Student thesis series INES nr 459

Glacial history of the upper Drac Blanc catchment (Écrins massif, French Alps)

Felix Martin Hofmann

2018
Department of
Physical Geography and Ecosystem Science
Lund University
Sölvegatan 12
S-223 62 Lund
Sweden

Felix Martin Hofmann (2018).

Glacial history of the upper Drac Blanc catchment (Écrins massif, French Alps)
Glaciationshistoria i området kring övre Drac Blanc, Écrinsmassivet, franska Alperna

Master degree thesis, 30 credits in Physical Geography and Ecosystem Analysis
Department of Physical Geography and Ecosystem Science, Lund University

Level: Master of Science (MSc)

Course duration: January 2018 until June 2018

Photo on the title page: aerial photo of the upper Drac Blanc catchment taken from a military aircraft in 1938. See the Sirac and its glaciers in the foreground. The Rougnoux valley (left) and the Prelles valley (right) can be seen in the background (unknown photographer).

Glacial history of the upper Drac Blanc catchment (French Alps)

Felix Martin Hofmann

Master thesis, 30 credits, in *Physical Geography and Ecosystem Analysis*

Supervisors:
Helena Alexanderson
Department of Geology, Lund University

Philippe Schoeneich
Department of Geography, Université Grenoble Alpes

Exam committee:
Ulrik Mårtensson, Lund University
Jesper Sjolte, Lund University

Felix Martin Hofmann

Glacial history of the upper Drac Blanc catchment (French Alps)

Glacier advances in the Écrins massif (French Alps) during the Late Glacial and the Early Holocene are poorly constrained. Based on field observations, a high-resolution digital elevation model and an orthophoto, glacial landforms in the upper Drac Blanc catchment were mapped. Thanks to 42 new ^{10}Be exposure ages, the timing of the stabilisation of selected moraines was constrained. The application of the accumulation area ratio method with a ratio of 0.67 enabled the determination of the Equilibrium Line Altitude (ELA) during the corresponding glacier advances and the amount it lowered compared to the end of the Little Ice Age.

The lowermost sampled moraine may have been reached by a first glacier advance at around 16.9 ± 1.6 ka. Not unexpectedly, multiple moraines in the upper Drac Blanc catchment stabilised during Greenland stadial 1 and in the Early Holocene. During the furthest glacier advance somewhat before 12.5 ± 0.6 ka, a prominent moraine was shaped or, alternatively, re-occupied. The ^{10}Be exposure ages provide evidence for further glacier advances or halts in glacier recession not later than 12.5 ± 0.6, 11.9 ± 1.0 and 11.2 ± 0.4 ka. According to the ELA reconstructions, these events were associated with ELA depressions between 160 and 220 m with respect to the end of the Little Ice Age. Exposure ages from three boulders indicate a still stand or a glacial re-advance not later than 10.7 ± 0.6 ka when the ELA was 150 m lower than at the end of the Little Ice Age.

Novel findings of this study are (1) the periods of moraine stabilisation at the latest at 11.9 ± 1.0, 11.2 ± 0.4 and 10.7 ± 0.6 ka which have hitherto not been dated in the Écrins massif and (2) the associated ELA lowering during these periods based on the accumulation area ratio method. The ^{10}Be exposure ages agree well with that of moraines at other sites in the Alps which have been correlated with the Egesen and the Kartell stadials.

Keywords: Physical Geography, ^{10}Be exposure dating, structure-from motion, geomorphological mapping, moraine, equilibrium line altitude, Alps

Advisors: **Helena Alexanderson** and **Philippe Schoeneich**
Master degree project 30 credits in Physical Geography and Ecosystem Analysis, 2018
Department of Physical Geography and Ecosystem Science, Lund University. Student thesis series INES nr 459

Felix Martin Hofmann

Glacial history of the upper Drac Blanc catchment (French Alps)

Glaciers shape characteristic landforms during the culmination of advances and during temporary halts in glacier recession. One of these landforms which can commonly be found in actual glacier forefields or formerly glaciated areas, are moraines. The elongated ridges which consist of loose sediments characterised by varying grain sizes up to large boulders, are deposited at the margin of a glacier. Different dating techniques enable the age of boulders on moraines to be determined. Hence, the age of the moraine and, therefore, the position of the glacier margin at a given time can be estimated.

Glaciers can be subdivided into two areas, an *accumulation area*, at a higher elevation where the mass balance is positive on a yearly timescale, and the *ablation area* at a lower elevation where the mass balance is negative on an annual timescale. Given the situation that the front of a glacier is stationary, the negative mass balance in the ablation area is compensated by ice flow. The transition between the accumulation and ablation areas occurs at the *equilibrium line altitude*, the elevation at which the mass balance is zero on a yearly timescale. Apart from a few exceptions, its position is believed to be influenced by changes in precipitation and/or temperature. Hence, the determination of the change of the *equilibrium line altitude* relative to the last period of stationary glaciers enables past changes in temperature and/or precipitation to be detected. This information can, in turn, be applied in future studies to predict the effects of anthropogenic climate change, as such forecasts require a detailed knowledge of past climatic variations. Therefore, the magnitude of past climatic changes in different parts of the world need to be determined. However, very little is known about previous climatic variations in the French Alps. This study aims at filling this gap by investigating past glacier variations as indications for former climatic fluctuations.

For the first step of this study, moraines and, therefore, the former position of glacier margins in two adjacent valleys in the southern Écrins massif (French Alps) were mapped. For the second part of this study, boulders on selected moraines in the upper Drac Blanc catchment were dated to reconstruct the changes in the extent of the former glaciers through time. Lastly, the lowering of the *equilibrium line altitude* relative to AD 1850 during the formation of the moraines in the two valleys in the upper Drac Blanc catchment was reconstructed.

Overall, the lowermost moraine from which rock samples were obtained, may have been reached by a glacier at around 16900 ± 1600 years before present. However, it is more likely that the moraine is slightly older than 12500 ± 600 years. Further glacier advances or halts in glacier recession occurred at around 12500 ± 600, 11900 ± 1000, 11200 ± 400 and 10700 ± 600 years before present. Considering that the dated moraines lie up to several kilometres down-valley from the areas which the former glaciers occupied before their final extinction, it can be inferred that the fronts of the glaciers were located at significantly lower elevations between 12500 ± 600 and 10700 ± 600 years before present. Hence, the climate then must have been more favourable for glaciers than today. As the aforementioned ages of glacier advances or halts in glacier recession fall in the cool period between 12900 and 11700 years before present, it can be assumed that the cooling caused the glaciers to advance and to stagnate, thereby leading to the deposition moraines at their margins.

The lowering of the equilibrium line altitude between 120 and 220 m with respect to its position at around AD 1850 during the glacier advances and halts in glacier recession between 12500 ± 600 and 10700 ± 600 years before present agrees well with studies of other sites in the Alps.

Hence, the climatic differences across the Alps at around 12000 years before present were possibly similar than today.

Keywords: Physical Geography, ^{10}Be exposure dating, structure-from motion, geomorphological mapping, moraine, equilibrium line altitude, Alps

Advisors: **Helena Alexanderson** and **Philippe Schoeneich**
Master degree project 30 credits in Physical Geography and Ecosystem Analysis, 2018
Department of Physical Geography and Ecosystem Science, Lund University. Student thesis series INES nr 459

Felix Martin Hofmann

Glacial history of the upper Drac Blanc catchment (French Alps)

Les stades glaciaires tardiglaciaires et holocènes dans le massif des Écrins (Alpes françaises) sont mal connus et peu datés. Dans le cadre de cette étude, une cartographie des moraines dans le bassin versant du Drac Blanc a été réalisée à partir d'un modèle numérique de terrain de haute résolution spatiale, d'une orthophoto et des observations de terrain. Les âges d'exposition (^{10}Be) obtenus sur les blocs morainiques sélectionnés ont permis d'établir une chronologie des avancées glaciaires et des phases de stationnement durant le Tardiglaciaire et le début de l'Holocène dans le bassin versant amont du Drac Blanc. L'altitude de la ligne d'équilibre glaciaire ainsi que ses valeurs de dépression par rapport à la période du Petit Age Glaciaire ont été reconstituées pour les différents stades en s'appuyant sur la méthode AAR (*accumulation area ratio* de 0,67).

Selon les âges d'exposition, il est possible que la moraine échantillonnée la plus basse ait été atteinte pour la première fois par un glacier vers 16.9 ± 1.6 ka. Plus probablement, cette moraine a certainement été déposée peu avant 12.5 ± 0,6 ka comme le suggère la dépression de la ligne d'équilibre de 220 m par rapport au Petit Age Glaciaire qui caractérise ce stade. Les âges d'exposition de blocs sur des moraines indiquent plusieurs avancées glaciaires ou phases de stagnation entre 12.5 ± 0.6 et 11.2 ± 0.4 ka qui sont caractérisées par des dépressions de la ligne d'équilibre comprises entre 220 et 160 m par rapport au Petit Age Glaciaire. Trois âges d'exposition obtenus sur une moraine latéro-frontale mettent en évidence une dernière avancée glaciaire ou phase de stationnement vers 10,7 ± 0,6 ka, associée à une baisse de la ligne d'équilibre de 150 m.

En tout, les avancées glaciaires ou phases de stationnement vers 11.9 ± 1.0, 11.2 ± 0.4 et 10.7 ± 0.6 ka ont été datées pour la première fois dans le massif des Écrins. De plus, cette étude a permis de reconstituer la baisse de la ligne glaciaire lors des stades glaciaires tardiglaciaires et holocènes dans le massif des Écrins en se basant sur la méthode AAR. Les âges des moraines dans le bassin versant du Drac Blanc sont cohérents avec les âges d'exposition recalculés obtenus par d'autres équipes dans les Alpes autrichiennes et suisses, et attribués aux stades d'Egesen et de Kartell. Le modèle des stades tardiglaciaires et début-Holocène des Alpes orientales semble donc aussi valable en partie pour la partie sud du massif des Écrins.

ACKNOWLEDGEMENTS

First of all, I would like to thank Helena Alexanderson and Philippe Schoeneich for their excellent supervision, as well as for their critical and helpful suggestions. I gratefully acknowledge the support of Didier Bourlès. This study would have been impossible without his offer to prepare the samples for ^{10}Be exposure dating in the Laboratoire National des Nucléides Cosmogéniques in Aix-en-Provence (France). The master thesis was financially supported by the German Academic Exchange Service (DAAD) through a one-year scholarship for graduate students to FMH. I would like to thank Sébastien Bolbenes and Philippe Schoeneich for their dedication and enthusiasm during the fieldwork in August 2017. Many thanks also go to the shepherd who transported the rock samples from the Pré de la Chaumette mountain cabin to the next parking lot. The help of Melaine Le Roy during fieldwork in November 2017 is warmly acknowledged. I would like to thank Jordan Mertes for the help with the establishment of the digital elevation model. I acknowledge also the support of Laëtitia Léanni, Valérie Guillou and Régis Braucher during the lab work. This study benefitted also from numerous suggestions and comments from colleagues. Especially the insightful discussions with Melaine Le Roy, Irene Schimmelpfennig, Lena Håkansson, Per Möller and Max Boxleitner are acknowledged. The thorough review of the manuscript by Isaac Smith, Sven Lukas and Melaine Le Roy is gratefully appreciated. I also would like to thank the administration of the Écrins National Park for the authorisation for the sampling. I dedicate this work to my father who has become severely sick during my master thesis project.

TABLE OF CONTENT

LIST OF ABBREVIATIONS

AAR	Accumulation Area Ratio
ASTER	Accélerateur pour les Sciences de la Terre, Environnement et Risques
CEREGE	Centre Européen de Recherche et d'Enseignement des Geosciences de l'Environnement
CRONUS	Cosmic-Ray Produced Nuclide Systematics
DEM	Digital Elevation Model
ELA	Equilibrium Line Altitude
GCP	Ground Control Point
GI-1	Greenland Interstadial 1
GPS	Global Positioning System
GRIP	Greenland Ice Core Project
GS-1	Greenland Stadial 1
GS-2.1	Greenland Stadial 2.1
IDW	Inverse Distance Weighting
IGN	French National Institute of Geographic and Forest Information
IGUL	Institute of Geography of Lausanne University
INTIMATE	INTegration of Ice-core, MArine and TErrestrial palaeoclimate records
LGM	Last Glacial Maximum
LIA	Little Ice Age
MU	Morphostratigraphical Unit
NGRIP	North Greenland Ice Core Project
PDB	Pee Dee Belemnite Standard
PdC	Pré de la Chaumette
PO	Preboreal Oscillation
SE	Surface Exposure
SfM	Structure-from Motion
SMOW	Standard Mean Ocean Water
VdP	Vallon de Prelles (Prelles valley)
VdR	Vallon de Rougnoux (Rougnoux valley)
YD	Younger Dryas

1 INTRODUCTION

It is nowadays widely accepted that the investigation of past glacier changes provides valuable palaeoclimatic information (Mackintosh *et al.* 2017). Smaller glaciers are especially suitable for palaeoclimatic reconstructions given their high sensitivity to short-term climatic changes (Moran *et al.* 2016). Since the mass balance of glaciers is predominantly controlled by climate, past variations of the extent of glaciers, which can be reconstructed based on geomorphic evidence, reflect changes in accumulation and ablation. A frequently used parameter for palaeoclimatic reconstructions is the Equilibrium Line Altitude (ELA) which corresponds to the zone of the glacier where the accumulation equals the ablation on a yearly timescale (Ohmura *et al.* 1992). As it is mainly influenced by precipitation in winter and temperature in summer, changes in the ELA are believed to reflect variations in one or both of these factors (Pellitero *et al.* 2015). Information about ELA changes can subsequently be used to infer past changes in summer temperature and precipitation during moraine deposition (Kerschner and Ivy-Ochs 2008). Information about past climate variations is, in turn, crucially needed for determining natural climatic variability and predicting future climate change (Masson-Delmotte *et al.* 2013).

Moreover, forecasts for future changes in glaciation rely on a detailed knowledge of past glacier variations (Briner 2011). Predictions of future glacier variability in mountainous areas are of particular interest, as these regions are particularly sensitive to global climate change, as the warming signal is amplified by higher heat fluxes owing to a declining snow cover (Haeberli *et al.* 2007). The average temperature in the European Alps has risen twice as fast the global mean since the end of the 19th century (Auer *et al.* 2007) leading to increasing retreat rates of the Alpine glaciers in the last decades (Vincent *et al.* 2017). The glacier shrinkage alters not only the hydrological cycle but also increases the likelihood and the magnitude of geomorphological hazards, such as rock falls, landslides and floods thereby strongly impacting human activity (Keiler *et al.* 2010).

In their pioneering study, Penck and Brückner (1909) provided a first stratigraphical framework for the Alpine Late Glacial , which can be defined as the period between the beginning of the retreat of the glaciers in the forelands of the Alps after the Last Glacial Maximum (LGM) and the end of the Greenland stadial 1 (ca. 18-11.7 ka, Heiri *et al.* 2014). The progressively warmer Late Glacial was interrupted by periods favourable for glacier advances, commonly referred to as Late Glacial stadials (Böhlert *et al.* 2011). Since the work of Penck and Brückner (1909), numerous studies focusing on Late Glacial and Holocene glacier variability have been undertaken (Ivy-Ochs *et al.* 2008; Ivy-Ochs *et al.* 2009; Ivy-Ochs 2015 and references therein) making the European Alps one of the best documented regions worldwide. However, the spatial distribution of dated sites is uneven. As pointed out by Le Roy *et al.* (2015), most geomorphological studies were conducted in the Eastern and Central Alps, while few studies have been undertaken in the French Alps, especially outside of the Mont-Blanc massif (Le Roy *et al.* 2017).

Until today, only few chronological constraints on glacier fluctuations in the Écrins massif (French Alps) prior to the Little Ice Age (LIA) have been published (Cossart *et al.* 2011; Chenet *et al.* 2016; Le Roy *et al.* 2017). Studies dealing with past glacier variations in the upper Drac Blanc catchment *(Fig. 1* and *2)*, hereinafter referred to as the upper part of the Champoléon valley and its lateral valleys (De la Pierre, Rougnoux and Prelles valleys), are very scarce.

The only glacio-geomorphological study in this area was carried out in the Rougnoux valley where a sequence of well-preserved moraines can be observed (Di Costanzo and Hofmann 2016). Although the prominent moraines were already described in a petrological (Biju-Duval 1975) and in a glacio-geomorphological study of the further down-valley glacial landforms in the Drac valley (Monjuvent 1978), the moraines in the Rougnoux valley were first mapped during a field course by Aix-Marseille University in April 2016. The mapping enabled a relative chronology of the moraines to be established. The preliminary map of the moraines in the Rougnoux valley was later improved with a Digital Elevation Model (DEM, Di Costanzo and Hofmann 2016).

Based on an ELA reconstruction, the moraines close to the margin of the permanent snow patch in the upper part of the Rougnoux valley were attributed to LIA advances. The application of the toe to headwall altitude ratio (Bakke and Nesje 2011) enabled the determination of an ELA depression of 380-480 m compared to the end of the LIA for the moraine stages further down-valley. Based on a similar ELA change in the Durance catchment (400-500m, Cossart *et al.* 2011), these moraines were cautiously attributed to the Egesen stadial which has been linked to Greenland stadial 1 (GS-1, Heiri *et al.* 2014). Due to the lack of chronological constraints it could not be ruled out that some of the moraines in the Rougnoux valley might have been deposited during the Early Holocene (Hofmann 2016).

Later field campaigns showed that some moraines were not recognised. Hence, a refinement of the geomorphological map of the Rougnoux valley and the application of an absolute dating method to numerically constrain the age of the moraines was deemed necessary. Well-preserved moraine systems can also be observed in the neighbouring Prelles valley and near the Pré de la Chaumette mountain cabin *(Fig. 2)* down-valley from the Rougnoux valley which have hitherto not been mapped or dated.

In the light of these uncertainties and the lack of chronological benchmarks concerning past glacier variations in the Écrins massif, this study aims at:

- Mapping the landforms in the Rougnoux valley, the Prelles valley and around the Pré de la Chaumette mountain cabin with a particular emphasis on glacial landforms;
- Determine the age of selected moraines in the Rougnoux valley, Prelles valley and near the Pré de la Chaumette mountain cabin through the use of Surface Exposure (SE) dating to reconstruct the spatial and temporal change of the glaciers in the upper Drac Blanc catchment;
- Reconstruct the ELA during the deposition of the moraines to be able to correlate moraines on the different sites, as ELA reconstructions are considered a useful tool for local stratigraphical correlations (Reitner *et al.* 2016).

In this study, the hypothesis that the moraines down-valley from the LIA in the Rougnoux valley can be linked to glacier advances during GS-1 or in the Early Holocene, is tested. Additionally, this study aims at evaluating the hypothesis that moraines of a similar age should also occur in the neighbouring Prelles valley. Due to limited resources, the glacier variations in the De la Pierre valley are beyond the scope of this study.

In the first section of this study, the study area is presented. The following section provides an overview about previous studies dealing with Late Glacial and Holocene glacier variability in the Écrins massif. The methods of this work are described in the third chapter. In the following two sections, the results are presented and discussed. The last section synthesises the main findings of this study.

2 REGIONAL SETTING

The Écrins massif as a part of the southern French Alps is located southeast of Grenoble *(Fig. 1)*. The highest summit of the Écrins massif is the Barre des Écrins (4102 m a.s.l, *Fig. 1)*. Mean annual precipitation in the massif varies strongly between 700 and more than 3000 mm (Chenet *et al.* 2016).

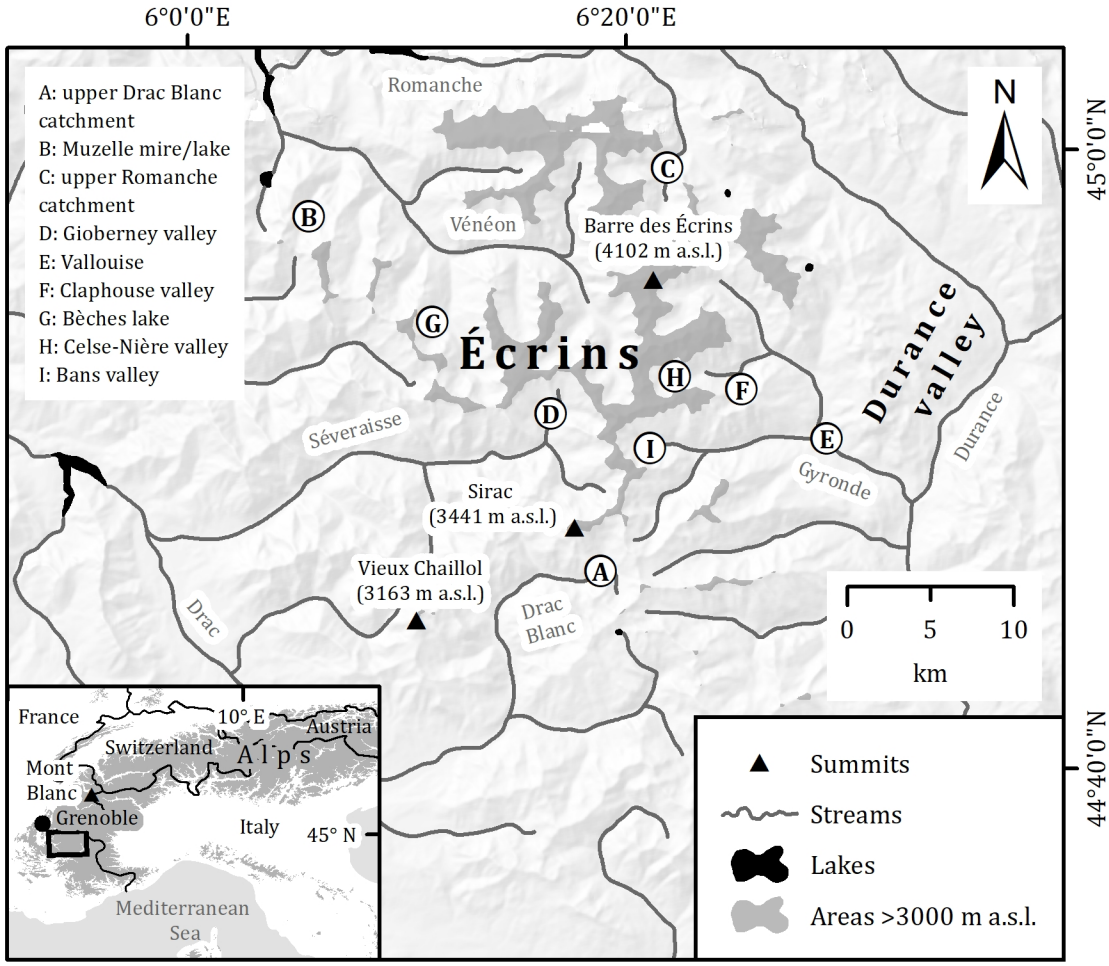

Date: 16.5.2018; Author: F.M. Hofmann; Data source: NASA 2014; Coordinate system: WGS 1984

Fig. 1. Location of the study area in the Écrins massif. The shaded relief is based on data from the Shuttle Radar Topography Mission (SRTM, version 4) with a spatial resolution of 250 m which was downloaded from the website of the CGIAR Consortium for Spatial Information (http://gisweb.ciat.cgiar.org/TRMM/SRTM_Resampled_250m, last accessed 23.3.2018).

The climate of the upper Drac Blanc catchment *(Fig. 1* and *2)* can be described as wet and cool. The mean annual temperature in the catchment varies between 4 and 6°C and average annual precipitation amounts to 1500-2000 mm. The snow cover in winter persists for more than 4 months (Ponel *et al.* 2011). The Écrins massif, which is one part of the external crystalline massifs in the Western Alps, was built up of blocks of the European basement. Granites intruded in these blocks and were subsequently metamorphosed during the Hercynian orogeny. The blocks of the crystalline substratum are separated by interspersed Jurassic sedimentary basins, which have been exhumed since the transitional period between the Oligocene and the Miocene (Dumont *et al.* 2008).

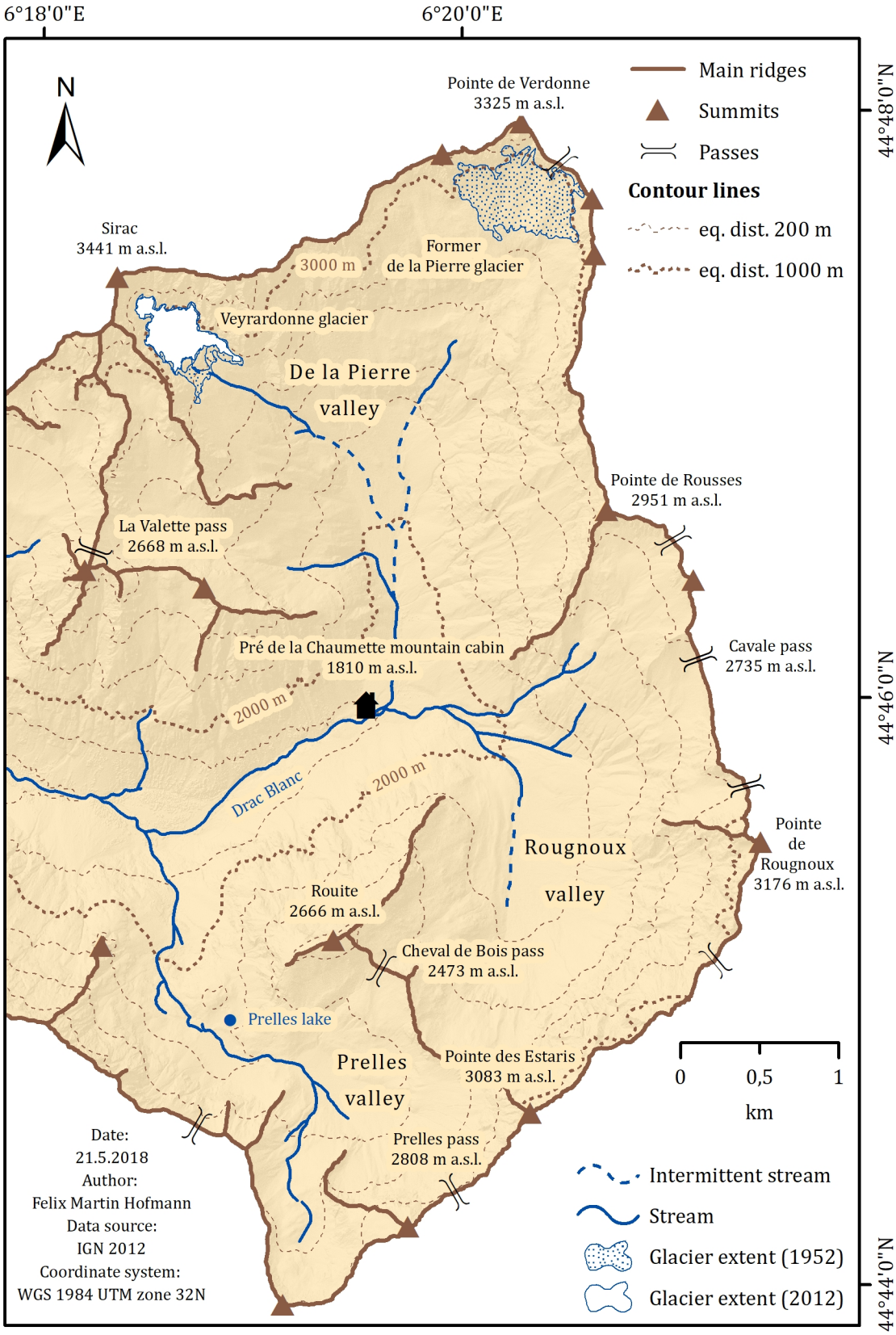

Fig. 2. Map of the upper Drac Blanc catchment. The glacier surface in 1952 is based on orthoimagery provided by the French National Institute of Geographic and Forest Information (IGN), whereas the glacier surface in 2012 was digitalised from the 2012 orthophoto.

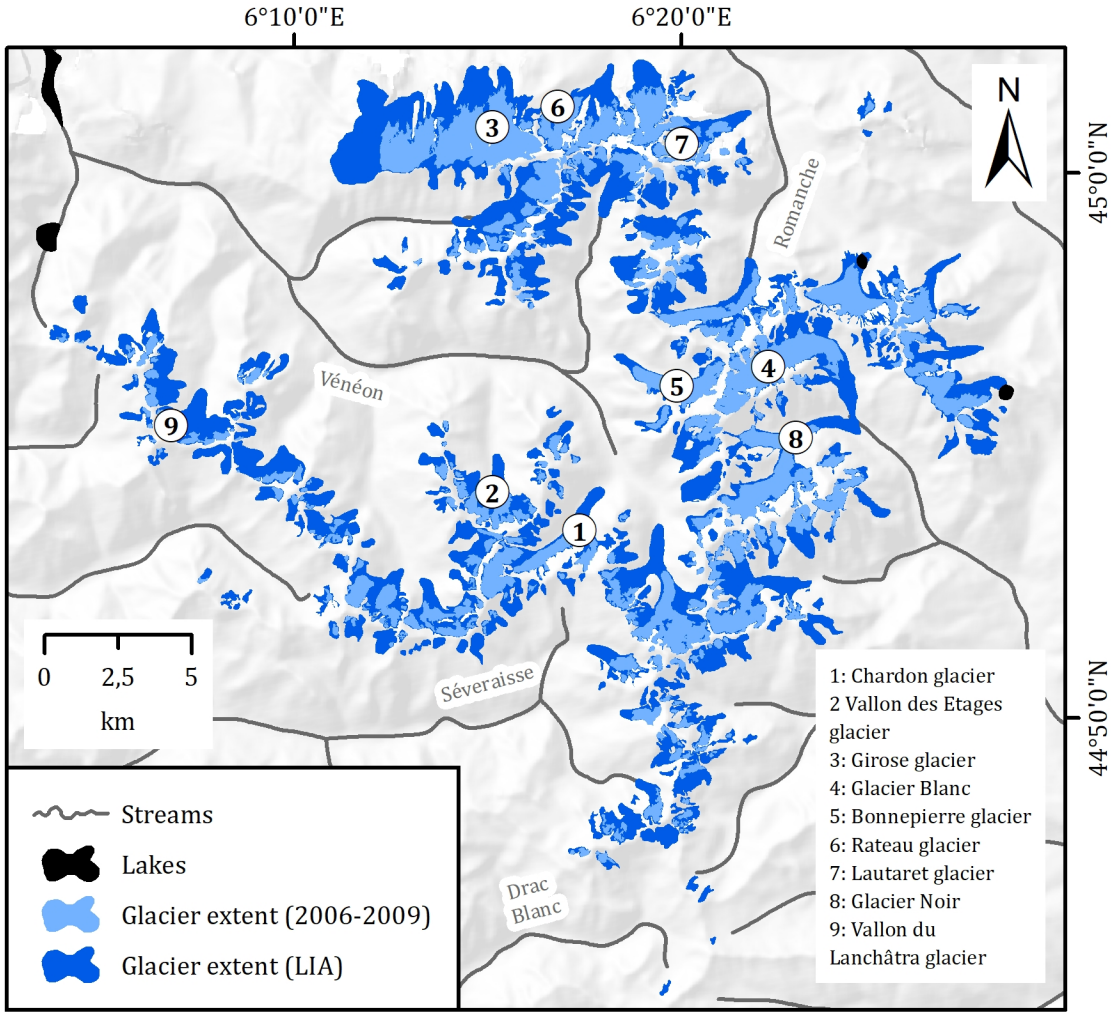

Date: 16.5.2018; Author: F.M. Hofmann; Data source: NASA 2014, Gardent 2014; Coordinate system: WGS 1984

Fig. 3. Extent of the glaciers in the Écrins massif at the end of the LIA and in 2006-2009 based on the most recent glacier inventory (Gardent 2014). See *Fig. 1* for the data source of the shaded relief.

The De la Pierre valley *(Fig. 2)* is dominated by migmatites and lenticular gneisses. In the lower part of the Rougnoux valley, migmatites, anatectic granites and lenticular gneisses are exposed. The south-eastern part of the Rougnoux valley consists of the feldspar-rich, partly conglomeratic Champsaur sandstone which is separated by a fault from the crystalline substratum. The higher part of the Rouite is made up of Triassic spilites. The eastern part of the Prelles valley consists of Champsaur sandstone and migmatites, whereas Jurassic marls and limestones dominate the southern part of the valley. In the lower part of the Prelles valley and around the Pré de la Chaumette mountain cabin, lenticular gneisses can be found (Debelmas *et al.* 1980).

The relief of the Écrins massif shows a strong imprint of past glaciations. Indeed, most valleys show a typical U-shaped cross section. Overdeepenings, hanging valleys and trimlines can frequently be found (van der Beek and Bourbon 2008). During the most extensive glaciations in the Quaternary, only the highest summits were not covered by ice and formed nunataks, whereas the main valleys were covered by thick glaciers (Delunel 2010). The Durance valley in the eastern part of the Écrins massif *(Fig. 1)* was, for example, covered by a roughly 1 km thick and 150 km long valley glacier during the LGM (Cossart *et al.* 2011).

Despite a strong glacier retreat from the LIA extent of about 170 km² *(Fig. 3,* Gardent 2014), the Écrins massif still hosts about 280 mostly debris-covered cirque and small valley glaciers covering a surface of about 68.5 km² according to the most recent glacier inventory in 2006-2009 (Gardent *et al.* 2014). The two biggest glaciers in the Écrins massif are the Girose and the Blanc glacier covering an area of 5.1 km² and 4.8 km², respectively *(Fig. 3,* Gardent *et al.* 2014). According to Le Roy *et al.* (2017), the Equilibrium Line Altitude (ELA) of the 11 largest glaciers in the Écrins massif was located at around 3100 ± 80 m in the AD 1984-2010 period. Based on the application of an accumulation area ratio of 0.65 for a set of 50 glaciers in the Écrins massif, Cossart (2011) reconstructed a mean ELA rise of about 250 m since the LIA.

Fig. 4. The Veyrardonne glacier south of the Sirac peak. The ice in the upper cirque is nowadays disconnected from the main ice body. Two generations of moraines (dotted lines) bear witness to recent advances of the small cirque glacier. Note the crevasses in both ice bodies (Photo: F.M. Hofmann, 22.8.2017)

The only remaining glacier in the upper Drac Blanc catchment is the Veyrardonne glacier *(Fig. 2, 4* and *5)*. This partly debris-covered, south-facing glacier is located in a small cirque below the Sirac peak. The ice in the small upper cirque is nowadays disconnected from the main ice body located below. The presence of small crevasses on the surface indicate that it can still be classified as an actual glacier. Two generations of fresh moraines on its forefield show that the glacier has reacted to recent climatic oscillations *(Fig. 4)*. The outermost of the fresh moraines on its forefield were probably deposited during the most extensive LIA advance (Gardent 2014). The surface of the cirque glacier amounted to 0.17 km² in the 1950s, when the two ice bodies were connected. Since then, the glacier experienced a reduction to 0.13 km² by 2012.

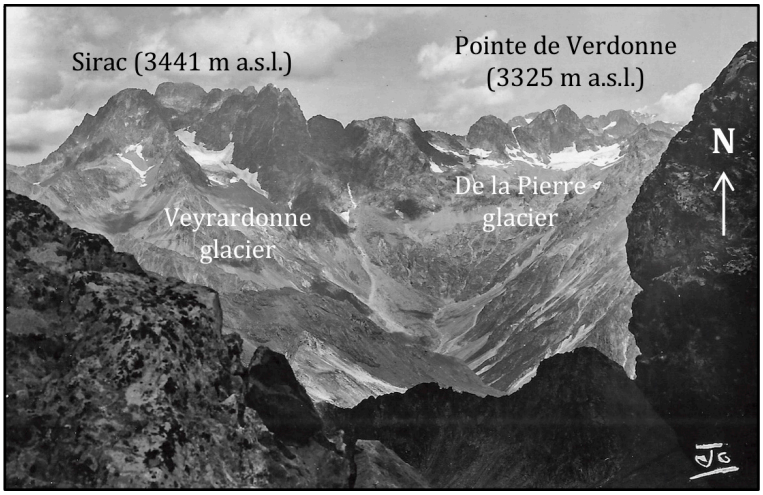

Fig. 5. Postcard from the 1950s showing both the De la Pierre glacier (right) and the Veyrardonne glacier (left). The photo was probably taken from the Prelles pass. Note the considerable larger extent of the Veyrardonne glacier (unknown photographer).

Only several permanent snow patches in the cirque south of the Pointe de Verdonne witness to the De la Pierre glacier which covered an area 0.29 km² in the 1950s *(Fig. 2* and *5)*. According to the caretaker of the Pré de la Chaumette mountain cabin, the south-facing glacier was even visible from the mountain cabin in the 1970s (Y. Ailloud, pers. comm. 13.8.2015).

3 LATE GLACIAL AND HOLOCENE GLACIER VARIATIONS IN THE ÉCRINS MASSIF

For the review of the existing studies about Late Glacial and Holocene glacier fluctuations in the Écrins massif, previously published exposure ages were recalculated with the Arctic ^{10}Be production rate of Young *et al.* (2013) using the CRONUS Earth (Cosmic-Ray Produced Nuclide Systematics on Earth Project) calculator (Balco *et al.* 2008). For the sake of comparability, neither snow shielding nor erosion were taken into account. Mean landform ages were computed by averaging the exposure ages from the same landform. Landform age uncertainties were calculated as outlined in section 4.2.3. The exposure ages of Le Roy *et al.* (2017) were not recalculated given the little effect on the resulting exposure ages (see the discussion in Le Roy *et al.* 2017).

Generally, Late Glacial and Holocene glacier variations in the Écrins massif prior to the LIA are not well constrained (Chenet *et al.* 2016; Le Roy *et al.* 2017). The scarcity of studies focusing on Late Glacial and Holocene glacier variability can mainly be attributed to three factors:

- The glaciers in the Mont-Blanc massif have received most attention from geomorphologists and glaciologists within the last decades (Deline and Le Roy 2008; Le Roy *et al.* 2015; Le Roy *et al.* 2017);
- Moraines older than the LIA are not very abundant in the Écrins massif thereby hampering the reconstruction of past glacier fluctuations (Delunel 2010);
- Most glaciers in the Écrins massif did not reach forested areas in the past, with few exceptions (Le Roy and Deline 2009), thereby preventing the use of subfossil wood and organic material incorporated in glacial deposits for the reconstruction of past glacier dynamics. Much like their precursors, Cossart *et al.* (2011) could not identify any organic material suitable for radiocarbon dating in glacial landforms in the Eastern Écrins massif. Until now, subfossil wood has only been found in the forefield of the Chardon and Etages glaciers *(Fig. 3*, Le Roy *et al.* 2017).

In contrast to other regions in the Alps (Ivy-Ochs *et al.* 2008), moraines deposited during the early phase of ice decay after the LGM (from 18 ka onwards) have not been described with only one exception. The remnants of lateral moraines at the entrance of the Chapeau-Roux valley close to the Muzelle mire *(Fig. 1)* were cautiously assigned to this period without any dating (Coûteaux 1983).

The absence of early Late Glacial moraines was explained with palynological data. Indeed, pollen data from different sites in the Écrins massif show no major climatic deterioration during the Late Glacial before the onset of the Younger Dryas (YD, Coûteaux 1984). Multiple glacier advances in the Écrins massif took place during GS-1, when pollen data from the Muzelle mire *(Fig. 1)* point towards a severe three-phased climatic downturn (Coûteaux 1983). Although moraines in several valleys of the Écrins massif have been attributed to GS-1 advances (see references in Le Roy *et al.* 2017) moraine deposits from that period have only been dated in the upper Romanche catchment *(Fig. 1)*.

In the upper Romanche catchment, the confluent Clot de Cavales and the La Plate des Agneaux glaciers deposited at least two moraines during the GS-1 (Chenet *et al.* 2016). Chenet *et al.* (2016) identified a moraine at around 1980 m a.s.l. which was dated to 12.1 ± 0.9 ka *(Fig. 6)*, whereas SE dating of another moraine 350 m up-valley yielded an exposure age of 11.6 ± 1.4 ka (recalculated from Chenet *et al.* 2016).

Based on a ^{10}Be exposure age of 12.8 ± 0.6 ka (recalculated from Delunel 2010) from a roche moutonée in Gioberney valley *(Fig. 1 and 6)*, Delunel (2010) linked the most external moraine complex to a GS-1 advance of the Condamine glacier. The glaciers in the Vénéon valley *(Fig. 1* and *6)* seem to have been affected by the climatic downturns during the GS-1. Indeed, the deposition of varved clay restarted in the Muzelle mire *(Fig. 1)* reflecting enhanced activity of the glaciers up-valley. Therefore, Coûteaux (1983) attributed a sequence of five moraines near the Muzelle mire to GS-1 advances.

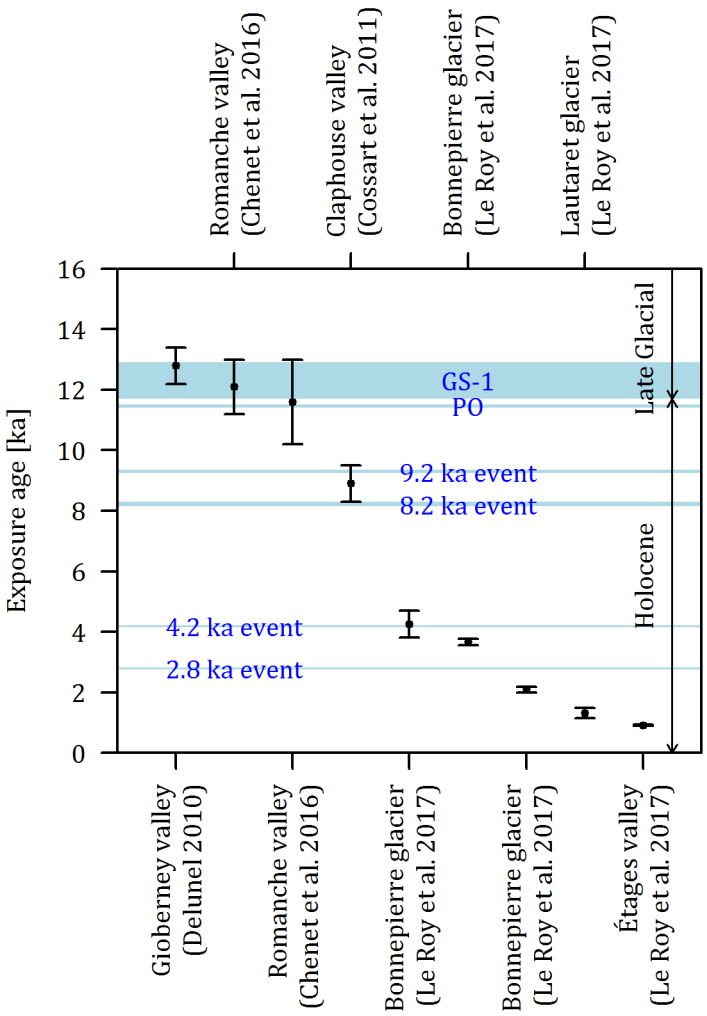

Fig. 6. Glacier advances in the Écrins massif according to recalculated ^{10}Be exposure ages. See *Fig. 1* and *3* for the location of the sites. All exposure ages, except those of Le Roy *et al.* (2017) were recalculated with the CRONUS Earth calculator (Balco *et al.* 2008) using the Arctic ^{10}Be production rate of Young *et al.* (2013). Neither snow shielding nor erosion rates were taken into account. The error bars indicate exposure age uncertainties or landform uncertainties. Mean exposure ages and average landform ages are highlighted as dots. GS-1 (12.9-11.7 ka, Rasmussen *et al.* 2014) and the Preboreal Oscillation (PO (11.5-11.4 ka), Rasmussen *et al.* 2014) are highlighted in light blue. See Lowe and Walker (2015), as well as Rasmussen *et al.* (2014) for the Holocene climatic downturns after the Preboreal oscillation.

Cossart *et al.* (2011) correlated the frontal moraine complex near Vallouise *(Fig. 1)* at around 1050 m a.s.l. with the second moraine generation in the Clarée valley *(Fig. 22)* located at a 300 m higher elevation, which has been dated to 12.2 ± 1.4 ka (recalculated from Cossart *et al.* 2012). Indeed, Cossart *et al.* (2011) argued that snow accumulation was more important in the eastern part of the Écrins massif than in the Clarée valley. Hence, the Gyronde valley was probably occupied by a valley glacier until the end of the Late Glacial. The associated ELA depression compared to the end of the LIA was determined to be 400-500 m (Cossart *et al.* 2011). SE dating of a riegel at the entrance of the Claphouse valley *(Fig. 1)*, on which a moraine has been deposited, yielded an exposure age of 8.9 ± 0.6 ka *(Fig. 6*, recalculated from Cossart *et al.* 2011). Hence, Cossart *et al.* (2011) drew the conclusion that the glaciers in the Gyronde valley were restricted to the cirques in the Early Holocene.

Before the onset of the LIA, the glaciers in the Écrins massif advanced at least five times during the Neoglacial and reached slightly larger extents than in the LIA (Le Roy *et al.* 2017)

Le Roy *et al.* (2017) dated the outermost right lateral moraine of the Bonnepierre glacier *(Fig. 3)* and obtained a mean exposure age of 4.25 ± 0.44 ka *(Fig. 6)*. Due to its large volume, Le Roy *et al.* (2017) supposed that it was built up during several pulses of the glacier implying that only the youngest advance had been dated. The last glacier advance shaping this lateral moraine was considered as the response to the 4.2 ka event thereby making the forefield of the Bonnepierre glacier the first site in the Alps where such a glacier advance has been dated (Le Roy *et al.* 2017).

Another glacier advance took place at around 3.7 ka *(Fig. 6)* when the Bonnepierre glacier deposited another lateral moraine and a small moraine segment close to its outermost lateral moraine. Simultaneously, the Rateau glacier *(Fig. 3)* shaped a lateral moraine. However, this interpretation should be considered carefully, since Le Roy *et al.* (2017) obtained younger exposure ages on the three outermost ridges of Rateau glacier which contradict the stratigraphy. The exposure age of a boulder on the innermost ridge (3.66 ± 0.45 ka) was considered the most reliable age for moraine deposition. Hence, Le Roy *et al.* (2017) suggested that the three outer moraines were also shaped during this 3.7 ka advance. During a subsequent advance, the Bonnepierre glacier built up its two innermost lateral moraines. Based on exposure ages from two boulders on the innermost ridge, this event was dated to 2.09 ± 0.10 ka *(Fig. 6)*. During this pulse, it is possible that boulders were reworked by the glacier, as indicated by the slightly 'too old' exposure ages of the blocs on the second innermost moraine (Le Roy *et al.* 2017).

Fouinat *et al.* (2017) identified a period of higher clastic sedimentation in the proglacial Muzelle lake *(Fig. 1)* between AD 370 and 500 indicating enhanced erosion by the glacier up-valley. The Lautaret glacier *(Fig. 3)* advanced at 1.31 ± 0.17 ka *(Fig. 6)* and deposited its left-hand side outermost lateral moraine (Le Roy *et al.* 2017). The Vallon des Étages glacier *(Fig. 3)* reached its Neoglacial maximum at around 0.92 ± 0.10 ka *(Fig. 6)* and a frontal moraine was shaped around 800 m down-valley from the current glacier front. During this advance, the glacier buried a log which possibly originated from a tree growing on the steep slope above the glacier's forefield (Le Roy *et al.* 2017). At the same time, a peak in clastic sedimentation occurred in the Muzelle lake. After a drop at around AD 1150, the detritic input in the Muzelle lake reached a new maximum between AD 1230 and 1325 marking the onset of the LIA in the Écrins massif (Fouinat *et al.* 2017).

According to palynological data from the Bèches lake *(Fig. 1)*, which was correlated with dendrochronological data from the Vanoise massif, the glacial activity up-valley from the Bèches lake peaked at around AD 1545, 1685 and 1820, thereby indicating periods favourable for glacial expansion (Tessier *et al.* 1986). However, contemporary moraines in the Écrins massif have not yet been dated. Minima in glacial erosion occurred around AD 1615, 1750 and 1870. Generally, the sedimentation rate dropped from AD 1750 on (Tessier *et al.* 1986). Multiple glaciers in the northern and eastern part of the Écrins massif reached their LIA maximum extent during the 19th century. At around AD 1815, the confluent Glacier Blanc and Glacier Noir *(Fig. 3)* reached an elevation of 1874 m a.s.l. The subsequent retreat led to the separation of the two glaciers at around AD 1853 (Cossart *et al.* 2006). The advancing Vallon des Etages glacier *(Fig. 3)* deposited a moraine between AD 1822 and 1853 (Le Roy 2012). The Bonnepierre glacier reached its maximum LIA extent and built up the outermost preserved frontal moraine at around AD 1854 (Le Roy and Deline 2009). Roughly at the same time, an advance of the Vallon du Lanchâtra glacier *(Fig. 3)* was underway leading to the deposition of a frontal moraine (Le Roy 2012). In the Celse-Nière valley *(Fig. 1)*, the Sélé glacier shaped its outermost moraine at around AD 1860. The oldest moraine generation in the Bans valley *(Fig. 1)* was deposited at about the same time (Cossart *et al.* 2006).

In summary, the glaciers in the Écrins experienced a re-advance during GS-1, as indicated by moraines in different valleys of the massif. Some of the glaciers, as the Bonnepierre glacier, advanced during the Neoglacial after 4.2 ka and reached a similar extent than at the end of the LIA. The last major glacial re-advances in the Écrins massif took place during the LIA.

4 METHODS

The landforms in the Rougnoux valley, the Prelles valley and around the Pré de la Chaumette mountain cabin were mapped using a combination of a high-resolution DEM, an orthophoto and field notes. The chapters 4.1 and 4.2 provide detailed information about the establishment of the DEM and the geomorphological mapping, respectively. The application of ^{10}Be exposure dating enabled the age of selected moraines in the upper Drac Blanc catchment to be determined. Methodological details are given in chapter 4.3. The ELA during the deposition of the moraines in the Rougnoux valley, in the Prelles valley and around the Pré de la Chaumette mountain cabin were reconstructed with two ArcGIS toolboxes (Pellitero *et al.* 2015; Pellitero *et al.* 2016). Their underlying principles and the application in this study are further outlined in chapter 4.4.

4.1 Establishment of the digital elevation model

The DEM of the southern Écrins massif was derived using the Structure-from Motion (SfM) approach. With this cost-effective method, DEMs and orthophotos can be established based on overlapping aerial photographs, satellite images or even photos taken with handheld cameras (Westoby *et al.* 2012). SfM-based DEMs have been widely used for geomorphological (e.g. Lucieer *et al.* 2014) or glaciological studies (e.g. Mertes *et al.* 2017) showing a similar precision to DEMs derived from costly terrestrial laser scanning data (Westoby *et al.* 2012).

Table 1. Main characteristics of the DEM of the southern Écrins massif.

	DEM of the southern Écrins massif
Aerial photographs	n = 61
Tie points (sparse point cloud)	n = 415,168
Points (dense point cloud)	n = 888,268,268
Size of the DEM [pixel]	36,699 ∗ 43,216
Pixel size [m]	0.569

The usual workflow in SfM involves the identification of common features in all images. In the next step, algorithms detect common points in multiple images. Simultaneously, erroneous correspondences are identified and removed. Subsequently, the 3D structure of the area under investigation is calculated. In contrast to conventional photogrammetry, a complete camera calibration is not required. A set of well-distributed Ground Control Points (GCP) can then be used to georeference the resulting sparse point cloud. Alternatively, the sparse point cloud can automatically be georeferenced when the camera positions are known. In a final step, the application of multiple algorithms densifies the sparse point cloud thereby significantly increasing the number of points (Smith *et al.* 2016).

For the establishment of both the DEM and the orthophoto of the southern Écrins massif *(Table 1)*, 61 aerial photographs taken by the IGN in summer 2012 were downloaded from http://remonterletemps.ign.fr (last accessed 21 February 2018).

The aerial images were first imported in Agisoft Photoscan™ and the black margin was subsequently removed using the mask tool. In the next step, the images were aligned, resulting in the identification of 415,168 key points. The subsequent densification of the sparse point cloud significantly increased the number of points *(Table 1)*. For this step, the high-quality setting and moderate depth filtering were chosen.

The dense point cloud was georeferenced with the WGS 1984 UTM zone 32N coordinate system. 22 well-distributed GCPs on boulders and other identifiable objects, which were not considered as likely to have changed their position, were selected on www.geoportail.fr (Last accessed 22 February 2018). The coordinates on www.geoportail.fr are based on the RGE ALTI® DEM with a spatial resolution of 5 m. Markers for the GCPs were first placed on a single aerial photograph. Subsequently, all other aerial photographs showing this point were automatically selected and the positioning of the marker was adjusted to improve the overall accuracy of the georeferencing. Subsequently, the x-, y-, and z-coordinates of the GCPS in Geoportail were manually added and a precision analysis was performed using the sfm-georef tool (James *et al.* 2017). Accordingly, 15 GCPs were selected for the georeferencing of the dense point cloud, whereas 7 GCPs served as check points. The overall error of the georeferencing was 0.83 m. A DEM and an orthophoto with a pixel size of 0.569 and 0.284 m, respectively, were finally derived from the dense point cloud *(Table 1)*. For the orthophoto, the 'mosaic' blending mode was chosen and the hole filling function was activated.

4.2 Geomorphological mapping

For the geomorphological mapping of the three sites under investigation, the Institute of Geography of Lausanne University's (IGUL) geomorphological map system (Maillard *et al.* 2011) was chosen. The geomorphological maps will later be integrated in a database of the Écrins massif. The IGUL legend, which is based on geomorphological legends from France, Germany and Switzerland (Schoeneich 1993), has been applied for several geomorphological studies (e.g. Pellitero Ondicol 2009; Lambiel *et al.* 2016).

The main principle of the legend is the distinction between erosion and accumulation. Indeed, erosional surfaces are intentionally left blank, whereas accumulation areas are highlighted in colour. The colours of the symbols, lines and surfaces have a genetic significance: fluvial (green), gravitational (ocre), glacial (purple), periglacial (pink), nival (dark red) and anthropogenic (grey). Although exposed bedrock is left blank, structural elements, as escarpments or rock steps are shown in red. The landforms' sedimentological composition is not represented (Schoeneich 1993).

The moraines in the Rougnoux valley, Prelles valley and around the Pré de la Chaumette were mapped at a scale of 1:1000 using the ArcGIS version of the IGUL legend (Maillard *et al.* 2011). A hillshade derived from the DEM, the orthophoto and field notes were jointly used to combine the advantages of both remotely sensed data and field notes. Based on a similar approach to that of Cossart *et al.* (2012), the identification of moraines was based on their morphometry (asymmetrical shape and a steeper proximal side), as well as on their sedimentary structure (diamict composed of different grain sizes) if outcrops were available. Fluvial, gravitational, periglacial and anthropogenic landforms were only mapped for the sake of completeness, as they are not the main scope of this study.

See the legends of the geomorphological maps in the appendices *(Appendix 10, 11 and 12)* for the taxonomy of the landforms.

4.3 Surface exposure dating

The scarcity of organic material suitable for radiocarbon dating in Late Glacial and Early Holocene moraines in the Alps, especially at high elevations, prevented most of their ages being constrained before the advent of SE dating (Ivy-Ochs and Kober 2008). As no organic material has been identified in the moraines in the upper Drac Blanc catchment, the only solution for overcoming this problem was the application of SE dating which only requires rock samples from large boulders on moraines. Therefore, this dating method has become the golden standard in glacial geomorphology (Heyman *et al.* 2016). As SE dating is the main tool of this study, its basic principles are first presented.

4.3.1 Basic principles of surface exposure dating

Cosmic rays are highly energetic particles which primarily originate from the Milky Way galaxy. During their passage through the earth's magnetic field, the high-energy cosmic rays collide with nuclei in the upper atmosphere, thereby releasing secondary nucleons and mesons. The flux of these secondary particles is increasingly dominated by neutrons towards the earth surface due to ionisation energy losses. When they hit the earth surface, the secondary particles cause target minerals in rock surfaces to fragment, a process which is commonly known as spallation. This process is reinforced by short-lived muons (Gosse and Phillips 2001).

However, the latter way of cosmic nuclide production can be considered negligible *(Fig. 7)*. Due to energy losses during the fragmentation of the target minerals, the neutrons lose their capability to fragment the nuclei and are ultimately absorbed by the target nuclei, commonly referred to as thermal neutron capture (Gosse and Phillips 2001). Hence, cosmic nuclide production in rock results mainly from spallation (I) and thermal neutron capture reactions (II). During spallation of target minerals by high-energy neutrons, cosmic nuclides, as ^{3}He, ^{10}Be, ^{14}C, ^{21}Ne, ^{26}Al or ^{36}Cl, are formed (Lowe and Walker 2015). The production of ^{10}Be, the nuclide used in this study, results from the spallation of both ^{28}Si and ^{18}O (Gosse and Phillips 2001).

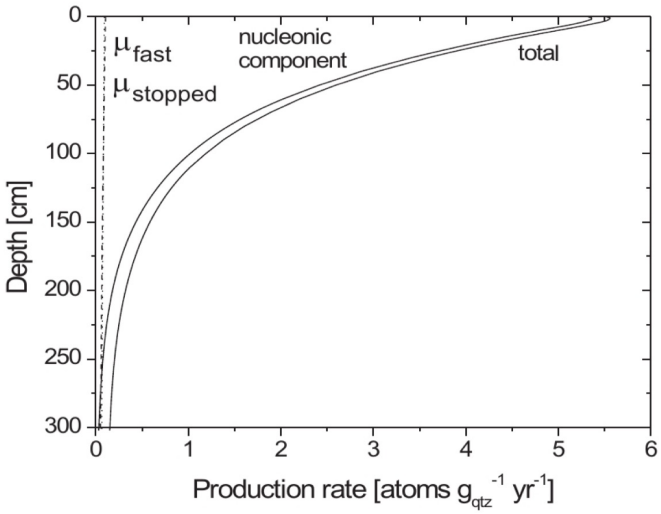

Fig. 7. ^{10}Be production rate [atoms g quartz^{-1} year^{-1}] at sea level and high latitudes. The ^{10}Be production rate is the result of muonic (μ) and spallogenic reactions. The muonic component in ^{10}Be production can be considered almost negligible. Note that the ^{10}Be production decreases with depth (Ivy-Ochs and Kober 2008, p. 184).

The formation of the cosmic nuclides is depth-dependent and decreases significantly within the first 3 m of the lithosphere *(Fig. 7)*. Since the concentration of cosmic nuclides is directly related to the duration of the exposure of a rock surface, the determination of their abundance enables the exposure age of the rock surface to be determined (Lowe and Walker 2015).

To constrain the exposure age of a given surface, the local cosmic nuclide production rate needs to be determined.

Considering that (I) the geomagnetic field deflects cosmic radiation, resulting in higher intensities of cosmic radiation at the poles than at lower latitudes, that (II) the earth's magnetic field has varied in the past and in space, that (III) topographic shielding exerts an influence on cosmogenic nuclide production and that (IV) cosmogenic nuclide production is depth-dependent (Ivy-Ochs and Kober 2008), a cosmogenic nuclide production model has to be applied which takes these four factors into account (Gosse and Phillips 2001). Commonly applied cosmic nuclide production models for ^{10}Be and ^{26}Al were developed by Lal (1991) and Stone (2000), the latter being the most-used scaling scheme in recent studies (Ivy-Ochs and Kober 2008).

According to Ivy-Ochs and Kober (2008), the concentration (C) of a cosmogenic nuclide [atoms g^{-1}] at a given time [a] can be determined as follows:

$$C_{(t)} = \frac{P_{(0)}}{\lambda + \frac{\rho\varepsilon}{\Lambda}} \left(1 - e^{-\left(\lambda + \frac{\rho\varepsilon}{\Lambda}\right)t}\right) + C_{in}e^{-\lambda t} \qquad (1)$$

where $P_{(0)}$ is the production rate at the given site [atoms g^{-1} a^{-1}], λ is the decay constant [a^{-1}], ρ the bedrock density [g cm^{-1}], ε the erosion rate [cm a^{-1}], Λ the attenuation length [g cm^{-2}] and C_{in} the initial cosmogenic nuclide concentration [atoms g^{-1}], which is also commonly referred to as inheritance. Frequently used values for the attenuation length and the bedrock density are 157 g cm^{-2} and 2.7 g cm^{-3}, respectively (Gosse and Phillips 2001).

For the use of SE dating in glacial geomorphology, it is commonly assumed that the surface was completely shielded prior to the glaciation and that it was continuously exposed to cosmic radiation after the onset of the deglaciation (Heyman *et al.* 2016). Equation 1 can be applied without the inheritance component at its end when the cosmogenic nuclide concentration has been zeroed prior to the exposure to cosmic radiation. Given the scenario that both the erosion during the exposure and the initial concentration of the nuclide are zero, equation 1 can be simplified as follows:

$$C_{(t)} = \frac{P_{(0)}}{\lambda} \left(1 - e^{-\lambda t}\right) \qquad (2)$$

Since $C_{(t)}$ can be measured with accelerator mass spectrometry, equation 2 can be solved for time (t).

The uncertainty in the ^{10}Be concentration in a sample originates mainly from (I) the error associated with the measurement of the ^{10}Be/^{9}Be ratio in the sample, (II) the uncertainty of the ^{9}Be concentration in the spike and from (III) the weighing error. Hence, the internal or analytical uncertainty in the ^{10}Be concentration in a sample (σC_{10Be}) in atoms g^{-1} can be determined by adding the aforementioned errors in quadrature:

$$\sigma C_{10Be} = \sqrt{\left(\frac{\sigma R_{10Be9Be}}{R_{10Be9Be}}\right)^2 + \left(\frac{\sigma C_{9Be\,spike}}{C_{9Be\,spike}}\right)^2 + \left(\frac{0.0001}{wt_{sample}}\right)^2} \qquad (3)$$

where $\sigma R_{10Be9Be}$ is the uncertainty in the measured ^{10}Be/^{9}Be ratio (corrected with respect to the chemical blanc), $R_{10Be9Be}$ the measured ^{10}Be/^{9}Be ratio corrected for the chemical blanc, σC_{9Be} the error in the ^{9}Be concentration in the spike [atoms], $C_{9Be\ spike}$ the ^{9}Be concentration in the spike [atoms] and wt_{sample} the weight of the sample [g].

For the comparison with the results of other dating methods, the external uncertainty has to be calculated. For the determination of the external uncertainty ($\sigma C_{external}$) in atoms g^{-1}, the error in the production rate (σP) and σC_{10Be} are added in quadrature:

$$\sigma C_{external} = \sqrt{\sigma C_{10Be}{}^2 + \sigma P^2} \qquad (4)$$

For the application of SE dating in glacial geomorphology, rock samples are taken from horizontal or near-horizontal boulders on moraines or polished rock surfaces. Surfaces which show signs of weathering and erosion should be avoided, as both factors lead to an underestimation of the exposure age (Lowe and Walker 2015). Particular attention should be drawn to the height of the boulders when constraining the age of moraines, as tall boulders generally yield more robust exposure ages which cluster better (Heyman *et al.* 2016).

Two main sources of errors should be borne in mind when using SE dating for dating boulders on moraines. SE dating often yields 'too-old' or 'too-young' exposure ages, thereby reflecting prior or incomplete exposure, respectively (Heyman *et al.* 2016). According to Heyman *et al.* (2016), prior exposure may result from limited glacial erosion or the transport of previously exposed material. Explanations for incomplete exposure include boulder toppling or post-depositional exhumation. The aforementioned sources of errors are discussed below with regard to the dataset from the upper Drac Blanc catchment.

4.3.2 Application to moraines in the study area

Rock samples for ^{10}Be exposure dating were taken from boulders on selected moraines in the upper Drac Blanc catchment during fieldwork in August 2017. 32, 5 and 4 samples were obtained from moraines in the Rougnoux valley, the Prelles valley and around the Pré de la Chaumette mountain cabin, respectively (*Appendix 1* and *2)*. The sampling strategies are presented in the first section. The analytical treatment of the samples, as well as the determination of the ^{10}Be exposure ages are described in the following two subchapters.

4.3.2.1 Sampling strategies

To avoid incomplete exposure associated with boulder toppling, only boulders which were well-embedded in the moraine matrix were chosen. Boulders on the moraine crests were prioritised *(Fig. 8)*. Given the higher risk for post-depositional exhumation, boulders on the proximal side of the moraines were only sampled if boulders on the moraine crest and the distal side were not available. To be partly able to detect 'too-young' and 'too-old' apparent exposure ages (Heyman *et al.* 2016), three samples were taken, in most cases, per moraine.

Topographic shielding was recorded using a SUUNTO© handheld clinometer and a compass. The azimuths and the elevations of the horizon of each sampled boulder were later converted into a shielding factor *(Appendix 1* and *2)*. The use of a handheld GPS (Global Positioning System) with a vertical and horizontal positioning error of about ± 5 m enabled the latitude, longitude and elevation of the boulders to be determined *(Appendix 1* and *2)*. To reduce the error associated with the handheld GPS, the coordinates were later corrected with the DEM of the southern Écrins massif. During sampling, the height and the lithology of each boulder were noted. The thickness of the rock fragments in each sample set was recorded with a caliper and subsequently averaged *(Appendix 1* and *2)*.

4.3.2.2 ^{10}Be geochemistry

Fig. 8. The VdR-7 boulder on the crest (dotted line) of a lateral moraine in the upper part of the Rougnoux valley. The boulder is well embedded in the moraine matrix and the exposure age of the corresponding sample taken from its surface is thus believed to reflect a minimum age for the deposition of the moraine (Photo: F.M. Hofmann, 22.8.2017).

The samples were prepared in the Laboratoire National des Nucléides Cosmogéniques in Aix-en-Provence (France) for subsequent accelerator mass spectrometry ^{10}Be measurements. The samples were first crushed and sieved. The grain size fraction between 0.25 and 1 mm was chosen for further analysis. The subsequent isolation of the quartz was performed in several steps. Magnetic grains were first removed with a magnetic Frantz© separator. For the next step, carbonates were removed with HCl 37% before subjecting the samples to 5 to 6 leaching steps with a mixture of two thirds H_2SiF_6 34% and one third HCl 37% to further remove unwanted minerals, such as felspars. Atmospheric ^{10}Be was removed during 3 subsequent leaching steps with HF 48%. In each step, roughly 10% of the quartz in each sample was dissolved. After the HF 48% leaching steps, the samples were spiked with 100 µl of a ^{9}Be carrier solution (3025 ± 9 µg ^{9}Be g^{-1}) and then completely dissolved using HF 48%. Chromatography on anionic and cationic exchange resins (DOWEX 1X8 and DOWEX 50WX8), as well as two precipitation stages enabled the separation and purification of beryllium. The final $Be(OH)_2$ precipitate was dried and oxidised at 700°C to obtain BeO.

The subsequent ^{10}Be measurements were performed at the Accélerateur pour les Sciences de la Terre, Environnement et Risques (ASTER) accelerator mass spectrometer (Arnold *et al.* 2013) at the CEREGE (Centre Européen de Recherche et d'Enseignement des Geosciences de l'Environnement) Research Centre in Aix-en-Provence (France). The measured ^{10}Be/^{9}Be ratios *(Appendix 3* and *4)* were normalised with respect to the in-house standard STD-11 using an assigned ^{10}Be/^{9}Be ratio of 1.191 ($\pm$ 0.013) $*$ 10^{-11} (Braucher *et al.* 2015) and the Be half-life of 1.387 $\pm$ 0.01 $*$ 10^{6} years (Chmeleff *et al.* 2010; Korschinek *et al.* 2010). The results of the ^{10}Be measurements are shown in the appendices *(Appendix 3* and *4)*

4.3.2.3 Determination of the exposure ages

In accordance with Chenet *et al.* (2016), four samples with an analytical error higher than 12% were excluded from further analysis. The ^{10}Be production rate was scaled to the recent physical position and topographical shielding of the boulders *(Appendix 1* and *2)*. Following Gosse and Phillips (2001), a sample density of 2.65 g cm^{-1} was assumed. Internal and external uncertainties were calculated according to equation 3 and 4.

Four different scenarios were applied for the determination of the exposure ages *(Appendix 5* and *6)*:

1. As the Arctic ^{10}Be production rate (3.93 ± 0.15 at ^{10}Be g^{-1} yr^{-1} at sea level and high latitudes, Young *et al.* 2013) has been commonly applied in studies about past glacier variability in the Alps (e.g. Schimmelpfennig *et al.* 2014; Chenet *et al.* 2016; Le Roy *et al.* 2017), it was chosen for the first scenario ('CRONUS Earth'). The exposure ages of the first scenario were determined using the CRONUS Earth calculator (Balco 2013). For the sake of comparability, the exposure ages were computed according to the common time-dependent 'Lm' cosmogenic nuclide production model (Lal 1991; Stone 2000). Neither erosion rates nor snow shielding were taken into account. The resulting exposure ages are only considered baseline values for a ready comparison with other studies, as the exposure ages are believed to be underestimated due to the lack of a snow shielding correction;
2. In their study of Late Glacial and Holocene glacier fluctuations in the upper Romanche valley *(Fig. 1)*, Chenet *et al.* (2016) took into account a snow shielding factor of 0.934 for the determination of ^{10}Be exposure ages of moraines due to their location in wind-sheltered positions on the valley bottom. The shielding factor corresponds to a snow cover of 0.5 m for six months. As the sampled boulders on the moraines in the upper Drac Blanc catchment are also located in relatively wind-sheltered locations and, specifically, the boulders on the moraines in the upper part of the Rougnoux valley had a thick snow cover during fieldwork in winter 2017 (F.M. Hofmann, pers. obs., 26.11.2017), a snow shielding factor of 0.934 was considered in the second scenario ('CRONUS Earth + snow'). Hence, the so-determined exposure ages with the CRONUS Earth calculator are directly comparable to the ^{10}Be exposure ages of Chenet *et al.* (2016);
3. A sensitivity test yielded on average 0.2 ka younger exposure ages than in the 'CRONUS Earth + snow' scenario when applying the only available regional ^{10}Be production rate of 4.16 ± 0.10 atoms ^{10}Be g^{-1} yr^{-1} from the Chironico landslide in southern Switzerland (Claude *et al.* 2014) instead. Due to a possible effect on the interpretation of the exposure ages, the exposure ages of the third scenario ('CREp') were computed with the ^{10}Be production rate of Claude *et al.* (2014) using the CREp programme (Martin *et al.* 2017). In the CREp calculator, the most recent parameters were chosen for the determination of the ^{10}Be exposure ages: the LSD cosmic ray model (Lifton *et al.* 2014), the ERA40 atmosphere (Uppala *et al.* 2005) and the Lifton-VDM2016 geomagnetic database (Lifton 2016) which takes past variations of the earth's magnetic field into account. Neither snow shielding or erosion was taken into account for the third scenario;
4. In addition to the third scenario, a snow shielding factor of 0.934 was taken into account for the exposure ages of the fourth scenario ('CREp + snow').

In most cases, multiple ^{10}Be exposure ages were available from each moraine. For the first step, reduced chi-squared statistics was applied to evaluate whether the variation of the exposure ages from the same landform can solely be attributed to analytical uncertainties (χ^2 close to 1) or if the scatter in the exposure ages originates from other sources (χ^2 considerably higher than 1), such as post-depositional exposure (Balco 2011). Reduced chi-squared (χ_R^2) can be determined as follows:

$$\chi_R{}^2 = \frac{1}{n-1} * \sum_{i=1}^{n} \left[\frac{t_i - t_{mean}}{\sigma t_i}\right] \qquad (5)$$

where t_i is the ^{10}Be exposure age, t_{mean} the average exposure age and σt_i the internal uncertainty of the exposure age (Balco 2011).

When χ_R^2 was ~1, the arithmetic mean of all exposure ages from the same moraine was considered the landform age, as averaging the exposure ages allows in that case for the elimination of the scatter due to measurement errors (Balco 2011). When equation 5 yielded a χ_R^2 value considerably higher than 1, the oldest ^{10}Be exposure age was chosen as the moraine age. This point of view is supported by Putkonen and Swanson (2003) who showed that the oldest exposure age from a boulder corresponds to ≥90% of the true age of a 20-100 ka-old, 10-20 m high moraine when four boulders are sampled for SE dating. Secondly, most samples for this study were collected from boulders with a height of less than 1.5 m. Such boulders are more susceptible to post-depositional exhumation and/or snow shielding and would thus yield 'too-young' exposure ages.

For the determination of the landform uncertainties, the methodology of Chenet *et al.* (2016) was adopted. It was assumed that each sample is part of a normal distribution defined by its exposure age and its uncertainty. A set of 1000 random derivates of the normal distribution of each sample was simulated using the R software. Subsequently, the sets were grouped according to the landforms and the standard deviation was empirically derived.

For the qualitative evaluation of the exposure ages in the discussion, stratigraphical relationships were taken into account. Indeed, significantly younger exposure ages from boulders on a moraine down-valley from a considerably older moraine were considered likely to be erroneous, as a glacier normally erodes all pre-existing moraines up to its front during an advance (Briner 2011). The ^{10}Be exposure age were interpreted with regard to the INTIMATE (INTegration of Ice-core, MArine and TErrestrial palaeoclimate records) event stratigraphy with the NGRIP (North Greenland Ice Core Project) ice cores as stratotype (Lowe and Walker 2015).

4.4 Equilibrium line altitude reconstructions

As mentioned above, not all moraines in the Prelles valley were sampled for ^{10}Be exposure dating. To be able to assign at least relative ages to the undated moraines in the Prelles valley, the ELA during moraine deposition was reconstructed. As mentioned above, the ELA corresponds to the zone of the glacier where the accumulation corresponds to the ablation on a yearly timescale (Ohmura *et al.* 1992). Subsequently, ELA changes (ΔELA) with respect to the ELA at the end of the LIA when the Alpine glaciers were last in equilibrium with the climate (Ivy-Ochs *et al.* 2008), were computed to finally make possible the establishment of stratigraphical correlations.

This method has, especially before the advent of SE dating, commonly been applied in studies of Late Glacial and Holocene glacier variability in the Alps, since the ELA depressions during the principal glacier advances after the LGM are nowadays well-known (Ivy-Ochs *et al.* 2008; Ivy-Ochs *et al.* 2009; Ivy-Ochs 2015). However, a recent study (Reitner *et al.* 2016) indicates that ΔELA-based stratigraphical correlations might yield erroneous results, especially when different sites across the Alps serve as references. Indeed, Reitner *et al.* (2016) challenged previous ΔELA-based stratigraphical correlations of moraines in the area around Lienz (Austrian Alps) and concluded that this approach should only be applied to nearby sites which are characterised by a similar bedrock lithology and topography. As these conditions are met in the Rougnoux and the Prelles valleys, ELA depression-based stratigraphical correlations are believed to be robust.

The ELA reconstructions for the LIA moraines as reference and the moraines further down-valley in the upper Drac Blanc catchment are based on the common Accumulation Area Ratio (AAR) method which is based on the assumption of a fixed ratio between the accumulation and the ablation zone of a glacier being in equilibrium with the climate (Bakke and Nesje 2011).

A proportion of 0.67 of the accumulation area is believed to be most appropriate for steady-state Alpine glaciers (Gross *et al.* 1977). The AAR method requires the extent and topography of a palaeoglacier to be known. The former glacier extent can be determined based on geomorphic evidence, such as moraines or trimlines. As in the southern Drac Blanc catchment, the landform record is mostly too fragmentary due to post-depositional erosion and incomplete deposition (Pellitero *et al.* 2016).

To overcome this issue, the available geomorphic evidence and basic principles of glacier motion can be combined to estimate the glacier's thickness. This method has been integrated in the GlaRe ArcGIS toolbox (Pellitero *et al.* 2016) which has been used as first ArcGIS toolbox in this study. It has to be assumed that the present-day topography corresponds to the surface of the former glacier bed and that the glacier was in a steady state with the climate (Pellitero *et al.* 2016). Based on the assumption of plastic ice flow, the surface elevation of a glacier *h* can be determined as follows:

$$h_{i+i} = h_i + \frac{\tau_{av}\,\Delta x}{F_i\,\rho g\,H_i} \qquad (6)$$

where τ_{av} is the basal shear stress [Pa], Δx the iteration length [m], *F* a shape factor (see equation 7), ρ the ice density (about 900 kg m^{-3}), *g* the acceleration due to gravity (9.81 ms^{-2}), *H* the glacier's thickness [m] and *i* corresponds to the number of the iteration. Equation 6 requires the basal shear stress as primary input (Pellitero *et al.* 2016).

The τ_{av} of a valley glacier varies usually between 50 and 150 kPa, whereas a basal shear stress of 190 kPa has been found to be appropriate for small cirque glaciers (Pellitero *et al.* 2016). As the τ_{av} of a palaeoglaciers is in most cases unknown, (Pellitero *et al.* 2016) suggest adjusting the standard value of 100 kPa to the geomorphic evidence. The bedrock conditions are not taken into account by the GlaRe toolbox (Pellitero *et al.* 2016). As the flow of topographically constrained glaciers is strongly influenced by lateral drag, the shape factor *F* can be determined as follows to refine the ice thickness reconstructions:

$$F = \frac{A}{Hp} \qquad (7)$$

A is the cross-section area at a given point, *H* the ice thickness and *p* the length of the ice-bed interface. Equation 7 relies on the assumption that the driving stress at the central flowline corresponds to the basal shear stress (Pellitero *et al.* 2016).

For the determination of the ELA during the deposition of the moraines in the upper Drac Blanc catchment, DEMs of the palaeoglaciers were first established. The headwalls with a slope angle >60° were left ice-free following Moran *et al.* (2016).

According to the most recent inventory of the glaciers in the French Alps (Gardent 2014), no glacier existed at the end of the LIA in the Prelles valley. Considering that a sequence of fresh moraines can be found in the uppermost part of the valley (see section 5.1.2.2), the moraines must have been shaped during quite recent glacier advances. Therefore, it was assumed that the outermost of these moraines were deposited during the furthest LIA glacier advance. Glacier flowlines were first digitised and interval nodes with a spacing of 25 m were subsequently created using the interval nodes tool in the GlaRe toolbox. Given the location of the assumed LIA glacier in a cirque, a shear stress of 190 kPa was considered appropriate for the determination of the ice surface elevation at the interval nodes. The resulting ice thickness was subsequently interpolated to the assumed LIA extent based on Inverse Distance Weighting (IDW).

Due to the presence of a permanent snow patch inside the LIA moraines in the Rougnoux valley, the bed elevation from ice surface tool in the GlaRe toolbox was first applied to reconstruct the elevation of the glacier bed along four main flowlines. The ice thickness at interval nodes with a spacing of 25 m was then computed assuming a basal shear stress of 190 kPa. The ice surface elevation was lastly interpolated to the LIA glacier extent (Di Costanzo and Hofmann 2016) using IDW.

For the reconstruction of the ELA during the deposition of the moraines further down the Prelles valley, flowlines were first digitised and interval nodes with a spacing of 50 m were created. As suggested by Pellitero *et al.* (2016), the shear stress for the calculation of the glacier's thickness was tuned to fit the moraines. Accordingly, the shear stress was set to 50 kPa near the former glacier front and for the rest of the glacier, the default shear stress of 100 kPa was used. Based on IDW, the ice surface elevation was ultimately interpolated to the whole glacier extent.

Considering the strongly asymmetrical shape of the upper part of the Rougnoux valley, the standard workflow described in Pellitero *et al.* (2016) was modified for the reconstruction of the glacier surface during the deposition of the moraines outside the LIA moraines. Indeed, interval nodes with a distance of 50 m were created along the main flowlines of the former glacier. Subsequently, the default shear stress of 100 kPa was used for the reconstruction of the ice thickness. Shape factors (Equation 7) were derived from manually created cross-sections and the ice thickness was subsequently corrected. Considering that the glacier extent during the deposition of the moraines outside the LIA extent can be well constrained, nodes within a distance of 25 m were created along the glacier extent and the ice thickness was subsequently set to zero. The ice surface elevation at the interval nodes derived from the flowlines and at the nodes on the glacier margin was finally interpolated to the whole glacier extent with IDW.

Given the location of the moraine near the Pré de la Chaumette mountain cabin near the confluence of the de la Pierre and the Rougnoux valleys, two different scenarios were performed: (I) built-up of the moraine by the Rougnoux glacier, (II) deposition of the landform by the confluent Veyrardonne, De la Pierre and Rougnoux glaciers. For both scenarios, interval nodes with a spacing of 50 m were created along the main flowlines and the shear stress was set to 100 kPa for the subsequent ice thickness calculation. The ice surface elevation was then interpolated to the whole glacier extent using IDW. See *Fig. 9* for the flowlines and the interval nodes which have been created for the establishment of the DEM of the palaeoglacier in the Rougnoux valley during the deposition of the frontal moraine near the Pré de la Chaumette mountain cabin. To be able to compute ΔELA for scenario 2, DEMs of the LIA ice surface elevation of the Veyrardonne and the de la Pierre glacier were derived. For the LIA extent of both glaciers, the glacier inventory of Gardent (2014) served as reference. Due to the presence of ice in the cirque of the Veyrardonne glacier, the bed elevation from ice surface tool was first applied for the reconstruction of the glacier bed. The ice thickness along the main flowlines of both glaciers was subsequently computed based on a shear stress of 190 kPa and finally interpolated with IDW to the whole glacier surface.

The corresponding ELAs for the moraines in the study area were computed with a second ArcGIS toolbox (Pellitero *et al.* 2015). The DEMs established with the GlaRe toolbox (Pellitero *et al.* 2016) served as input. The contour line interval was set to 10 m resulting in an uncertainty of 5 m of the so-determined ELA, as the error of the determined ELA is half of the contour line interval (Pellitero *et al.* 2015).

For the scenario that the moraine near the Pré de la Chaumette mountain cabin was deposited by the confluent Veyrardonne, De la Pierre and Rougnoux glacier, separate ELA depressions were computed for the Veyrardonne/De la Pierre and the Rougnoux glacier.

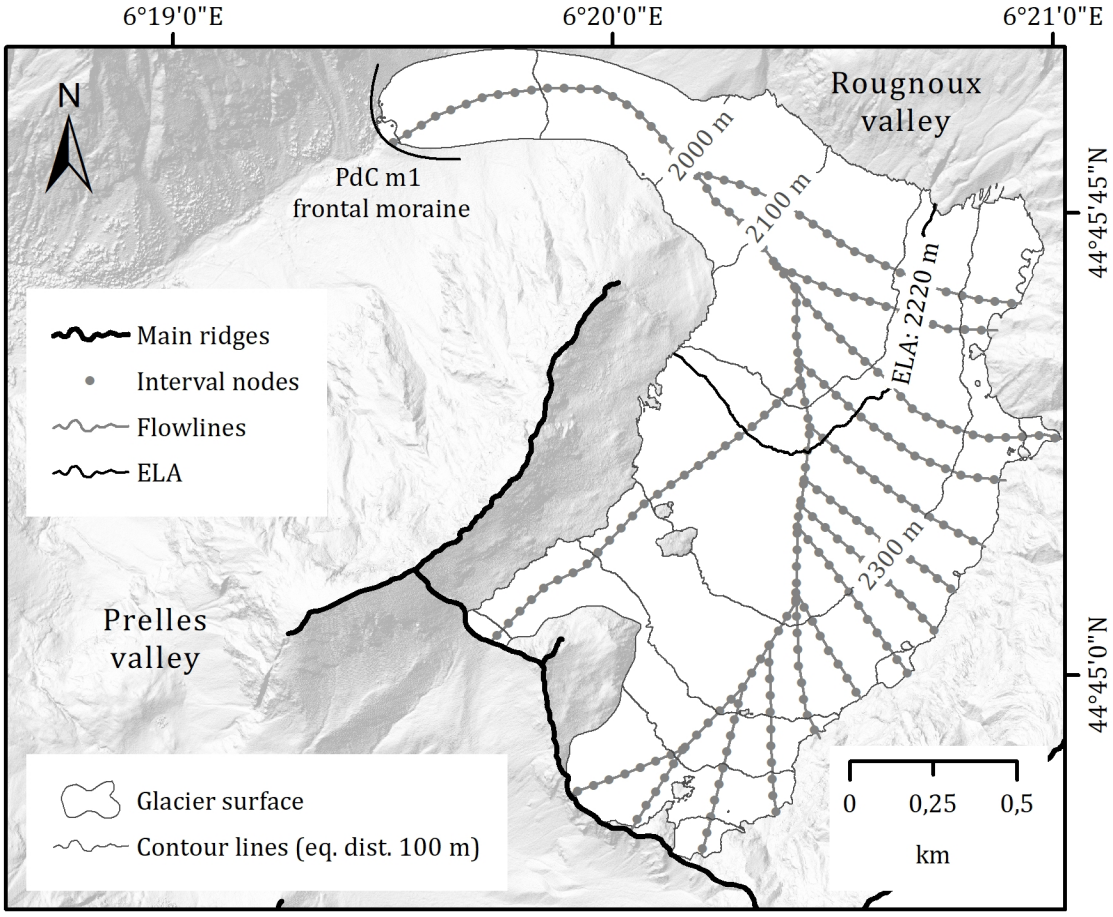

Date: 28.6.2018; Author: Felix Martin Hofmann; Data source: IGN 2012; Coordinate system: WGS 1984 UTM zone 32N

Fig. 9. ELA during the deposition of the PdC m1 frontal moraine. The interval nodes were created along the main flowlines of the palaeoglacier with a spacing of 50 m. The default shear stress of 100 kPa was assigned to the interval nodes (Pellitero *et al.* 2016). The ice thickness at the interval nodes was determined using equation 6. IDW allowed for the surface elevation at the interval nodes to be interpolated to the whole glacier surface. The ArcGIS tollbox of Pellitero *et al.* (2015) enabled the determination of the ELA assuming an AAR of 0.67.

5 RESULTS

In the first subchapter, the different landforms in the Rougnoux valley, in the Prelles valley and in the area around the Pré de la Chaumette mountain cabin are described and interpreted. The 42 ^{10}Be new exposure ages and corresponding landform ages are presented in the following subchapter. The results of the ELA reconstructions can be found in the third subchapter.

5.1 Geomorphological mapping

The geomorphological maps of the three mapped areas can be found in the appendices *(Appendix 10, 11* and *12)*. Thus, they can easily be compared to the description and the interpretation of the geomorphological units in the following three subsections.

The first three letters of the landform names refer to their locality (e.g. VdR stands for 'Rougnoux valley'). The number after the letter 'm' for 'moraine' simply refers to the order in which the moraines have been sampled and has thus no chronological implication.

5.1.1 Moraines in the Rougnoux valley

Most of the glacial landforms in the Rougnoux valley have already been described. In summary, six well-preserved lateral moraines in the upper part of the valley at an elevation of about 2100 m a.s.l., as well as multiple latero-frontal moraines up to the entrance of the valley were identified. See Di Costanzo and Hofmann (2016), as well as Hofmann (2016) for further details. Therefore, only relevant updates of the previous geomorphological map are presented in the following paragraphs.

Description. – Uphill from the lateral moraine VdR m1, which has been described in the aforementioned publications, two elongated ridges can be observed: the first is located slightly uphill from moraine VdR m1, whereas the second is situated at a significantly higher elevation *(Fig. 10* and *11)*. Both ridges are roughly parallel to the lateral moraines downhill. The ridge slightly uphill from moraine VdR m1 emerges in a north-westerly direction from the slope downhill of the upper ridge and change subsequently its direction to the north *(Fig. 10* and *11)*. Both ridges are characterised by an asymmetric profile, as their eastern flanks are considerably steeper than the western counterparts. Both ridges are covered by a denser vegetation compared to the surrounding slope *(Fig. 10)*. South of the uppermost ridge, a distinct shift in slope angle can be observed *(Fig. 10)*. On the steeper part of the slope below, polished bedrock is exposed.

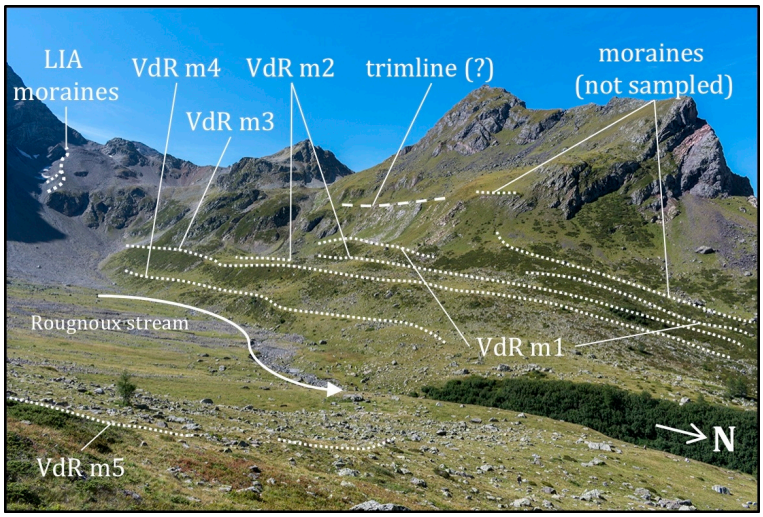

Fig. 10. Moraines (dotted lines) on the western side of the Rougnoux stream viewed from the lateral moraine VdR m5. The two lateral moraines uphill from moraine VdR m1 can be differentiated from the surrounding slope by a denser vegetation cover. Note the LIA moraines of the Rougnoux glacier in the background. See *appendix 9* for the location from which the photo was taken (Photo: F.M. Hofmann, 23.8.2017).

Thanks to the high-resolution DEM and new field evidence, two subtle, elongated ridges were identified uphill from the previously mapped latero-frontal moraine VdR m9 *(Fig. 11* and *12)*. The north-eastern flank of both ridges is considerably steeper than their almost horizontal south-western side. An arch-shaped ridge (VdR m8) can be found downhill from moraine VdR m9. It consists entirely of very angular, wedged boulders with a diameter up to 4 m *(Fig. 12)*. No finer matrix can be observed between the boulders. Hence, the sediments of the VdR m8 ridge can be described clast-supported. According to a lithological assessment during the fieldwork campaign in August 2017, only sandstone boulders were identified on its surface.

North of the lateral moraine VdR m5, a two-crested ridge (VdR m6) can be observed *(Fig. 11* and *13)*. Its southern and northern end are eroded by a stream and a gully, respectively. The slope of its south-west facing sides can be described as gentler than their north-eastern counterparts.

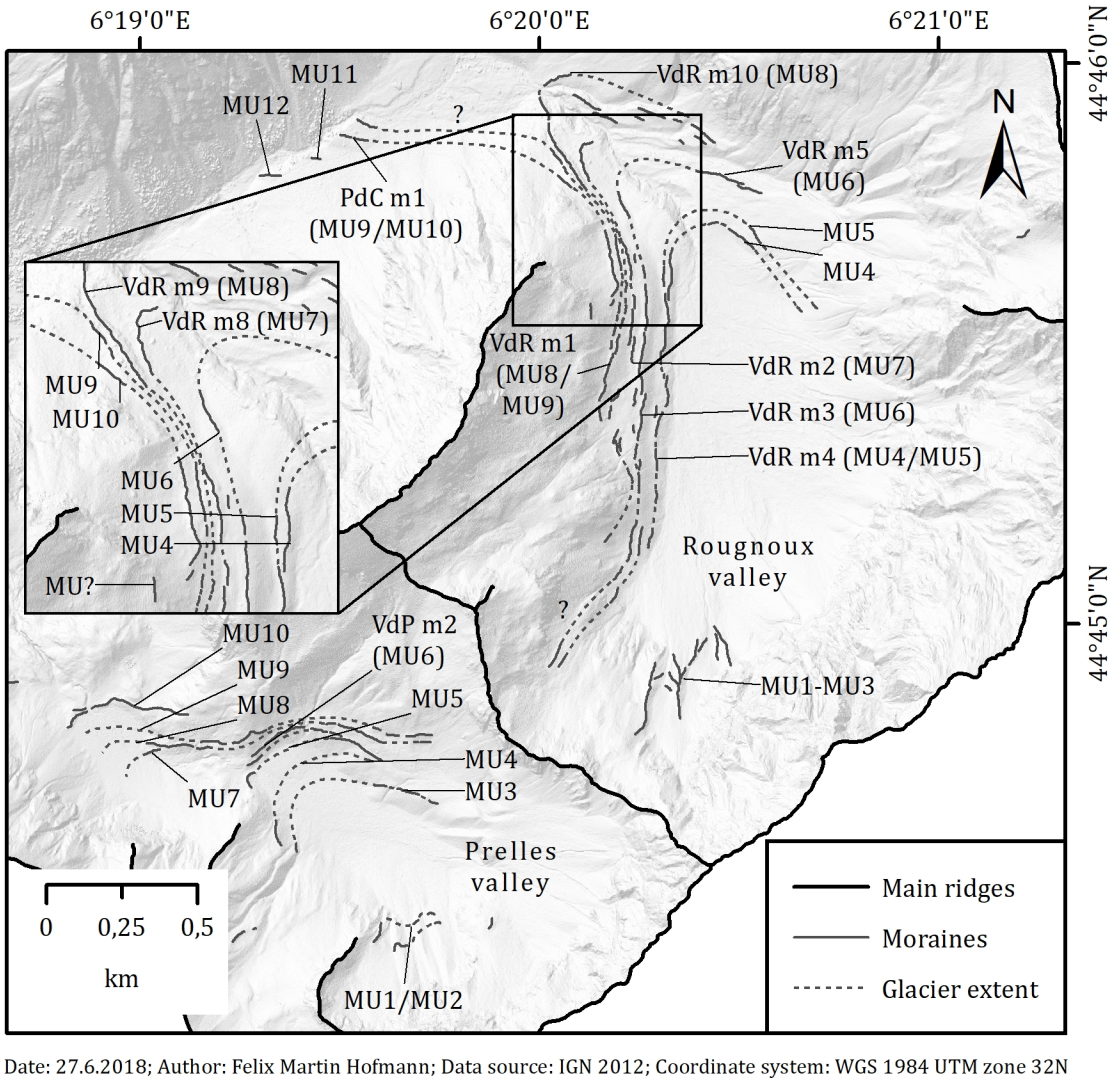

Fig. 11. Moraines and Morphostratigraphical Units (MU) in the southern part of the upper Drac Blanc catchment. Possible correspondencies are marked with question marks.

At the southern tip of the VdR m6 ridge, a matrix-supported diamict is exposed *(Fig. 13)*. Another short, subdued ridge can be found downhill of the VdR m6 ridge *(Fig. 13).* North of the gully, a prominent two-crested ridge can be observed. Its northern tip has partially been eroded by a stream. In contrast to the upper one, its lower crest can be described as subtle *(Fig. 13)*. A steep south-west facing side and a gentle north-eastern slope characterise a ridge (VdR m7) further downhill. Another ridge with a similar orientation can be observed north-west of the ridge VdR m7. At the entrance of the Rougnoux valley, a very subtle, arcuate crest (VdR m10) emerges from the talus slope on the eastern side of the Rougnoux stream *(Fig. 11)*. In contrast to its northern flank, the southward facing side of this ridge can be characterised as steep. The angle between the valley bottom and the crest is about 45° *(Fig. 11)*.

Interpretation. – The asymmetrical shape of the two ridges uphill from the VdR m1 moraine, which resembles that of the four lateral moraines downhill *(Fig. 10)*, as well as the fact that crests parallel the valley bottom and therefore former ice flow direction suggest that both ridges can be classified as lateral moraines. The denser vegetation cover on both ridges might be explained by the occurrence of finer sediments compared to the surrounding slope. The distinct change in the slope angle south of the uppermost lateral moraine is considered to be a trimline *(Fig. 10)*.

The exposure of polished bedrock below this distinct shift in slope angle supports this interpretation. According to a geological map of the area (Debelmas *et al.* 1980), the marked change in slope angle coincides with a boundary between gneisses on the steeper portion of the slope and spilites further uphill. Alternatively, the change in inclination might thus reflect their differential resistance to weathering and erosion. However, the location of a lateral moraine at a similar elevation nearby supports the trimline interpretation.

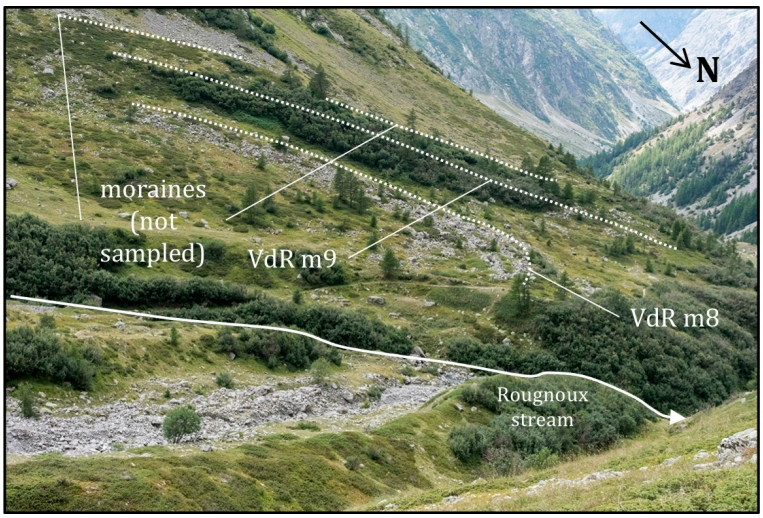

Fig. 12. Moraines (dotted lines) in the lower part of the Rougnoux valley viewed from the VdR m7 moraine. Note the arcuate form of the dump moraine VdR m8 on the western side of the Rougnoux stream. The two moraines uphill can be easily identified by their denser vegetation cover. See *appendix 9* for the location from which the photo was taken (Photo: F.M. Hofmann, 23.8.2017).

Considering the similar shape to that of the lateral moraine VdR m9, the two ridges slightly uphill can be interpreted as lateral moraines. Given the angularity of the boulders which form the arcuate ridge (VdR m8) downhill from moraine VdR m9, it can be assumed that the boulders were supraglacially transported.

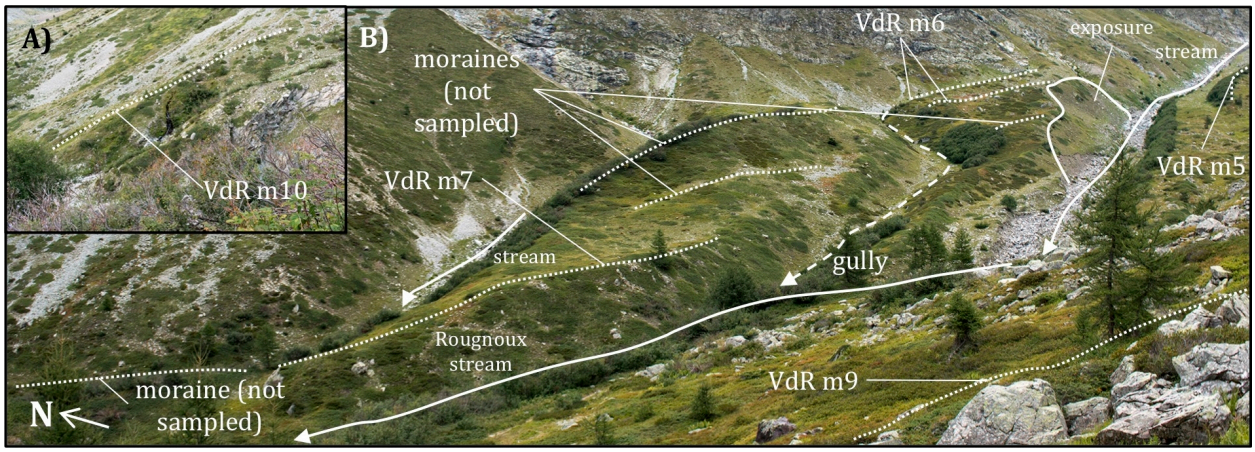

Fig. 13. Moraines (dotted lines) on the north-eastern side of the Rougnoux stream viewed from the latero-frontal moraine VdR m9. A) The latero-frontal moraine at the entrance of the Rougnoux valley. A large part of the moraine is covered by scree of graviational origin. B) Between a stream and a gully, a two-crested lateral moraine (VdR m6) and smooth crest further downhill can be observed. A matrix-supported diamict is exposed at the southern tip of the lateral moraine VdR m6. Four lateral moraines can be found north of the gully. All lateral moraines except the lateral moraine VdR m5 parallel the valley bottom and therefore former ice flow; See *appendix 9* for the location from which the photos were taken (Photos: F.M. Hofmann, 24.8.2017).

The boulders originate most likely from discrete rockfalls from the escarpment in the south-eastern part of the Rougnoux valley, as this is the only area in the Rougnoux valley where sandstones are exposed. Considering that the boulders form a discrete ridge and do not spread not over a large area *(Fig. 12)*, VdR m8 can tentatively be classified as dump moraine.

According to Bennett and Glasser (2009), a halt in glacier recession or a stationary ice margin, high ice velocities, as well as a steep ice front favour the development of dump moraines. Therefore, it can be assumed that moraine VdR m8 was deposited during a stationary phase of the former Rougnoux glacier when the supraglacially transported boulders accumulated in front of its margin. Given its asymmetrical profile, the exposure of a diamict at its southern end and the orientation parallel to the valley bottom, the VdR m6 ridge can be interpreted as lateral moraine. The overall similar morphology indicates that all ridges north of the gully including the ridge VdR m7 can be classified as lateral moraines. Based on an angle of about 45° between the crest and the valley bottom, VdR m10 is hereinafter referred to as latero-frontal moraine.

Morphostratigraphical interpretation. – The uppermost lateral moraine on the western side of the Rougnoux stream can be considered the oldest moraine in the Rougnoux valley, as it can be inferred that the ice of the Rougnoux glacier was thickest during its deposition *(Fig. 11)*. Due to its association to the trimline, it can be assumed that the lateral moraine was probably shaped during the LGM. The lateral moraine slightly uphill from the lateral moraine VdR m1 can be considered the second oldest landform *(Fig. 11)*, whereas the lateral moraine VdR m4 represents the youngest landform outside the LIA moraines on the western side of the Rougnoux stream *(Fig. 11)*. Thus, this moraine can be assigned to the Morphostratigraphical Unit (MU) 4. Due to their position at a higher elevation, the moraines uphill from the lateral moraine VdR m9 must be older than the VdR m9 moraine. As the latero-frontal moraine VdR m9 terminates at the entrance of the Rougnoux valley, the glacier front must have been advanced further during the deposition of the two lateral moraine fragments uphill. Therefore, the two lateral moraines might be correlated with the frontal moraine complex down-valley from the Pré de la Chaumette mountain cabin (MU9/MU10, *Fig. 11)*.

Considering its location furthest down-valley, the latero-frontal moraine VdR m10 can be considered to be the oldest moraine on the eastern side of the Rougnoux stream. Since its western tip is located close to the northern limit of the latero-frontal moraine VdR m9, it can be assumed that both landforms were simultaneously deposited. They can thus be assigned to the same morphostratigraphical unit (MU8, *Fig. 11)*. Considering that the moraines between the latero-frontal moraine VdR m10 and the lateral moraine VdR m5 have been affected by substantial reworking since their deposition *(Fig. 13)*, stratigraphical correlations prove difficult. For instance, whether the two-crested lateral moraine uphill from moraine VdR m7 can be correlated with the two crests of the lateral moraine VdR m6 remains an open question.

5.1.2 Glacial landforms in the Prelles valley

A transversal ridge associated with a narrowing of valley profile divides the Prelles valley into a higher and a lower part *(Fig. 14* and *15)*. In the first subsection, this landform is described and interpreted. The following subsection focuses on the moraines on each side of the transversal ridge.

5.1.2.1 Transversal ridge

Description. – Down-valley from a gently sloping area in the upper part of the Prelles valley, a roughly 20 m high ridge can be observed. The ridge is oriented perpendicular to the valley bottom. It exhibits an asymmetric profile, as its up-valley facing side is considerably steeper than its down-valley facing flank (*Fig. 14* and *15)*. The up-valley facing side of the ridge is covered by boulders and finer sediments, whereas bedrock is exposed on its down-valley facing flank. The surface of the up-valley facing flank of the ridge can be described as smooth, whereas the down-valley facing side is characterised by a rugged surface.

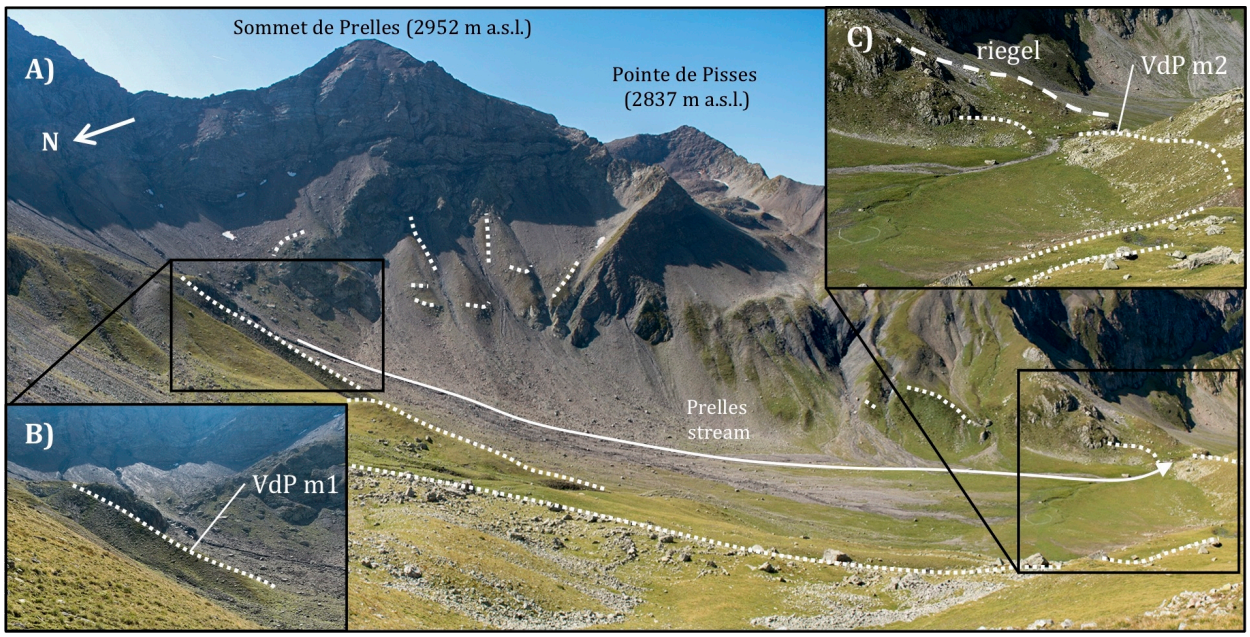

Fig. 14. Moraines (dotted lines) in the upper part of the Prelles valley. A) Panorama of the upper Prelles valley viewed from the Cheval de Bois pass *(Fig. 2)*. Small, unvegetated ridges can be observed downhill from the Sommet de Prelles. Note the two arcuate latero-frontal moraines in the foreground. Three latero-frontal moraines can be observed south of the Prelles stream. B) The sparsely vegetated, sharp crested ridge VdP m1 downhill from an escarpment. C) The prominent latero-frontal moraine VdP m2 north of the Prelles stream. Another latero-frontal moraine, as well as a transversal ridge (riegel) can be observed south of the Prelles stream (Photos: F.M. Hofmann, 25.8.2017).

Interpretation. – The smooth surface on the up-valley facing side can probably explained by subglacial abrasion of pre-existing bedrock. The rugged relief on the down-valley facing side is probably due to plucking. Given that the ridge is oriented almost perpendicular to the valley bottom and associated with a narrowing of the valley profile, the transversal ridge can be interpreted as a riegel. Given its lower elevation than the ridge, the area directly east of the ridge can be considered to be an overdeepening *(Fig. 14)*. The formation of the riegel and the overdeepening was probably promoted by the presence of different bedrock types in the transitional zone between the lower and the upper part of the Prelles valley. Indeed, the riegel is made up of spilites in contrast to the area further up-valley, where limestones and sandstones are exposed (Debelmas *et al.* 1980). Thus, it can be assumed that the limestones and the sandstones up-valley from the riegel were more readily removed than the spilites.

5.1.2.2 Moraines in the Prelles valley

Description. – Downhill from the Sommet de Prelles, a sequence of relatively small ridges can be found *(Fig. 14)*. The ridges are composed of boulders of various sizes and covered by sparse pioneering plants in contrast to the surrounding areas. According to the DEM, the subtle ridges are characterised by an asymmetrical profile. A sharp-crested ridge (VdP m1) can be observed downhill from an escarpment on the northern side of the Prelles stream *(Fig. 14)*. Both flanks of the ridge are covered by pioneering plants. The ridge itself consists of angular to sub-rounded boulders residing in a sandy matrix. The profile of the ridge can be described as slightly asymmetric considering that the southward facing side is slightly steeper than its northern counterpart. North-west of the ridge VdP m1, four well-preserved arcuate ridges including VdP m2 can be found *(Fig. 11)*. They can be differentiated from the ridges downhill of the Sommet de Prelles, as well as from the ridge VdP m1 by their significantly denser vegetation cover *(Fig. 14)*.

The arcuate ridges exhibit an asymmetric profile, as their south-facing sides are considerably steeper than their northern flanks. Their crests can be described as smooth *(Fig. 14)*. The ridges are divided into segments by four gullies. Around the four gullies, a matrix-supported diamict is exposed. The easternmost of the four ridges is partly overlaid by a vegetation-covered alluvial fan. North-east of the arcuate ridges, small east-west oriented ridges can be observed. Like the arcuate ridges further downhill, they exhibit an asymmetric profile given their steeper south-facing sides. The easternmost two ridges are partly overlain by an alluvial fan. On the southern side of the Prelles stream, four arcuate ridges can be observed. Their eastward facing slopes are significantly steeper than their western flanks. Four ridges can be found north-west of the riegel *(Fig. 11)*. The ridges parallel the valley bottom and exhibit a strongly asymmetric profile, as their south-facing sides are considerably steeper than their northern flanks. The tips of the two westernmost ridges turn towards the Prelles stream. South of the Prelles lake, a prominent, arc-shaped ridge can be observed. The ridge is divided by the Prelles stream in two parts *(Fig. 11* and *15)*.

Fig. 15. Moraines (dotted lines) in the lower part of the Prelles valley. A) Moraines in the lower part of the Prelles valley viewed from the Prelles lake. The large latero-frontal moraine can be seen in the foreground. The part of the latero-frontal moraine on the south-western side of the Prelles stream features two crests. Another latero-frontal moraine, as well as the riegel can be seen in the background. B) The well-preserved latero-frontal moraine south of the Prelles lake viewed from the south-east. Note the considerably steeper southward-facing side of the moraine. North-west of the latero-frontal moraine, a ridge with an assymetric profil can be observed. Due to its profile, it is considered a moraine. See *appendix 7* for the locations from which the photos were taken (Photos: F.M. Hofmann, 25.8.2017).

The eastern part emerges from the slope north of the four previously described ridges and subsequently changes its orientation to the south-west. Both parts of the arcuate ridge consist predominantly of very angular boulders *(Fig. 15)*. The part west of the Prelles stream can be differentiated from its eastern counterpart, as it features two distinct crests *(Fig. 15)*. The southward facing slope of the arc-shaped ridge is steeper than its northern flank. Three north-south oriented, smooth ridges can be observed south-east of the Prelles lake *(Appendix 12)*. North-west of the large arc-shaped ridge, an asymmetrical ridge can be found *(Fig. 15)*.

Interpretation. – The sparsely vegetated ridges downhill from the Sommet de Prelles are thought to be moraines based on their asymmetrical profile.

Given their non-symmetrical profile and the exposure of a diamict around the gullies, the four arcuate ridges north-west of the VdP m1 ridge are hereinafter considered latero-frontal moraines. Based on their orientation perpendicular to the slope, the four ridges at a higher elevation northeast of the latero-frontal moraines are interpreted as lateral moraines.

An explicit interpretation of the ridge VdP m1 proves difficult. The fact that its sediments resemble macroscopically those of the four latero-frontal moraines further down-valley and the similar orientation compared to the easternmost latero-frontal moraine suggest classification as a latero-frontal moraine. However, three arguments contradict this hypothesis. Firstly, the ridge is located directly down-valley from an escarpment. Under such circumstances, moraine deposition should be unlikely. Secondly, the presence of debris flows and alluvial fans around the VdP m1 ridge indicates that this area has substantially modified by fluvial reworking after the retreat of the ice. Under such circumstances, a good preservation of glacial landforms consisting of sediments seems rather unlikely. Thirdly, the VdP m1 ridge exhibits a sharp crest in contrast to the arcuate ridges further down-valley. Based on this reasoning, the ridge VdP m1 is cautiously mapped a fluvial deposit in the geomorphological map *(Appendix 11)*. A grain size analysis could help to evaluate if the ridge VdP is a fluvial landform or a glacial deposit. To be interpreted as a fluvial landform, its sediments would have had to exhibit at least some degree of sorting and finer grain sizes would have had to have been washed away. Based on the asymmetrical shape that resembles that of the arc-shaped ridges on the right-hand side of the Prelles stream, the three arcuate ridges on the left-hand side of the Prelles stream are interpreted as latero-frontal moraines.

Considering their asymmetric profiles and their orientation parallel to the valley bottom, the easternmost two ridges in the lower part of the Prelles valley are classified as lateral moraine fragments. Based on the fact that the ends of the two westernmost ridges turn towards the valley bottom, they are hereinafter referred to as latero-frontal moraines. The prominent ridge south of the Prelles lake *(Fig. 11* and *15)* is thought to be a latero-frontal moraine. The presence of two crests on the part west of the Prelles lake, as well as the large volume indicate that the latero-frontal moraine was shaped during an important glacier advance. It cannot be excluded that it was reached during several glacier pulses. The subtle ridges south-east of the Prelles lake are believed to be eroded moraines, as indicated by their smooth surface. The peculiar shape of the ridge north-west of the prominent latero-frontal moraine hampers an explicit interpretation. Due to its asymmetrical profile, the ridge north-west of the large latero-frontal moraine is tentatively considered as lateral moraine *(Fig. 15)*.

Morphostratigraphical interpretation. – Based on their freshness, the moraines in the uppermost part of the Prelles valley are attributed to LIA advances. As this hypothesis relies solely on their location in the glacial cirque in the upper part of the Prelles valley, the ridges should be dated in a future study. Considering its location close to the riegel furthest down-valley, the latero-frontal moraine VdP m2 is probably the oldest moraine in the upper part of the Prelles valley (MU6). As the lateral moraine fragments and latero-frontal moraines on the right-hand side of the Prelles stream imply a location of the glacier front south-east of the spectacular latero-frontal moraine near the Prelles lake (MU10, *Fig. 11)*, they can be assigned to be younger morphostratigraphical units (MU7-MU9, *Fig. 11)*. Given their location furthest-down-valley, the eroded moraines south-east of the Prelles lake are believed to be older than the large latero-frontal moraine.

5.1.3 Pré de la Chaumette

Despite substantial reworking since their deposition, glaciofluvial deposits and moraines are preserved around the Pré de la Chaumette mountain cabin *(Fig. 16* and *17)*.

5.1.3.1 Pré de la Chaumette moraines

Description. – A two-crested ridge (PdC m1) which is almost perpendicular to the Drac Blanc, can be observed southwest of the Pré de la Chaumette mountain cabin *(Appendix 10, Fig. 16* and *17)*. The north-eastern sides of both crests can be described as slightly steeper than the south-west facing flanks. Near the Drac Blanc, a blocky, matrix-supported diamict is exposed *(Fig. 16)*. Except for the area around the mountain hut between the two crests, numerous, well-embedded boulders with a height up to 4 m can be found on the south-western part of the ridge *(Fig. 16)*. A small gravel road to the mountain hut divides the south-western crest of the ridge in two parts. On the right-hand side of the Drac Blanc, a smooth ridge can be observed. Its southern tip has been eroded by the Drac Blanc. The position of its south-eastern end corresponds roughly to the north-western limit of the north-eastern crest of the PdC m1 ridge. Two additional, east-west oriented ridges can be observed down-valley from the two-crested ridge PdC m1 *(Appendix 10* and *Fig. 11)*. Their western tips have been eroded by the Drac Blanc. Their eastern ends intertwine with sediments of alluvial and gravitational origin. Due to the vegetation cover, the sediments on their western ends are hardly visible from right-hand side of the Drac Blanc.

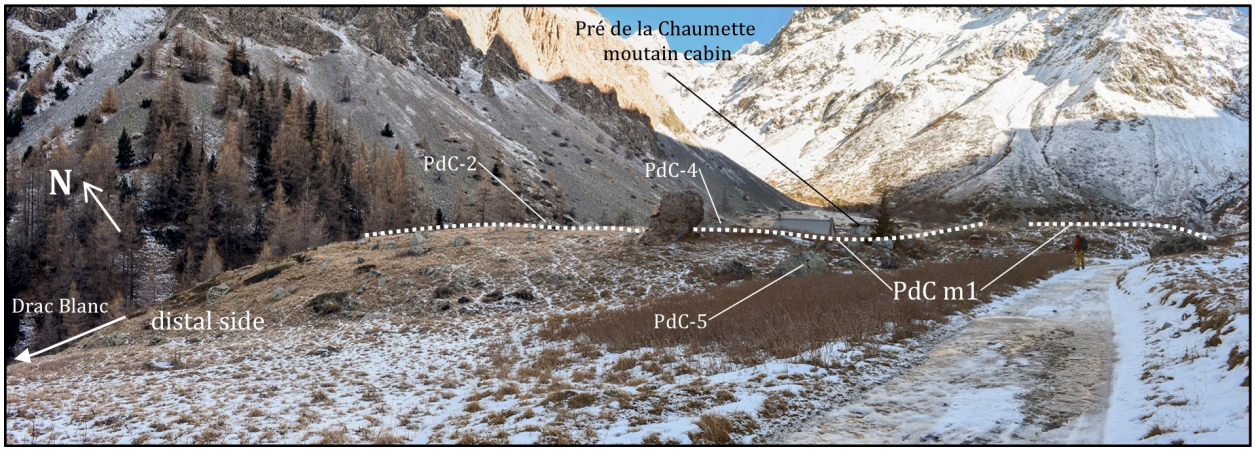

Fig. 16. Distal side of the south-western crest of the frontal moraine PdC m1. See the person in the right part of the photo for scale. Three samples for ^{10}Be exposure dating (PdC-1, PdC-2 and PdC-4) were taken from boulders close to the smooth moraine crest, whereas sample PdC-5 was obtained from a boulder at the end of the distal side. The large boulder in the centre of the photo consists of a carbonate-rich conglomerate and was thus not sampled for ^{10}Be exposure dating. See *appendix 8* for the locations from which the photo was taken (Photo: F.M. Hofmann, 26.11.2017).

Interpretation. – Based on the exposure of a diamict near the Drac Blanc and the slightly non-symmetrical profile (Bennett and Glasser 2009), the two-crested ridge PdC m1 is interpreted as a frontal moraine. A more precise genetical interpretation would have required additional sedimentological investigations. Given the very smooth morphometry of the frontal moraine, it can be assumed that the moraine was affected by substantial degradation after its deposition. It is likely that the morphology of the moraine might have been considerably modified by the construction of the mountain hut and the corresponding gravel road. As the north-western tip of the inner crest of the frontal moraine corresponds to the southern end of the eroded ridge on the right-hand side of the Drac Blanc, both landforms can presumably be correlated.

Due to the large volume of the frontal moraine PdC m1 and the presence of two crests, it can be assumed that the frontal moraine was built up during an important glacier advance. It is likely that it has even been reached during several glacier advances. Based on their similar morphometry, the two eroded ridges further down-valley are considered remnants of latero-frontal moraines. Considering their significantly smaller volume, the subtle ridges further down-valley might have been formed during minor ice advances or a temporary halt in glacier recession.

Morphostratigraphical interpretation. – Given their location further down-valley from the frontal moraine PdC m1, the two latero-frontal moraines must be stratigraphically older than the frontal moraine complex PdC m1. Based on its location further down-valley, the frontal moraine PdC m1 must be older than the moraines in the Rougnoux valley (MU9 and MU10, *Fig. 11)*.

5.1.3.2 Glacio-fluvial deposits

Description. – The plateau around the Pré de la Chaumette mountain cabin exhibits an uneven surface. However, its overall strike and dip can be considered as fairly constant. About 1-2 m deep, nowadays dry channels divide the area south-west and west of the mountain cabin into small, bar-shaped plateaus *(Fig. 17)*. Some sparse boulders, which are poorly embedded in the finer sediments, occur around the mountain cabin. Sediments composed of sand, as well as pebbles and cobbles exhibiting various degrees of rounding are exposed in very few unvegetated areas. The deposits southeast of the mountain cabin, as well as those at the entrance of the Rougnoux valley are separated by an about 5 m high slopes from the topographically lower area around the Drac Blanc and the Rougnoux stream. The sediments at the entrance of the Rougnoux valley differ from those around the mountain cabin, as they consist almost entirely of sub-angular to well-rounded pebbles, cobbles and boulders.

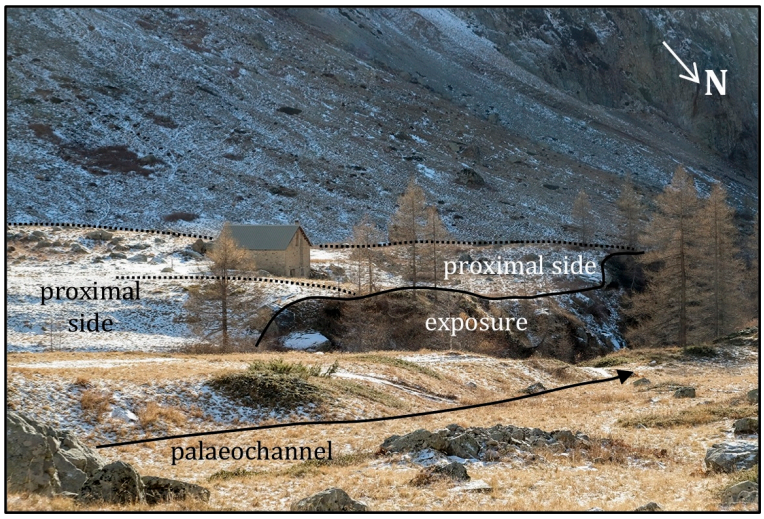

Fig. 17. Proximal side of the PdC m1 moraine complex taken from the glacio-fluvial deposit south of the Pré de la Chaumette mountain cabin. The crests of the frontal moraine (dotted lines) on each side of the small mountain hut are smooth and indicate intense post-depositional degradation. Note that only few boulders are exposed on the ridge up-valley from the mountain hut. Near the Drac Blanc, a matrix-supported diamict is exposed. Note the roughly 2 m deep palaeochannel in the foreground. (Photo: M. Le Roy, 26.11.2017).

Interpretation. – The presence of palaeochannels *(Fig. 17)* and bar-shaped plateaus around the mountain cabin imply a deposition of the sediments by flowing water. Biju-Duval (1975) classified the plateau around the mountain cabin as a fluvial terrace. However, the overall constant strike and dip, as well as the presence of numerous palaeochannels on its surface imply that the plateau was not deposited by a single river, but rather by a braided river network. As such an environment can typically be found in a proglacial setting (Bennett and Glasser 2009), the area around the mountain cabin should accordingly be interpreted as a glacio-fluvial deposit. Considering its up-valley location from the frontal moraine PdC m1, the plateau must be stratigraphically younger, as any pre-existing sediments were probably reworked during the ice advance up to the frontal moraine.

The lack of kettle holes on the surface around the mountain cabin might indicate that that the melt-out of any buried ice came to an end before the outwash surface was finally abandoned (Bennett and Glasser 2009). Given the coarse grain size of the sediments, it cannot be ruled out that the plateau at the entrance of the Rougnoux valley is an older fluvial terrace which formed during a phase of higher water supply than today. In any case, the slope southeast of the Pré de la Chaumette mountain cabin, as well as around the plateau at the entrance of the Rougnoux valley point towards a later phase of fluvial incision. The poorly embedded boulders around the Pré de la Chaumette mountain cabin can be linked to rock falls from the escarpment further northwards and would thus not directly date a glacial event.

5.2 ^{10}Be exposure ages

The ^{10}Be exposure ages were computed in ka (kiloyears before ~ AD 2000). If not otherwise stated, the exposure ages in the following three subchapters refer to the 'CREp + snow' scenario. Detailed information about the ^{10}Be measurements, as well as the exposure ages according to the other scenarios can be found in in the appendices *(Appendix 5* and *6)*.

^{10}Be dating of the VdR-1, VdR-2 and VdR-3 boulders on the lateral moraine VdR m1 in the upper part of the Rougnoux valley yielded exposure ages of 11.0 ± 0.4, 10.4 ± 0.5 and 10.0 ± 0.4 ka *(Appendix 9)*. A reduced chi-squared value of 2.3 was computed, thereby implying that measurement errors do not alone account alone for scatter in the exposure ages (Balco 2011). Accordingly, the oldest exposure age of the VdR-1 boulder (11.0 ± 0.4 ka) was considered to be the landform age.

Based on the ^{10}Be concentration in samples from three boulders (VdR-4, VdR-5 and VdR-6) on the lateral moraine (VdR m2) further downhill, exposure ages of 10.7 ± 0.5, 11.2 ± 0.6 and 10.9 ± 0.4 ka were computed *(Appendix 9)*. Considering that reduced χ^2 turned out to be 0.3, the landform age of 10.9 ± 0.6 ka was determined by averaging all three exposure ages. ^{10}Be exposure dating of three boulders (VdR-7, VdR-8, VdR-9) on the second innermost lateral moraine (VdR m3) on the western side of the Rougnoux stream yielded exposure ages of 11.5 ± 0.5, 11.2 ± 0.7 and 10.6 ± 0.4 ka. As the variations in the exposure ages from the moraine VdR m3 can mainly be attributed to measurement errors (reduced chi-squared of 1.3), the average ^{10}Be exposure age of the lateral moraine was determined to be 11.1 ± 0.7 ka *(Appendix 9)*.

Samples for ^{10}Be exposure dating were collected from three boulders (VdR-10, VdR-11, VdR-12) on the innermost lateral moraine (VdR m4) on the western side of the Rougnoux stream. The ^{10}Be concentration in the samples indicates exposure ages of 11.2 ± 0.5, 11.9 ± 1.0 and 7.3 ± 0.4 ka *(Appendix 9)*. Based on the aforementioned exposure ages, a reduced χ^2 of 30.6 was computed. Therefore, the differences in the exposure ages cannot solely be explained by measurement uncertainties. Accordingly, the oldest exposure age from boulder VdR-11 (11.9 ± 1.0 ka) was considered the landform age *(Appendix 9)*. Based on landform ages and the landform uncertainties, the moraines VdR m1, VdR m2, VdR m3 and VdR m4 cannot be distinguished in terms of chronology.

Samples from three boulders (VdR-13, VdR-14, VdR-15) were obtained from the second innermost moraine (VdR m5) outside the LIA moraines on the right-hand side of the Rougnoux stream *(Appendix 9)*. ^{10}Be measurements yielded exposure ages of 1.3 ± 0.1, 11.2 ± 0.4 and 10.7 ± 0.5 ka. Since a reduced chi-squared of 2163 was computed, the oldest exposure age from the boulder VdR-14 (11.2 ± 0.4 ka) was selected as the landform age.

Samples for ^{10}Be exposure dating were taken from three boulders on both crests of the lateral moraine VdR m6. Based on the ^{10}Be concentration in the samples, exposure ages between 10.7 ± 0.5 and 11.9 ± 0.5 ka were inferred.

Considering that a reduced chi-squared of 2.3 was computed, the oldest exposure age from the boulder VdR-16 (11.9 ± 0.5 ka) was chosen as the landform age *(Appendix 9)*. As the landform ages of the lateral moraines VdR m5 and VdR m6 overlap, a chronological distinction between the two landforms is impossible.

Given the good embeddedness in the moraine matrix and the lack of suitable boulders for SE dating on the two-crested lateral moraine uphill, a boulder situated slightly downhill was sampled for SE dating yielding an exposure age of 12.7 ± 0.8 ka *(Appendix 9)*. Exposure ages between 7.9 ± 0.4 and 9.9 ± 0.5 ka were obtained from three boulders (VdR-20, VdR-21 and VdR-22) on the lateral moraine VdR m7 *(Appendix 9)*. A reduced chi-squared of 10.5 was computed, thereby indicating that the variation in the exposure ages from the moraine VdR m7 cannot alone be attributed to the measurement errors. Accordingly, the oldest exposure age (9.9 ± 0.5 ka) was selected as the landform age.

Four exposure ages were obtained from boulders (VdR-23, VdR-24, VdR-25-1, VdR-25-2) on the dump moraine (VdR m8) on the south-western side of the Rougnoux stream *(Appendix 9)*. The samples VdR-25-1 and VdR-25-2 were obtained from the same boulder, as quartz veins were abundant on its surface. Based on the results of the ^{10}Be measurements, exposure ages of 10.5 ± 0.5, 12.5 ± 0.7, 11.9 ± 0.5 and 10.8 ± 0.4 ka were inferred. The oldest exposure age from boulder VdR-24 (12.5 ± 0.7 ka) was chosen as the landform age *(Appendix 9)*, as indicated by the reduced χ^2 value of 4.7.

Three ^{10}Be exposure ages were obtained from boulders (VdR-26, VdR-27, VdR-28) on the latero-frontal moraine (VdR m9) slightly uphill from the dump moraine VdR m8 *(Appendix 9).* According to the ^{10}Be concentration in the samples, exposure ages between 12.2 ± 0.6 and 12.7 ± 0.5 ka were computed. As the reduced chi-squared was determined to equal exactly 1, the mean landform age (12.5 ± 0.6 ka) was derived by averaging all three ^{10}Be exposure ages. Considering that the landform age of the moraine VdR m9 equals that of the VdR m8 moraine, both landforms cannot be distinguished.

Based on the ^{10}Be concentrations in samples from three boulders (VdR-29, VdR-30, VdR-31) from the latero-frontal moraine furthest down-valley on the north-eastern side of the Rougnoux stream (VdR m10), corresponding exposure ages were determined to be 8.0 ± 1.3, 7.9 ± 1.3 and 3.4 ± 1.1 ka *(Appendix 9)*. Considering that the analytical uncertainties were higher than 12%, the exposure ages were considered unreliable and, thus, no landform age was computed.

Two samples were collected from boulders on the sharp crest of a ridge (VdP m1) in the upper part of the Prelles valley *(Appendix 7)*. The ^{10}Be concentration in the samples indicates that the boulders were exposed at 1.7 ± 0.2 and 1.9 ± 0.3 ka to cosmic radiation. The ^{10}Be exposure age of the VdP-2 boulder was considered not reliable due to an analytical error >12%. Therefore, no landform age was computed.

SE dating of three boulders (VdP-4, VdP-5, VdP-6) on the latero-frontal moraine VdP m2, in the upper part of the Prelles valley *(Appendix 7)*, resulted in ^{10}Be exposure ages of 10.3 ± 0.4, 11.3 ± 0.5 and 10.5 ± 0.4 ka. Considering the reduced χ^2 value of 1.3, the landform age (10.7 ± 0.6 ka) of the latero-frontal moraine VdP m2 corresponds to the arithmetic mean of all three exposure ages.

Four samples (PdC-1, PdC-2, PdC-4 and PdC-5) for ^{10}Be dating were obtained from boulders on the two-crested frontal moraine near the Pré de la Chaumette mountain cabin *(Appendix 8)*. ^{10}Be exposure dating of two boulders (PdC-1 and PdC-2) close to the outer smooth moraine crest yielded exposure ages of 11.1 ± 1.2 ka and 12.2 ± 1.1 ka.

Based on the ^{10}Be concentration of sample PdC-4 which was collected from a boulder on the distal side of the moraine, an exposure age of 10.5 ± 0.6 ka was derived. Sample PdC-5 was taken from a well-embedded boulder close to the end of the distal side of the moraine *(Appendix 8)*. ^{10}Be dating of the boulder yielded an exposure age of 16.9 ± 1.6 ka. Based on all exposure ages and associated internal uncertainties, a reduced chi-squared value of 7.3 was derived. As it can be inferred that the scatter in the exposure ages is not only due to analytical errors, the oldest exposure age (16.9 ± 1.6 ka) from the boulder PdC-5 was considered the landform age *(Appendix 8)*.

5.3 Determination of the equilibrium line altitudes

The ELA was located at around 2440 m a.s.l. during the most extensive LIA glacier advance in the Rougnoux valley. As mentioned in section 4.4, the LIA ELA serves as reference value for all glacier advances surpassing the LIA extent. The ELA lowered to about 2280 m a.s.l. when the lateral moraine VdR m4 was deposited and the ice reached the inner crest of the southernmost lateral moraine on the right-hand side of the Rougnoux stream. Hence, this advance was associated with an ELA depression of 160 m *(Fig. 21)*. During the time when the ice reached the outer crest at the northern end of the lateral moraine VdR m4 and the upper crest of the southernmost lateral moraine on the right-hand side of the Rougnoux stream, the ELA was located at around 2270 m a.s.l., thereby implying an ELA lowering of 170 m *(Fig. 21)*.

Table 2. Reconstructed ELAs during the deposition of the frontal moraine near the Pré de la Chaumette mountain cabin. According to the first scenario, the moraine was deposited by the former Rougnoux glacier. For the second scenario, it was assumed that the former Rougnoux, Veyrardonne and De la Pierre glaciers were confluent. ΔELA are stated with respect to the LIA ELAs.

Scenario	Reconstructed ELA (m a.s.l.)	ΔELA (m)
Former Rougnoux glacier	2220	220
Confluent Veyrardonne, De la Pierre and Rougnoux glaciers	2370 (Veyrardonne and de la Pierre glaciers)	500 (Veyrardonne glacier)
		600 (De la Pierre glacier)
	2230 (Rougnoux glacier)	210 (Rougnoux glacier)

For the time of the deposition of the lateral moraines VdR m3 and VdR m5, which have already been correlated (Di Costanzo and Hofmann 2016), an ELA at 2260 m a.s.l. and an ELA depression of 180 m were reconstructed *(Fig. 21)*. During the deposition of the dump moraine VdR m8 on the left-hand side of the Rougnoux stream, the ELA was located at a slightly lower elevation of 2550 m a.s.l. (ΔELA of 190 m). The ELA reconstructions show that when the former Rougnoux glacier advanced up to the entrance of the Rougnoux valley and deposited the latero-frontal moraines VdR m9 and VdR m10, the ELA was situated at 2220 m a.s.l. Hence, an ELA lowering of 220 m compared to the end of the LIA was inferred *(Fig. 21)*.

Based on the LIA extent in the most recent glacier inventory (Gardent 2014), the LIA ELAs of Veyrardonne and the De la Pierre glacier were situated at 2870 m a.s.l. and 2970 m a.s.l., respectively. As outlined in section 4.4, two different scenarios were performed for the frontal moraine PdC m1 further down-valley *(Table 2)*. Based on the assumption that the frontal moraine was solely deposited by the former Rougnoux glacier, the ELA must have been situated at around 2220 m a.s.l. Therefore, an ELA lowering of 220 m was determined *(Table 2)*.

According to the second scenario that the PdC m1 moraine was shaped by the confluent Rougnoux, Veyrardonne and De la Pierre glaciers, the ELA of the Rougnoux glacier was located at 2230 m a.s.l., whereas the ELA of the Veyrardonne and the De la Pierre glacier was situated 140 m higher. Consequently, the ELA of the De la Pierre, Veyrardonne and the former Rougnoux glaciers lowered by 600, 500 and 210 m, respectively *(Table 2)*.

During the deposition of the now sparsely vegetated moraines in the upper part of the Prelles valley, which can probably be correlated with the LIA maximum glacier advance in the Prelles valley, an ELA at 2570 m a.s.l. was reconstructed. The ELA reconstructions indicate that the ELA was situated between 2450 and 2420 m a.s.l. during the formation of the four well vegetated, latero-frontal moraines further down-valley including VdP m2. Hence, the ELA lowered between 120 and 150 m during their deposition *(Fig. 21)*. When the former glacier reached the moraines in the lower part of the Prelles valley, the ELA was located between 2390 and 2370 m a.s.l. thereby implying ELA depressions of 180-200 m. The build-up of the large latero-frontal moraine near the Prelles lake was associated with an ELA lowering of 200 m.

6 DISCUSSION

In the first subsection, the ^{10}Be exposure ages are interpreted. A local stratigraphy is proposed in the following section. The exposure ages from the moraines in the upper Drac Blanc catchment are subsequently discussed with regard to recalculated exposure ages from key sites in the Alps and palaeoclimatic proxies other than glaciers.

6.1 Interpretation of the exposure ages of the moraines

Generally, exposure ages from boulders on moraines provide minimum ages of both moraine stabilisation and the associated glacier advance (Heyman *et al.* 2016). As moraines are also formed during periods of glacier recession (e.g. Benn and Evans 2010), the ^{10}Be exposure age of boulders on moraines may also reflect periods of stationary ice margins. As ^{10}Be exposure ages from boulders on moraines provide minimum ages of their stabilisation, all interpretations regarding the timing of both moraine build-up and the corresponding glacier advance or still stand are minimum estimates.

The mean landform ages of the lateral moraines in the upper part of the Rougnoux valley (VdR m1, VdR m2, VdR m3, VdR m4) disagree slightly with the stratigraphy *(Fig. 11),* as the oldest landform age was determined for the stratigraphically youngest ridge (VdR m4). Based on the relatively similar landform ages *(Fig. 18)*, it can be assumed that the four moraines were shaped during glacier advances or still stands within a quite short period. Given that all sampled boulders on the moraines VdR m1, VdR m2, VdR m3 and VdR m4 were considered to be well-embedded in the moraine matrix, boulder toppling as an explanation for the slightly incoherent landform ages seems not appropriate. Inheritance is equally unlikely, as it would have probably caused a stronger scatter in the exposure ages.

Due to the lack of suitable large boulders, most of the samples from the moraines in the upper Rougnoux valley were collected from boulders with a height of less than 1 m. Only the samples VdR-7 and VdR-11 were chiselled off from boulders with a height of 1.20 and 1.75 m, respectively *(Appendix 1)*. Considering that small boulders are more prone to post-depositional exposition and snow shielding, their ^{10}Be exposure ages are likely to underestimate the timing of both the moraine stabilisation and the corresponding glacier advance or still stand (Heyman *et al.* 2016).

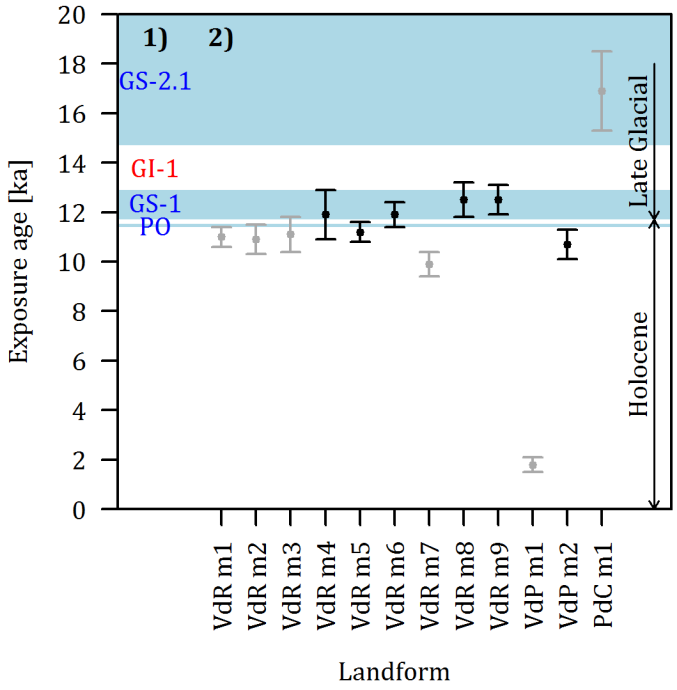

Fig. 18. Landform ages and associated uncertainties from the upper Drac Blanc catchment with regard to the INTIMATE event stratigraphy. 1) Stadials, interstadials and events according to the INTIMATE event stratigraphy: Greenland stadial 2.1 (GS-2.1, 22.9 –14.7 ka), Greenland interstadial 1 (GI-1, 14.7-12.9 ka), GS-1 and PO (Rasmussen *et al.* 2014); 2) Landform ages and uncertainties according to the 'CREp + snow' scenario. Robust mean landform ages and associated uncertainties are highlighted as black dots and error bars, respectively. Inconclusive landform ages and corresponding uncertainties are shown in grey.

Hence, post-depositional exhumation and snow shielding are believed to be the most likely explanations for the slightly incoherent landform ages of the moraines VdR m1, VdR m2, VdR m3 and VdR m4. Le Roy *et al.* (2017) encountered similar problems when dating the four outermost Neoglacial moraines of the Rateau glacier, as the oldest exposure age was obtained from a boulder on the innermost sampled ridge. Based on a significant correlation between the boulder height and the corresponding exposure ages, the age from the tallest boulder on the innermost moraine ridge was suggested as the minimum age for all four moraines (Le Roy *et al.* 2017).

The ^{10}Be exposure ages of the boulders on the moraines VdR m1, VdR m2, VdR m3 and VdR m4 seem to be associated to a certain degree with the boulder height, as it explains 37% of the variance of the exposure ages *(Fig. 19)*. However, it is noteworthy that most samples were collected from boulders with a height of about 0.5 m and, therefore, the coefficient of determination should not be considered meaningful *(Fig. 19)*. In any case, it is striking that SE dating of the tallest boulder (VdR-11) yielded the oldest exposure age. Therefore, the ^{10}Be exposure age from the VdR-11 boulder (11.9 ± 1.0 ka) is believed to reflect the timing of the stabilisation of the lateral moraine VdR m4, thereby implying that the three lateral moraines uphill (VdR m1, VdR m2 and VdR m3) were shaped before 11.9 ± 1.0 ka.

In conclusion, the lateral moraine VdR m4 was deposited during a glacier advance or a temporary still stand no later than in the Early Holocene *(Fig. 18)*, as indicated by the exposure age of boulder VdR-11 (11.9 ± 1.0 ka), whereas the three moraines uphill (VdR m1, VdR m2 and VdR m3) were shaped at some hitherto unknown time before.

Regarding the ^{10}Be exposure ages from the moraine VdR m5, the considerably younger exposure age of boulder VdR-13 might be due to analytical problems. In fact, ^{10}Be was purified from only 2.28 g of quartz, whereas for most of the samples, 21 g quartz was used *(Appendix 4)*. Therefore, it can be expected that the amount of ^{10}Be in the sample was simply too low to yield a robust ^{10}Be/^{9}Be ratio. Considering the exposure ages of the tallest boulder VdR-14 (11.2 ± 0.4 ka), the lateral moraine VdR m5 stabilised after a glacier advance or a halt in glacier recession at the latest in the Early Holocene *(Fig. 18)*.

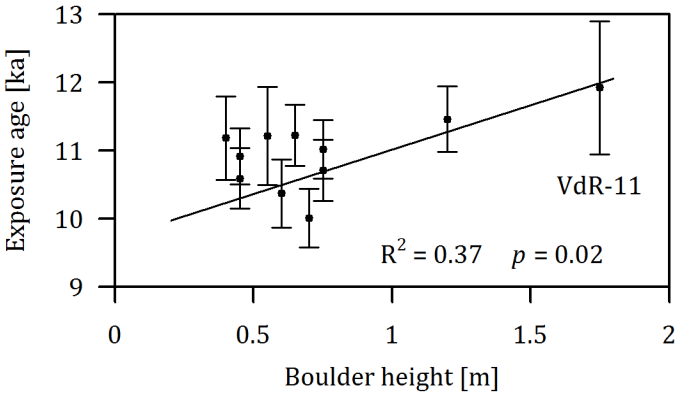

Fig. 19. Height of the sampled boulders on the lateral moraines VdR m1, VdR m2, VdR m3 and VdR m4 versus the corresponding exposure age. The considerably younger exposure age of the boulder VdR-12 is considered to be an outlier and is therefore not included. The correlation is statistically significant at a 95% confidence level (p = 0.02). The boulder height accounts for 37% of the variance of the exposure ages. However, R^2 is thouht to be not meaningful, as most samples were collected from boulders with a height of about 0.5 m. Due to the fact that the oldest exposure age was obtained from the tallest boulder (VdR-11), its ^{10}Be exposure age is considered the minimum age of the lateral moraine VdR m4 and the distant minimum age for the three sampled lateral moraines uphill.

As rock samples were taken from boulders on both crests of the lateral moraine VdR m6, the landform age *(Fig. 18)* is thought to reflect the timing of the built-up of the whole landform. The landform age of the two-crested moraine VdR m6 (11.9 ± 0.5 ka) agrees with the stratigraphy considering that it is older than that of the stratigraphically younger moraine VdR m5 (11.2 ± 0.4 ka). According to the landform age 11.9 ± 0.5 ka, which corresponds to the oldest exposure age of the VdR-16 boulder, VdR m6 was deposited no later than in the Early Holocene *(Fig. 18)*.

A single exposure age (12.7 ± 0.8 ka) was obtained from the VdR-19 boulder uphill from moraine VdR m7 *(Appendix 9)*, as no suitable boulders for SE dating were available on the two-crested lateral moraine uphill. Accordingly, the exposure age of boulder VdR-19 is believed to provide a minimum age for the undated lateral moraine uphill thereby implying that it was deposited at the end of the Late Glacial. Hence, moraine stabilisation in the Early Holocene can be ruled out.

The landform age of the lateral moraine VdR m7 (9.9 ± 0.5 ka) disagrees with the stratigraphy. Indeed, the landform age is younger than that of the moraine m5 (11.2 ± 0.4 ka) which can be considered to be the next stratigraphically younger landform *(Fig. 11)*. Given the fact that the Rougnoux stream has eroded at least a part of the lateral moraine VdR m7, it can be assumed that it was not the stabilisation of the moraine, but a single erosional event that has instead been dated. The hypothesis, that the ^{10}Be ages indicate the exposure after erosion is supported by the similar exposure ages of the VdR-20 and VdR-21 boulders. It is noteworthy that the VdR-20 boulder is partially shielded by a *Larix decidua.* However, tree shielding accounts only for a change of less than 4% in ^{10}Be production (Böhlert *et al.* 2011) and, therefore, a considerable effect on the resulting exposure age can be ruled out.

The landform age of the dump moraine VdR m8 (12.5 ± 0.7 ka) is in agreement with the stratigraphy, as it equals the landform age (12.5 ± 0.6 ka) of the latero-frontal moraine VdR m9 uphill. As the sediments of the VdR m8 are clast-supported, boulder toppling as reason for the scatter in the exposure ages can be ruled out. However, as VdR m8 is tentatively interpreted as a dump moraine consisting of boulders derived from discrete rockfall events (see section 5.1.1.1), it cannot be excluded that the detachment of the boulders and the simultaneous exposure to cosmic radiation has instead been dated. However, it can be anticipated that the supraglacial transport of the boulder required less time than the uncertainties of the ^{10}Be exposure ages.

In any case, the landform age of moraine VdR m8 should thus be considered an approximate estimate for the deposition of the moraine. Given that the formation of a discrete dump moraine requires a stationary ice margin or a slow glacier retreat rate (Bennett and Glasser 2009), the landform age of the moraine VdR m8 is thought to reflect a halt in the recession of the former Rougnoux glacier at the end of the Late Glacial or in the Early Holocene *(Fig. 18)*.

Considering that the northern end of the latero-frontal moraine VdR m9 is located at the entrance of the Rougnoux valley, its landform age (12.5 ± 0.6 ka) provides a minimum age of the furthest glacier advance in the Rougnoux valley or the earliest still stand after the glacial retreat from the moraine near the Pré de la Chaumette moraine to the entrance of the Rougnoux valley *(Fig. 11)*. Both the samples VdR-27 and VdR-28 were taken from boulders which are shielded by a *Larix decidua*. Again, a noticeable effect on the exposure ages can be ruled out (Böhlert *et al.* 2011). Due to the height of the sampled boulders (1.25-1.90 m), the exposure ages are believed to provide a robust estimate of the timing of moraine stabilisation. As indicated by the landform age, the latero-frontal moraine was deposited no later than during GS-1. It can be ruled out that the moraine stabilised in the Early Holocene *(Fig. 18)*.

As it could not be explicitly evaluated whether the sharp-crested ridge (VdP m1) in the upper part of the Prelles valley can be classified as a moraine or a fluvial deposit, the lack of a clear genetical assignment prevents a conclusive interpretation of the exposure ages. According to the hypothesis that VdP m1 is a moraine, the exposure ages of the VdP-1 boulder indicates moraine stabilisation at around 1.7 ± 0.2 ka. The ^{10}Be exposure age should be considered as minimum age of the corresponding glacier advance given the small size of the dated boulders (0.60-0.65 m). Following the interpretation as fluvial deposit, the exposure ages might indicate the timing of an erosional event. As pointed out above, further sedimentological investigations are needed to reveal the depositional history of the ridge VdP m1 which would, in turn, facilitate the interpretation of the exposure ages.

The exposure ages from the latero-frontal moraine VdP m2 vary between 10.3 ± 0.4 and 11.3 ± 0.5 ka. Given the height of the sampled boulders 0.9 and 1.3 m, the exposure ages from VdP m2 are believed to be a good proxy for the corresponding glacier advance. Accordingly, the latero-frontal moraine stabilised at the latest in the Early Holocene *(Fig. 18)*.

The exposure ages of the boulders PdC-1, PdC-2 and PdC-4 on the frontal moraine down-valley from the Pré de la Chaumette mountain cabin cluster in the period between 10.5 ± 0.6 and 12.2 ± 1.1 ka *(Appendix 8)*. In contrast, ^{10}Be exposure dating of the PdC-5 boulder at the end of the distal side of the moraine resulted in a significantly older exposure age of 16.9 ± 1.6 ka. Overall, the exposure ages from the PdC m1 moraine should be interpreted with caution. In fact, the smooth crests of the moraine indicate substantial post-depositional degradation.

Therefore, it can be anticipated that the nowadays exposed boulders on the outer crest weathered out of the till and became exposed to cosmic radiation when the glacier retreat was already well under way. Therefore, the exposure ages from the boulders PdC-1, PdC-2 and PdC-4 which are situated close to the moraine crest, can be classified as 'too-young' exposure ages. Conversely, only the exposure age of the PdC-5 boulder is believed to be a good proxy for moraine build-up, as the PdC-5 boulder is the only sampled boulder from the PdC m1 moraine which has probably not been affected by significant post-depositional degradation due to its location near the end of the distal side of the moraine.

It can be excluded that the frontal moraine stabilised after 12.5 ± 0.6 ka, as the stratigraphically younger latero-frontal moraine in the Rougnoux valley (VdR m9) was deposited at 12.5 ± 0.6 ka, when the former Rougnoux glacier reached the entrance of the Rougnoux valley *(Fig. 11)*. As the landform age of the latero-frontal moraine VdR m9 is based on three coherent exposure ages, it can be inferred that the moraine PdC m1 must be older than 12.5 ± 0.6 ka. Thus, arises the question as to whether the frontal moraine was deposited slightly before 12.5 ± 0.6 ka or significantly earlier at 16.9 ± 1.6 ka, as indicated by the ^{10}Be exposure age from the PdC-5 boulder. Three preliminary hypotheses for the age of the moraine can thus be formulated:

1. The PdC m1 moraine stabilised slightly before 12.5 ± 0.6 ka thereby implying that the significantly older exposure age of boulder PdC-5 (16.9 ± 1.6 ka) reflects pre-exposure to cosmic radiation prior to moraine deposition. According to this scenario, it might be also possible that the boulder PdC-5 stabilised after a glacier advance at around 16.9 ± 1.6 ka and was later picked up by the ice somewhat before 12.5 ± 0.6 ka. Hence, the boulder was subsequently incorporated in the frontal moraine;
2. The moraine formed around 16.9 ± 1.6 ka and was not reached during a later glacier advance. Consequently, the exposure ages of the boulders PdC-1, PdC-2 and PdC-4 reflect their exposure to cosmic radiation during the subsequent degradation of the moraine and not the timing of the corresponding glacier advance;
3. The moraine was deposited at around 16.9 ± 1.6 ka and was re-occupied during a later glacier re-advance at some hitherto unknown time before 12.5 ± 0.6 ka.

Furthermore, it raises the question as to which glacier shaped the frontal moraine near the Pré de la Chaumette mountain cabin considering that it is situated slightly down-valley from the confluence of the Rougnoux and the De la Pierre valleys. In the following chapter, this question, as well as the three hypotheses for the age of the frontal moraine PdC m1 are further discussed with regard to the ELA reconstructions.

6.2 Establishment of a local stratigraphy

Relative ages have been assigned to the moraines (see section 5.1) based on the concept of morphostratigraphy (Lowe and Walker 2015). As the age of most moraines has been constrained through the use of SE dating, the moraines can be classified in terms of time and therefore be assigned to chronostratigraphical units *(Fig. 20 and 21)*. Accordingly, the terms 'stage' and 'substage' are employed. The first number after 's' for stage refers to the main stage, whereas the second number indicates the number of the substage *(Fig. 20* and *21)*. All undated moraines are correlated with dated moraines based on ΔELA.

It should be noted that that the reconstructed LIA ELA of the palaeoglaciers in the Rougnoux and the Prelles valley might not correspond to the climatic ELA at that time. Indeed, the LIA glaciers were located downhill from steep escarpments. In such a topographical situation, it can be anticipated that shading caused a local ELA well below the climatic ELA. This becomes especially evident in the Rougnoux valley, where a permanent snow patch can still be found inside the LIA moraines at an elevation of about 2400-2600 m a.s.l. although the current ELA in the Rougnoux valley might be situated at around 3000 m a.s.l. or higher. See also Hofmann (2016) for a discussion of the LIA ELA in the Rougnoux valley.

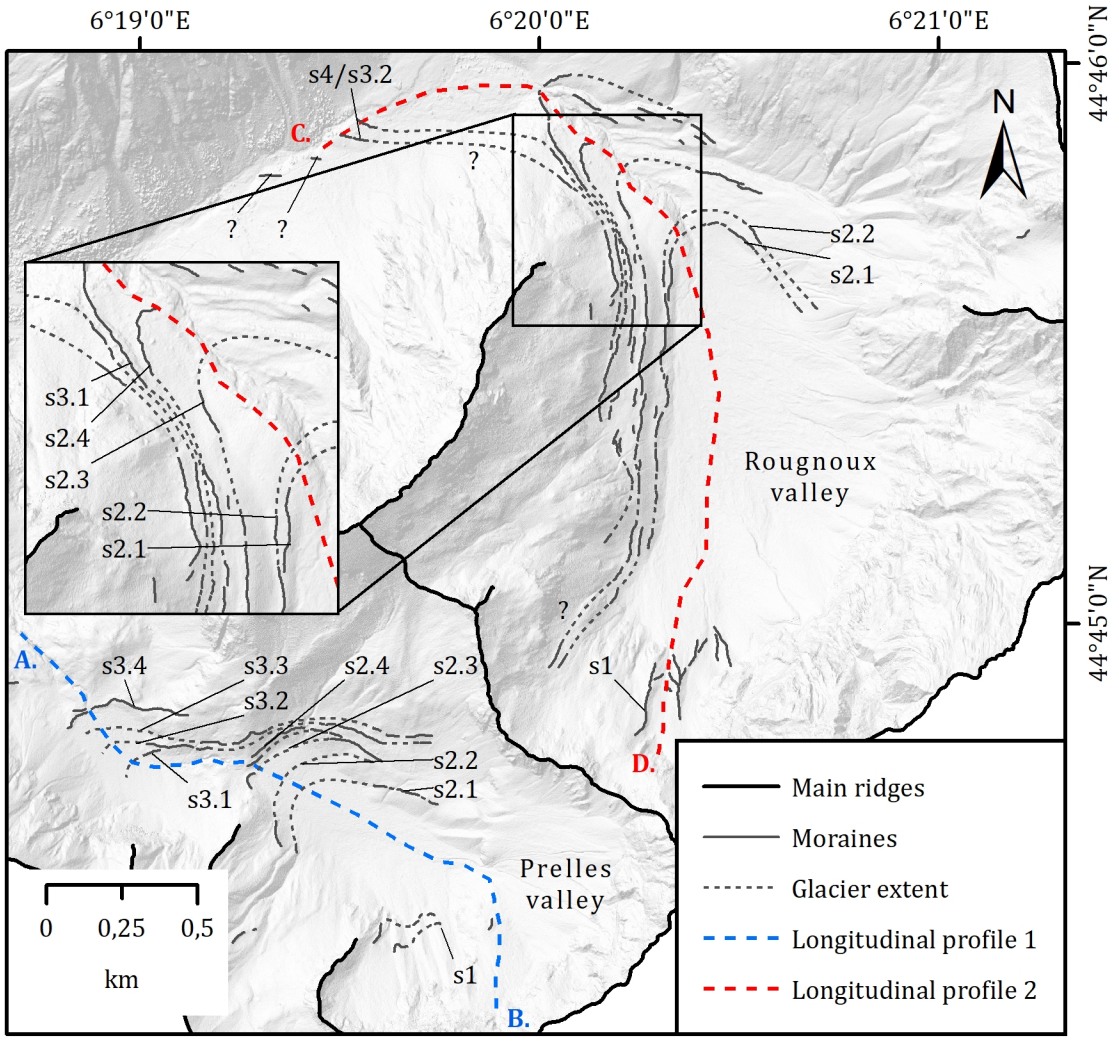

Date: 24.5.2018; Author: Felix Martin Hofmann; Data source: IGN 2012; Coordinate system: WGS 1984 UTM zone 32N

Fig. 20. Moraine stages and substages in the southern part of the upper Drac Blanc catchment. Possible correspondencies are marked with question marks.

On the other hand, the reconstructed ELAs during the deposition of the moraines further down-valley can be considered more robust, as the topographical constraint in the upper part of the accumulation area probably exerted a lesser influence. In light of this reasoning, the reconstructed ELA depressions should strictly be seen as minimum values. Nevertheless, as the topographical context in the Prelles valley resembles that of the upper Rougnoux valley, comparisons between the two valleys are believed to be conclusive.

The moraines in the upper Prelles and Rougnoux valleys, which were deposited during the LIA and subsequent glacier re-advances, can be subsumed as first stage (s1, *Fig. 20* and *21)*.

As most exposure ages from the Rougnoux and Prelles valleys fall into the last part of the Late Glacial and in the Early Holocene, a subdivision in a last Late Glacial stage and an Early Holocene stage would be desirable. However, the uncertainties associated with the exposure ages prevent drawing a clear boundary between GS-1 and Early Holocene moraines. A clear subdivision is further complicated by the fact that no distinct groups of closely spaced moraines can be observed in the Rougnoux valley *(Fig. 20* and *21)*. Considering that the ^{10}Be exposure ages provide minimum estimates for the timing of the corresponding glacier advances *sensu stricto*, it might also be possible that all moraines outside the LIA moraines stabilised before the onset of the Holocene.

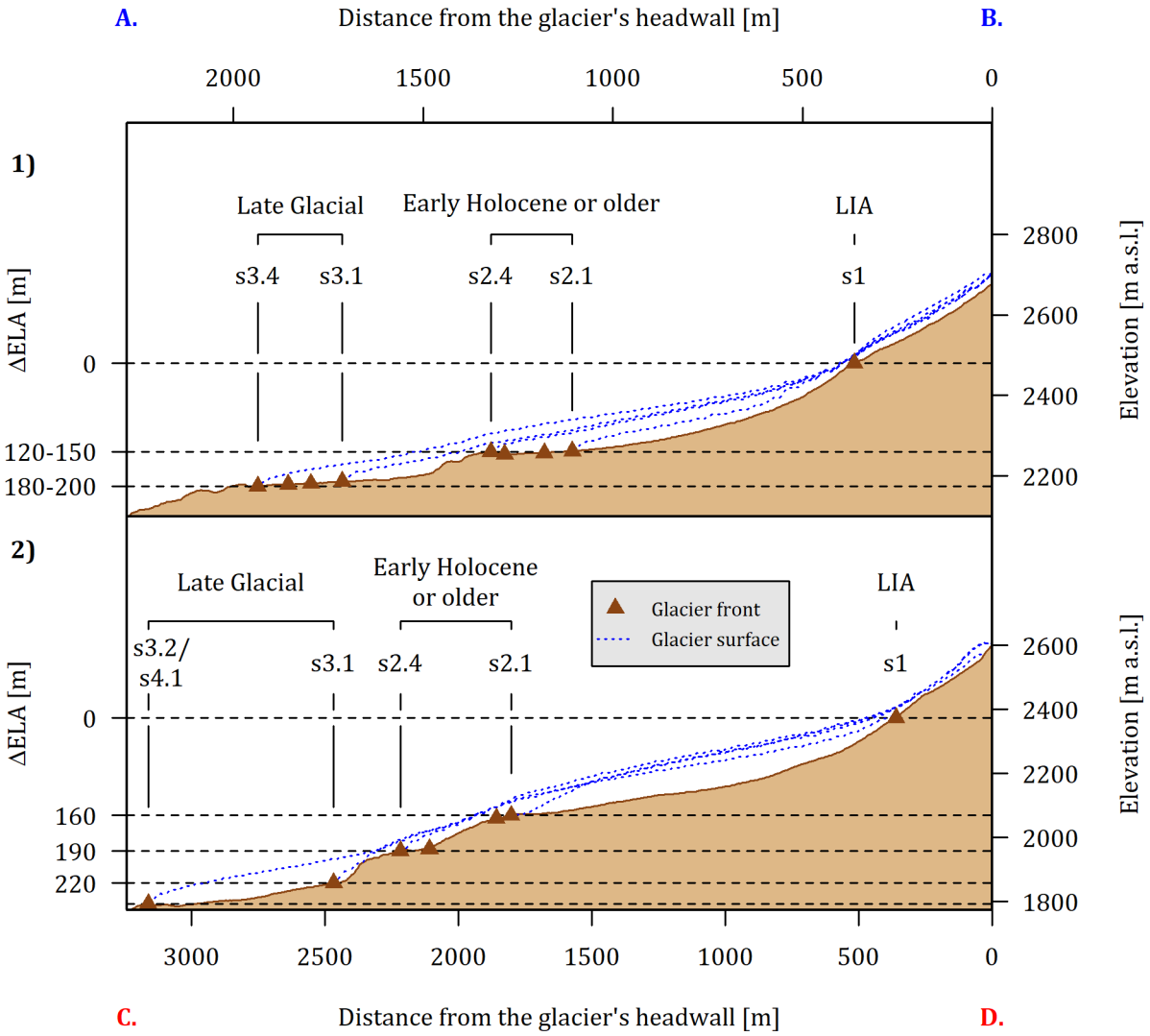

Fig. 21. Longitudinal profile of the 1) Prelles valley and the 2) Rougnoux valley. See *fig. 20* for the location of the longitudinal profiles. The reconstructed ice thickness with the GlaRe toolbox during the deposition of the outermost and the innermost moraine of a stage is shown as dotted blue line. See section 4.4 for further methodological details.

Despite this fact, a subdivision into moraines which might have been deposited during the Early Holocene and moraines shaped before the onset of the Holocene is proposed *(Fig. 20* and *21)*. Accordingly, all moraines in the Rougnoux valley which might have been deposited in the Early Holocene, are grouped as stage 2 (s2). Stage 2 can be further subdivided in four substages *(Fig. 20* and *21)*.

Given that the dump moraine VdR m8 is the furthest down-valley landform which might have stabilised in the Early Holocene (see section 6.1), it is considered the oldest substage (s2.4) of stage 2. As the lateral moraines VdR m3 and VdR m5 are the next stratigraphically younger landforms further up-valley, they can accordingly be classified as substage 2.3. The outer crest at the northern tip of the lateral moraine VdR m4, as well as the outer crest of the southernmost lateral moraine on the right-hand side of the Rougnoux stream are hereinafter referred to as substage 2.2 *(Fig. 20* and *21)*. The inner crest at the northern end of the lateral moraine VdR m4 and the inner crest of the corresponding lateral moraine on the right-hand side of the Rougnoux stream are the innermost landforms outside of the LIA moraines *Fig. 20* and *21)*. Therefore, they are classified as the youngest substage (s2.1).

In contrast to the Rougnoux valley, two distinct group of moraines outside of the LIA moraines can be differentiated in the Prelles valley. Therefore, the moraines in the upper part of the valley outside the LIA moraines including the VdP m2 moraine are assigned to a Late Glacial/Early Holocene stage (s2, *Fig. 20* and *21)* based on the exposure ages from the latero-frontal moraine VdP m2. It is noteworthy that the reconstructed ELA depressions during the deposition of the moraines of the second stage in the Rougnoux valley (160-190 m) are larger than in the Prelles valley (120-150 m).

The two-crested lateral moraine uphill from the boulder VdR-19 is assigned to a third stage (s3, *Fig. 20* and *21)*, as its exposure age (12.7 ± 0.8 ka) indicates moraine formation before the onset of the Holocene. Due to the strong degradation of the moraine record on the right-hand side of the Rougnoux stream, correlations with other moraines in the vicinity prove difficult. Hence, the lateral moraine is simply considered part of s3 and not assigned to a specific substage. As it can be excluded that the correlated latero-frontal moraines VdR m9 and VdR m10 stabilised during the Early Holocene, they are assigned to the first substage of stage 3 (s3.1). Accordingly, the landform age of the moraine VdR-9 (12.5 ± 0.6 ka) is the minimum age of the moraines attributed to the third stage *(Fig. 20* and *21)*.

The frontal moraine near the Pré de la Chaumette mountain cabin (PdC m1) can be assigned to the second substage of stage 3 (s3.2, *Fig. 20* and *21*), since the ELA reconstructions show that only a subtle ELA change of a few meters was required to cause the former Rougnoux glacier to advance to the frontal moraine down-valley from the mountain cabin. Therefore, it is near certain that the former Rougnoux glacier reached the frontal moraine PdC m1 shortly before 12.5 ± 0.6 ka.

In consequence, this reasoning suggests excluding the second preliminary hypothesis in section 6.1 that the frontal moraine PdC m1 was shaped solely during an advance at around 16.9 ± 1.6 ka. Furthermore, it seems very unlikely that the frontal moraine PdC m1 was formed in front of the confluent Veyrardonne, De la Pierre and Rougnoux glaciers slightly before 12.5 ± 0.6 ka. Indeed, the ELA reconstructions suggest that ELA depressions of roughly 500-600 m compared to the end of the LIA would have been required to cause the De la Pierre and the Veyrardonne glaciers to advance up to the frontal moraine near the mountain cabin, whereas a considerably smaller ELA lowering of 220 m would have been sufficient for an advance of the former Rougnoux glacier up to the moraine. Hence, it can be concluded that the moraine PdC m1 was either built-up by the former Rougnoux glacier or re-occupied somewhat before 12.5 ± 0.6 ka.

It may be possible for the lateral moraines uphill from the latero-frontal moraine VdR m9 to be correlated with the frontal moraine PdC m1 *(Fig. 20)*.

As it cannot be excluded, that the frontal moraine PdC m1 was reached by an earlier glacier advance at or before 16.9 ± 1.6 ka, the moraine can also be assigned to a fourth stage (s4, *Fig. 20* and *21)*.

The moraines in the lower part of the Prelles valley constitute a last Late Glacial stage (s3, *Fig. 20* and *21).* The ELA reconstructions show that the deposition of the moraines in the lower part of the Prelles valley must have been associated with ΔELA of 180-200 m. Thus, the moraines in the lower part of the Prelles valley can be correlated with the moraines of the third stage in the Rougnoux valley (ΔELA of 190-220 m), thereby implying that the prominent latero-frontal moraines near the Prelles lake was probably shaped during the maximum re-advance of the palaeoglacier in the Prelles valley around 12.5 ± 0.6 ka.

6.3 Glacier variations in the upper Drac Blanc catchment in the Alpine context

For the comparison of the exposure ages from the upper Drac Blanc catchment with previous studies from other localities in the Alps *(Fig. 22)*, published ^{10}Be exposure ages were recalculated with the CRONUS Earth calculator (Balco *et al.* 2008) using the Arctic ^{10}Be production rate of Young *et al.* (2013). The necessary parameters for the determination of the exposure ages were taken from the original publications. Missing information was retrieved from Heyman (2018). No corrections were made for snow shielding or erosion. Outliers were excluded as done in the original publications. Landform ages and uncertainties were computed as outlined in section 4.3.2.3. For the sake of comparability, landform ages and associated uncertainties from the upper Drac Blanc catchment in this section correspond to the 'CRONUS Earth' scenario.

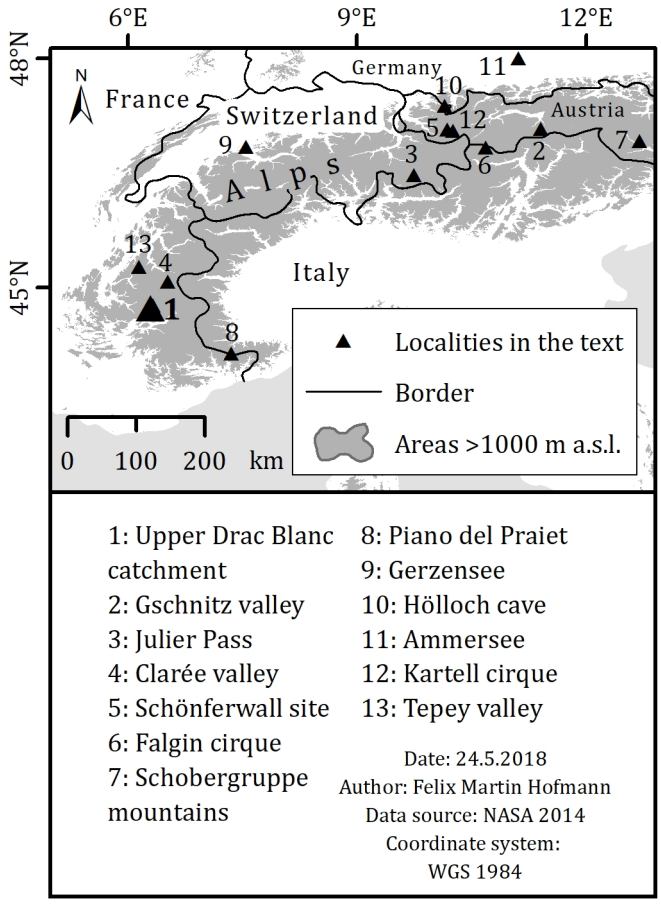

Fig. 22. Location of key sites in the Alps. The numbering of the localities refers to their appearance in the text. See *fig. 1* for the data source.

The phase of ice decay following the LGM and the subsequent retreat of the Alpine glaciers to the interior of the Alps, a first clear glacial re-advance occurred in the early part of the Late Glacial. A prominent moraine system in the Gschnitz valley *(Fig. 22)* near the village of Trins was defined as the type-locality for this first clear Late Glacial re-advance in the pioneering study by Penck and Brückner (1909). ^{10}Be exposure dating of boulders on the moraine complex showed that the moraine must have stabilised before 16.6 ± 1.2 ka *(Fig. 23,* Ivy-Ochs *et al.* 2006a).

The similarity between the ^{10}Be exposure age (16.2 ± 1.7 ka) of the PdC-5 boulder from the frontal moraine PdC m1 and the landform age of the moraine near Trins raises the question of a possible correlation.

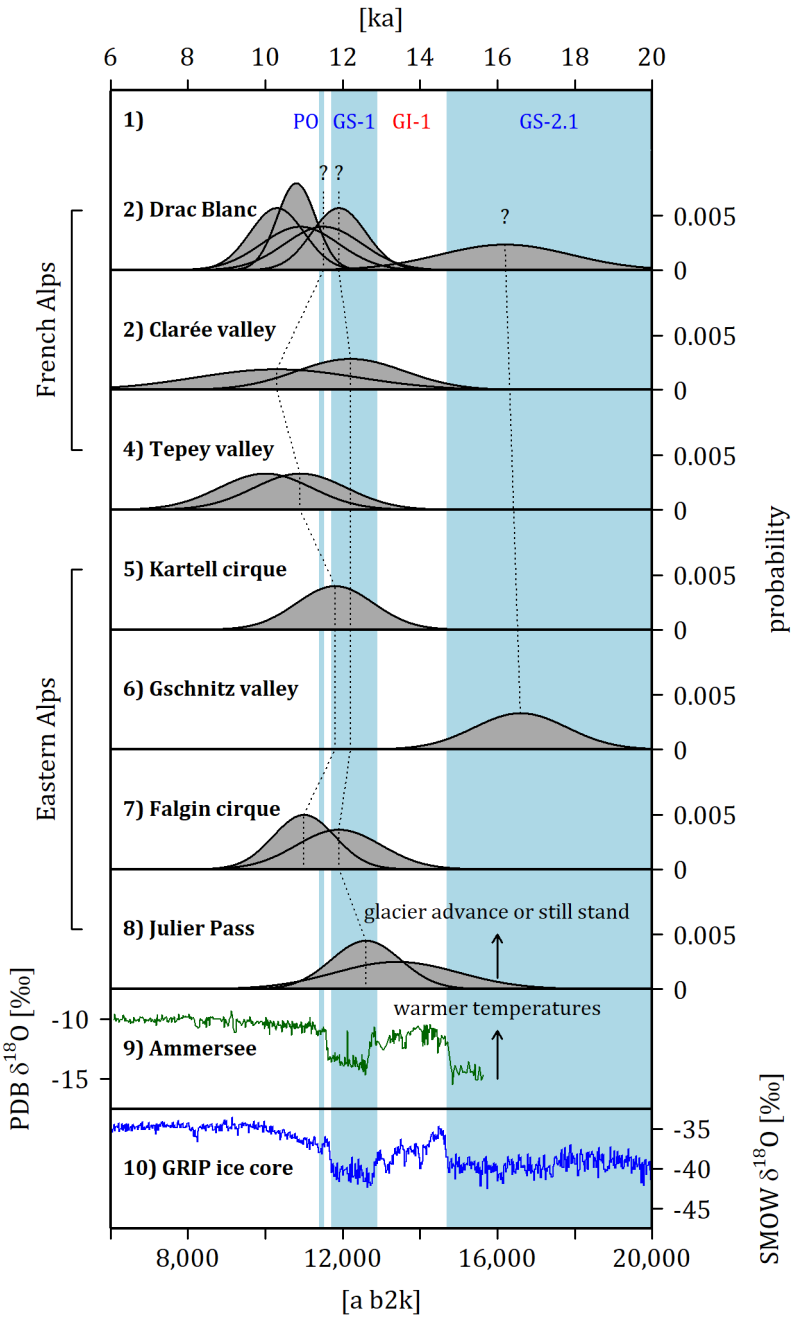

Fig. 23. Probability density functions of glacier advances or still stands at different sites in the Alps based on recalculated ^{10}Be exposure ages, as well as data from regional and hemispheric palaeoclimatic proxies. See *fig. 22* for the location of the sites in the Alps. 1) Events according to the INTIMATE event stratigraphy: GS-2.1 (22.9-14.7 ka), GI-1 (14.7-12.9 ka), GS-1 (12.9-11.7 ka), and PO (11.5-11.4 ka, Rasmussen *et al.* 2014); 2-8) Probability density functions of glacier advances or still stands in the 2) upper Drac Blanc catchment (this study), 3) upper Clarée valley (Cossart *et al.* 2012), 4) Tepey valley (Le Roy 2012 and Le Roy, unpublished data), 5) Kartell cirque (Austria, Ivy-Ochs *et al.* 2006b), 6) Gschnitz valley (Austria, Ivy-Ochs *et al.* 2006a), 7) Falgin cirque (Italy, Moran *et al.* 2016) and 8) to Julier Pass (Switzerland, Ivy-Ochs *et al.* 2006b). Possible correlations are marked with dotted lines and question marks. 9) Ostracod-based reconstruction of $\delta^{18}O$ in precipitation with respect to the Pee Dee Belemnite (PDB) standard from Ammersee (southern Germany, von Grafenstein *et al.* 1999); $\delta^{18}O$ compared to the Standard Mean Ocean Water (SMOW) in the GRIP (Greenland Ice Core Project) ice core (Rasmussen *et al.* 2014).

However, fact that an ELA lowering of only 220 m was sufficient to trigger an advance of the Rougnoux glacier to the frontal moraine PdC m1 casts doubts on a link between the deposition of the PdC m1 moraine and the formation of the prominent moraine in the Gschnitz valley. In fact, an ELA reconstructions based on the AAR method indicates that the formation of the moraine at the type locality in the Gschnitz valley required a considerably larger ELA depression in the order of 700 m (Ivy-Ochs *et al.* 2006a).

Therefore, the exposure age of the PdC-5 boulder should be regarded as an indication that a glacier advance of a similar age than in the Gschnitz valley may have occurred in the upper Drac Blanc catchment. Due to the strong post-depositional degradation of the PdC m1 moraine and the fact that most suitable boulders on the distal side of the moraine were sampled for ^{10}Be exposure dating, an assessment of this hypothesis proves difficult. The only way for overcoming this issue would be to constrain the age of the large conglomerate boulder on the outer crest of the PdC m1 moraine *(Fig. 16)* through the use of ^{36}Cl exposure dating and the exposure age of boulders on the outermost moraine further down-valley with ^{10}Be exposure dating.

Several lines of evidence suggest that the moraines of stage 2 and 3 in the upper Drac Blanc catchment can be correlated with the Egesen stadial *sensu* Heuberger (1968). The term 'Egesen stadial' is nowadays widely employed for glacial re-advances during GS-1, although it was originally introduced as appendix of the Daun stadial (Reitner *et al.* 2016). Considering that they often represent prominent landforms, Egesen-like moraines have been described in numerous valleys in the Austrian, French, Italian and Swiss Alps (Ivy-Ochs *et al.* 2008; Ivy-Ochs *et al.* 2009; Ivy-Ochs 2015 and references therein). In most cases, two or more distinct groups of Egesen-like moraines can be distinguished owing to the pronounced climatic instability during GS-1 (Ivy-Ochs *et al.* 2009).

The good agreement between the inferred age of the PdC m1 moraine (slightly older than 11.9 ± 0.7 ka according to the 'CRONUS Earth + snow' scenario) and ^{10}Be exposure ages from boulders on moraines in different parts of the Alps which have been attributed to the furthest glacier advances during the Egesen stadial *(Fig. 23)*, suggest that the frontal moraine PdC m1, as well as the prominent latero-frontal moraine in the lower part of the Prelles valley can be considered Egesen maximum positions. For instance, SE dating of the outer Egesen stadial moraine at the Julier Pass *(Fig. 22)* yielded a landform age of 13.4 ± 1.6 (Ivy-Ochs *et al.* 2006b). Cossart *et al.* (2012) dated a moraine of the second glacial stage in the upper part of the Clarée valley *(Fig. 22)* in the southern French Alps to 12.4 ± 1.4 ka (recalculated from Cossart *et al.* 2012). ^{10}Be exposure dating of boulders on a prominent Egesen-like moraine at the Schönferwall site *(Fig. 22)* resulted in a landform age of 13.2 ± 1.0 ka (recalculated from Ivy-Ochs *et al.* 2006b). A mean exposure age of 11.9 ± 1.2 ka (recalculated from Moran *et al.* 2016) was obtained from an Egesen maximum moraine in the Falgin cirque *(Fig. 22)* in the Ötztal Mountains. However, the compilation of ^{10}Be exposure ages from boulders on Egesen maximum moraines shows slight variations *(Fig. 23)*. The slightly different exposure ages can possibly be attributed to local factors, such as the topography, which probably led to a modification of the common climatic signal.

Although it has been demonstrated that comparisons of ELA depressions compared to the end of the LIA on different sites of the Alps may exhibit significant regional differences (Reitner *et al.* 2016), ΔELA during the glacier advances in the upper Drac Blanc catchment agree surprisingly well with reconstructed ELA depressions during advances on other sites in the Eastern Alps. For example, Ivy-Ochs (2015) showed that the outer Egesen-like moraine at the Julier Pass *(Fig. 22)* formed when the ELA was roughly 220 m lower compared to the end of the LIA. According to Böhlert *et al.* (2011), the formation of the Egesen-like moraines in two valleys close by (Val Tschitta and Val Mulix) was associated with an ELA depression of between 220 and 230 m. Moran *et al.* (2016) inferred an identical ELA depression for the date when the outermost Egesen-like moraine in the Falgin cirque *(Fig. 22)* was deposited. The formation of Egesen maximum moraines in the Schobergruppe mountains *(Fig. 22)* was associated with an ELA depression between 265 and 300 m (Reitner *et al.* 2016).

In contrast, Federici *et al.* (2016) showed that during the build-up of the Piano del Praiet moraine *(Fig. 22)* which has been correlated with the Egesen stadial, the ELA must have lowered by 500 m compared to the end of the LIA. Overall, the similar ELA depressions in the Eastern Alps and in the southern part of the Écrins massif during GS-1 suggest that the climatic differences between the two regions were not considerably different from the pattern at the end of the LIA.

Data from palaeoclimatic records other than glaciers indicate that the advance of the former glacier in the Rougnoux valley up to the PdC m1 moraine can be considered a clear re-advance which was triggered by a climatic downturn of larger spatial relevance in the first place *(Fig. 23)*. Indeed, palynological data, as well as chironomid records from the Austrian and the Swiss Alps point towards a simultaneous decrease of 1.5-3 K in summer temperature (Heiri *et al.* 2014). For example, $\delta^{18}O$ in the sediments of Gerzensee in the Alpine foreland in Switzerland *(Fig. 22)* decreased by 3 ‰ from 12.7 to 12.5 ka (Schwander *et al.* 2000). A speleothem record from the Hölloch cave *(Fig. 22)* shows a drop of 2 ‰ in $\delta^{18}O$ at around 12.6 ka (Wurth *et al.* 2004). Moreover, an ostracod-based reconstruction from sediments of the Ammersee in southern Germany *(Fig. 22)* indicates a lowering of about 3 ‰ in $\delta^{18}O$ of precipitation in the foreland of the northern Alps at the beginning of GS-1 *(Fig. 23*, von Grafenstein *et al.* 1999). This lowering of $\delta^{18}O$ in precipitation corresponds to a drop of 5 ‰ in $\delta^{18}O$ in both the GRIP and the NGRIP ice cores after 12.9 ka *(Fig. 23,* Rasmussen *et al.* 2014). In conclusion, the advance of the former Rougnoux glacier and the subsequent deposition of the frontal moraine PdC m1 were probably triggered by the major climatic shift at the onset of GS-1 which was probably caused by a weakening or shutdown of the Atlantic meridional overturning circulation due to the injection of meltwater in the North Atlantic (Lowe and Walker 2015).

Stage 3.2 in the Rougnoux valley can probably be correlated with the second phase of the Egesen stadial. Indeed, the landform age of the latero-frontal moraine VdR m9 (11.9 ± 0.7) agrees with the Egesen II moraine mean landform age of 12.6 ± 0.9 ka at Julier Pass *(Fig. 23,* recalculated from Ivy-Ochs *et al.* 2006b). The mean landform age is also in agreement with the mean ^{10}Be exposure age (12.1 ± 0.9 ka) of the second outermost moraine in the upper Romanche catchment *(Fig. 1*, recalculated from Chenet *et al.* 2016). Again, the good agreement between the landform age of the latero-frontal moraine VdR m9 and the mean ^{10}Be exposure age of the moraines at the two aforementioned sites suggests a common climatic origin of the corresponding glacier advances. As mentioned above, the slight variations in the exposure ages can be attributed to local factors which caused an individual reaction of the glaciers despite a common climatic signal.

The innermost moraines of stage 2 in the Prelles and Rougnoux valleys can probably be considered the local expression of the Kartell stadial. The ^{10}Be exposure age from the tallest boulder on the lateral moraine VdR m4 (11.5 ± 1.0 ka according to the 'CRONUS Earth' scenario) agrees well with the landform age of a moraine in the Kartell cirque *(Fig. 22)*. Indeed, SE dating of three boulders on the Kartell moraine yielded a mean exposure age of 11.8 ± 1.0 ka (recalculated from Ivy-Ochs *et al.* 2006b), thereby indicating that the Kartell stadial is nothing else than the final advance of the Egesen stadial (Ivy-Ochs 2015). Moraines of a similar age have been dated through the use of ^{10}Be exposure dating in two valleys in the French Alps. Cossart *et al.* (2012) obtained exposure ages from 8 boulders on the frontal moraine at the entrance of the Muandes cirque in the upper Clarée valley *(Fig. 22)*, thereby implying a landform age of 10.3 ± 2.2 ka (recalculated from Cossart *et al.* 2012).

^{10}Be dating of three boulders on the third innermost moraine in the Tepey valley *(Fig. 22)* resulted in a mean exposure age of 10.9 ± 1.2 ka (recalculated from Le Roy 2012 and Le Roy, unpublished data).

Based on an AAR of 0.67, the ELA was probably lowered by 180 m during the deposition of the moraines at the latter site (Le Roy 2012) which agrees roughly with the ELA depression at the time when the innermost moraines outside the LIA moraines in the Prelles and Rougnoux valleys stabilised (120 and 160 m). However, The ΔELA values from the upper Drac Blanc catchment and from the Tepey valley are slightly larger than the reconstructed ELA change during the formation of the Kartell moraine in the Ferwall group (ca. 120 m, Ivy-Ochs 2015). Therefore, it can be assumed that the slight variation in the ELA depressions indicates that the differences in terms of precipitation and temperature between the French Alps and the Eastern Alps were different during the Late Glacial/Holocene transitional period than at end of the LIA.

6.4 Open questions

As pointed out above, the frontal moraine PdC m1 was most likely shaped during the furthest advance of the Rougnoux glacier at the onset of GS-1. However, this hypothesis relies solely on ELA reconstructions, as ^{10}Be dating of boulders on the PdC m1 moraine yielded no conclusive results due to its strong post-depositional degradation (see section 5.2). Therefore, a more detailed investigation of the sediments of the moraine would be of great value. Indeed, the presence of sandstone in the moraine matrix would strengthen the hypothesis that the moraine was shaped by the former Rougnoux glacier, as sandstones are only exposed in the upper part of the Rougnoux valley (Debelmas *et al.* 1980). Conversely, the lack of sandstone would suggest that the moraine was deposited by the Veyrardonne and the De la Pierre glaciers. Furthermore, the exposure age of conglomerate boulder on the outer crest of the PdC m1 moraine should be constrained with ^{36}Cl exposure dating to evaluate the hypothesis of a glacier still stand or advance in the upper Drac Blanc catchment at the latest at 16.2 ± 1.7 ka.

Secondly, the age of the lowermost moraine in the upper Drac Blanc catchment, down-valley from the PdC m1 moraine, should be constrained with ^{10}Be exposure dating. Additional exposure ages from boulders would help to evaluate if it was deposited during an older Late Glacial advance or if it can be considered the GS-1 maximum position of the former Rougnoux glacier, although the latter scenario seems unlikely due to the large volume of the PdC m1 moraine.

Although the ΔELA-based correlations of the undated moraines in the Prelles valley with dated moraines in the Rougnoux valley are considered to be robust, the stabilisation of the large latero-frontal moraine near the Prelles lake should, at least, be dated with ^{10}Be exposure dating to remove any doubts on the correlation with the PdC m1 moraine. As pointed out above, the sediments of the VdP m1 ridge should also be investigated to be able to infer its depositional history.

According to Heiri *et al.* (2014), two major shortcomings of glacier records are that the age of moraines indicates, with some exceptions, cool periods favourable for glacier expansion and that moraines are often overridden during important glacial re-advances. These two major disadvantages prevent the use of glacier-based evidence for continuous palaeoclimatic reconstructions (Heiri *et al.* 2014). Therefore, the findings of this study should be put in a wider perspective by extracting quantitative information from nearby palaeoclimatic archives other than glaciers.

Such a study has already been undertaken by Ponel *et al.* (2011) who reconstructed vegetation changes in the Isola valley, a lateral valley of the Champoléon valley, through the analysis of beetle assemblages and pollen in the sediments of the former Lauzons lake. However, the late deglaciation of the site prevented the palaeoenvironmental change during the major part of the Late Glacial to be reconstructed. Considering that the Prelles lake was probably not overrun by glacier advances during GS-1, it can be anticipated that more information about climatic variability during the Late Glacial could be inferred from its sediments.

Lastly, well-preserved moraines close to the upper Drac Blanc catchment, as east of the Vallonpierre mountain cabin, up-valley from the hamlet of Dormillouse or around the Chabournéou mountain cabin should be dated through the use of SE dating to evaluate if the palaeoglaciers on the aforementioned sites reacted in a similar fashion than in the Rougnoux and the Prelles valleys. The reconstruction of associated ELA depressions compared to the end of the LIA would enable to test the validity of ΔELA-based stratigraphical correlations within the Écrins massif.

7 CONCLUSION

Based on the available geomorphic evidence, as well as the ^{10}Be exposure ages of moraines, the glacial history of the upper Drac Blanc catchment can be summarised as follows: It cannot be excluded that the frontal moraine near the Pré de la Chaumette mountain cabin was shaped for the first time during a glacier advance or a still stand at around 16.2 ± 1.7 ka. The palaeoglacier in the Rougnoux valley reacted to the climatic downturn at the onset of GS-1 and advanced up to the prominent frontal moraine near the Pré de la Chaumette mountain cabin shortly before 12.5 ± 0.6 ka. According to the ELA reconstructions, this advance was triggered by an ELA lowering of 220 m compared to the end of the LIA. At the same time, the palaeoglacier in the Prelles valley shaped the prominent latero-frontal moraine complex near the Prelles lake. During this advance, the ELA in the Prelles valley must have been 200 m lower than the LIA ELA. The ^{10}Be exposure ages from boulders on a moraine at the entrance of the Rougnoux valley provide evidence for a second GS-1 advance or a stationary period at the latest at 12.5 ± 0.6 ka.

A halt in glacier recession occurred shortly thereafter, as indicated by four ^{10}Be exposure ages from a dump moraine. The following glacial re-advance or still stand not later than 11.2 ± 0.4 ka led to the build-up of the moraines VdR m2 and VdR m5. The geomorphic evidence, as well as three ^{10}Be exposure ages suggest that the palaeoglacier in the Rougnoux valley surpassed for the last time its LIA extent at around 11.9 ± 1.0 ka when the innermost lateral moraine on the left-hand side of the Rougnoux stream was deposited. The palaeoglacier in the Prelles valley shaped the outermost latero-frontal moraine in the upper part of the valley not later than 10.7 ± 0.6 ka. The occurrence of three latero-frontal moraines nearby indicate that three re-advances or halts in glacier recession occurred after the built-up of the VdP m2 moraine.

Overall, the ^{10}Be exposure ages provide unanimous support for the first hypothesis that the moraines in the Rougnoux valley were deposited during GS-1 and in the Early Holocene. The ^{10}Be ages from the VdP m2 moraine, as well as the ELA depressions indicate that the palaeoglaciers in the Prelles and the Rougnoux valleys reacted in a similar way to the climatic oscillations during GS-1 and in the Early Holocene, thereby confirming the second hypothesis that moraines of a similar age than in the Rougnoux valley can also be observed in the Prelles valley.

Considering that the previous assignment of the moraines in the Rougnoux valley to GS-1 and Early Holocene advances based on similar ELA depressions than in the Durance catchment turned out to be correct, this study provides evidence that ΔELA-based stratigraphical correlations may work on a regional scale if (I) possible sources of bias (e.g. debris cover) are taken into account and if (II) moraines serve as reference whose age has been constrained with a geochronological method. However, this study demonstrates that the combination of ^{10}Be exposure dating and ELA reconstructions enables the establishment of a chronology of glacier variations whose temporal solution goes well beyond a mere ΔELA-based approach.

In conclusion, novel findings of this study are

- The glacier advances or still stands not later than 11.9 ± 1.0, 11.2 ± 0.4 and 10.7 ± 0.6 ka which have been dated for the first time in the Écrins massif. The ^{10}Be exposure ages of the corresponding moraines agree well with recalculated ^{10}Be exposure ages of moraines on different sites in the Alps which have been attributed to the Egesen and Kartell stadials;
- The reconstructed ELA depressions with respect to the end of the LIA during glacier advances or still stands at the end of the Late Glacial and in the Early Holocene in the southern part of the Écrins massif.

REFERENCES

Arnold, M., G. Aumaître, D. L. Bourlès, K. Keddadouche, R. Braucher, R. C. Finkel, E. Nottoli, L. Benedetti, et al. 2013. The French accelerator mass spectrometry facility ASTER after 4 years: Status and recent developments on ^{36}Cl and ^{129}I. *Nuclear Instruments and Methods in Physics Research Section B: Beam Interactions with Materials and Atoms,* 294**:** 24-28. DOI: 10.1016/j.nimb.2012.01.049

Auer, I., R. Böhm, A. Jurkovic, W. Lipa, A. Orlik, R. Potzmann, W. Schöner, M. Ungersböck, et al. 2007. HISTALP—historical instrumental climatological surface time series of the Greater Alpine Region. *International journal of climatology,* 27**:** 17-46. DOI: 10.1002/joc.1377

Bakke, J., and A. Nesje. 2011. Equilibrium-Line Altitude (ELA). In *Encyclopedia of Snow, Ice and Glaciers,* eds. V. P. Singh, P. Singh, and U. K. Haritashya, 268-277 pp. Dordrecht: Springer Netherlands.

Balco, G., J. O. Stone, N. A. Lifton, and T. J. Dunai. 2008. A complete and easily accessible means of calculating surface exposure ages or erosion rates from ^{10}Be and ^{26}Al measurements. *Quaternary geochronology,* 3**:** 174-195. DOI: 10.1016/j.quageo.2007.12.001

Balco, G. 2011. Contributions and unrealized potential contributions of cosmogenic-nuclide exposure dating to glacier chronology, 1990–2010. *Quaternary Science Reviews,* 30**:** 3-27. DOI: 10.1016/j.quascirev.2010.11.003

Balco, G. 2013. ^{10}Be - ^{26}Al exposure age calculator. Young et al. (2013) Baffin Bay/Arctic calibration data set. . Retrieved 22.5.2018, from. http://hess.ess.washington.edu/math/al_be_v22/alt_cal/Young_Baffin_age_input.html

Benn, D. I., and D. J. A. Evans. 2010. *Glaciers and Glaciation*. London: Hodder Education.

Bennett, M., and N. F. Glasser. 2009. *Glacial geology : ice sheets and landforms*. Chichester, UK ; Hoboken, NJ Wiley-Blackwell.

Biju-Duval, J. 1975. Etude pétrologique des terrains cristallins de la région du Sirac (sud du massif des Ecrins-Pelvoux-Haut Dauphiné). PhD Thesis. Grenoble: Grenoble University

Böhlert, R., M. Egli, M. Maisch, D. Brandová, S. Ivy-Ochs, P. W. Kubik, and W. Haeberli. 2011. Application of a combination of dating techniques to reconstruct the Lateglacial and early Holocene landscape history of the Albula region (eastern Switzerland). *Geomorphology,* 127**:** 1-13. DOI: 10.1016/j.geomorph.2010.10.034

Braucher, R., V. Guillou, D. L. Bourlès, M. Arnold, G. Aumaître, K. Keddadouche, and E. Nottoli. 2015. Preparation of ASTER in-house ^{10}Be/^{9}Be standard solutions. *Nuclear Inst. and Methods in Physics Research, B,* 361**:** 335-340. DOI: 10.1016/j.nimb.2015.06.012

Briner, J. P. 2011. Dating Glacial Landforms. In *Encyclopedia of Snow, Ice and Glaciers,* eds. V. P. Singh, P. Singh, and U. K. Haritashya, 175-186 pp. Dordrecht: Springer Netherlands.

Chenet, M., D. Brunstein, V. Jomelli, E. Roussel, V. Rinterknecht, F. Mokadem, M. Biette, V. Robert, et al. 2016. ^{10}Be cosmic-ray exposure dating of moraines and rock avalanches in the Upper Romanche valley (French Alps): Evidence of two glacial advances during the Late Glacial/Holocene transition. *Quaternary Science Reviews,* 148**:** 209-221. DOI: 10.1016/j.quascirev.2016.07.025

Chmeleff, J., F. von Blanckenburg, K. Kossert, and D. Jakob. 2010. Determination of the ^{10}Be half-life by multicollector ICP-MS and liquid scintillation counting. *Nuclear Instruments and Methods in Physics Research Section B: Beam Interactions with Materials and Atoms,* 268**:** 192-199. DOI: 10.1016/j.nimb.2009.09.012

Claude, A., S. Ivy-Ochs, F. Kober, M. Antognini, B. Salcher, and P. W. Kubik. 2014. The Chironico landslide (Valle Leventina, southern Swiss Alps); age and evolution. *Swiss Journal of Geosciences,* 107**:** 273-291. DOI: 10.1007/s00015-014-0170-z

Cossart, E., M. Fort, V. Jomelli, and D. Grancher. 2006. Les variations glaciaires en Haute Durance (Briançonnais, Hautes-Alpes) depuis la fin du XIXe siècle: mise au point d'après les documents d'archives et la lichénométrie. *Quaternaire. Revue de l'Association française pour l'étude du Quaternaire,* 17**:** 75-92. DOI: 10.4000/quaternaire.694

Cossart, E., D. Bourlès, R. Braucher, J. Carcaillet, M. Fort, and L. Siame. 2011. L'englacement du haut bassin durancien (Alpes françaises du sud) du Dernier Maximum Glaciaire à l'Holocène: synthèse chronologique. *Géomorphologie: relief, processus, environnement,* 17**:** 123-142. DOI: 10.4000/geomorphologie.9336

Cossart, E. 2011. Mapping glacier variations at regional scale through equilibrium line altitude interpolation: GIS and statistical application in Massif des Écrins (French Alps). *Journal of Geographic Information System,* 3**:** 224. DOI: 10.4236/jgis.2011.33020

Cossart, E., M. Fort, D. Bourles, R. Braucher, R. Perrier, and L. Siame. 2012. Deglaciation pattern during the Lateglacial/Holocene transition in the southern French Alps; chronological data and geographical reconstruction from the Clarée Valley (upper Durance Catchment, southeastern France). *Palaeogeography, Palaeoclimatology, Palaeoecology,* 315-316**:** 109-123. DOI: 10.1016/j.palaeo.2011.11.017

Coûteaux, M. 1983. Fluctuations glaciaires de la fin du Würm dans les Alpes françaises, établies par des analyses polliniques. *Boreas,* 12**:** 35-56. DOI: 10.1111/j.1502-3885.1983.tb00359.x

Coûteaux, M. 1984. Les particularités pollenanalytiques de sédiments glaciaires en Oisans (Isère, France). *La Houille Blanche,* 6-7**:** 433-444. DOI: 10.1051/lhb/1984028

Debelmas, J., C. Kerckhove, G. Monjuvent, R. Mouterde, and A. Pêcher. 1980. Carte géologique de la France (1/50 000), feuille Orcières (846). Orléans: Bureau de Recherches géologiques et minières.

Deline, P., and M. Le Roy. 2008. Fluctuations des glaciers des alpes occidentales depuis 5000 ans: un état des connaissances. *Collection EDYTEM. Cahiers de Paléoenvironnement,* 6**:** 13-28.

Delunel, R. 2010. Evolution géomorphologique du massif des Ecrins-Pelvoux depuis le Dernier Maximum Glaciaire–Apports des nucléides cosmogéniques produits in-situ. PhD Thesis. Grenoble: Grenoble University

Di Costanzo, H., and F. M. Hofmann. 2016. Le retrait du glacier du Drac Blanc (massif des Écrins, Alpes françaises). *Méditerranée. Revue géographique des pays méditerranéens,* Varia. DOI: 10.15496/publikation-13788

Dumont, T., J.-D. Champagnac, C. Crouzet, and P. Rochat. 2008. Multistage shortening in the Dauphine zone (French Alps): the record of Alpine collision and implications for pre-Alpine restoration. *Swiss Journal of GeoSciences,* 101**:** 89-110. DOI: 10.1007/s00015-008-1280-2

Federici, P. R., A. Ribolini, and M. Spagnolo. 2016. Glacial history of the Maritime Alps from the Last Glacial Maximum to the Little Ice Age. In *Quaternary Glaciation in the Mediterranean Mountains,* eds. P. D. Hughes, and J. C. Woodward, 137-159 pp. London: The Geological Society of London.

Fouinat, L., P. Sabatier, J. Poulenard, D. Etienne, C. Crouzet, A.-L. Develle, E. Doyen, E. Malet, et al. 2017. One thousand seven hundred years of interaction between glacial activity and flood frequency in proglacial Lake Muzelle (western French Alps). *Quaternary Research,* 87**:** 407-422. DOI: 10.1017/qua.2017.18

Gardent, M. 2014. Inventaire et retrait des glaciers dans les alpes françaises depuis la fin du Petit Age Glaciaire. PhD Thesis. Grenoble: Grenoble University

Gardent, M., A. Rabatel, J.-P. Dedieu, and P. Deline. 2014. Multitemporal glacier inventory of the French Alps from the late 1960s to the late 2000s. *Global and Planetary Change,* 120**:** 24-37. DOI: 10.1016/j.gloplacha.2014.05.004

Gosse, J. C., and F. M. Phillips. 2001. Terrestrial in situ cosmogenic nuclides: theory and application. *Quaternary Science Reviews,* 20**:** 1475-1560. DOI: 10.1016/S0277-3791(00)00171-2

Gross, G., H. Kerschner, and G. Patzelt. 1977. Methodische Untersuchungen über die Schneegrenze in alpinen Gletschergebieten. *Zeitschrift für Gletscherkunde und Glazialgeologie,* 12**:** 223-251.

Haeberli, W., M. Hoelzle, F. Paul, and M. Zemp. 2007. Integrated monitoring of mountain glaciers as key indicators of global climate change: the European Alps. *Annals of glaciology,* 46**:** 150-160. DOI: 10.3189/172756407782871512

Heiri, O., K. A. Koinig, C. Spötl, S. Barrett, A. Brauer, R. Drescher-Schneider, D. Gaar, S. Ivy-Ochs, et al. 2014. Palaeoclimate records 60–8 ka in the Austrian and Swiss Alps and their forelands. *Quaternary Science Reviews,* 106**:** 186-205. DOI: 10.1016/j.quascirev.2014.05.021

Heuberger, H. 1968. Die Alpengletscher im Spät-und Postglazial: Eine chronologische Übersicht. *E&G–Quaternary Science Journal,* 19**:** 270-275. DOI: 10.23689/fidgeo-1106

Heyman, J., P. J. Applegate, R. Blomdin, N. Gribenski, J. M. Harbor, and A. P. Stroeven. 2016. Boulder height–exposure age relationships from a global glacial ^{10}Be compilation. *Quaternary Geochronology,* 34**:** 1-11. DOI: 10.1016/j.quageo.2016.03.002

Heyman, J. 2018. A global compilation of glacial ^{10}Be and ^{26}Al data. Retrieved 27.4.2018 2018, from. http://expage.github.io/index.html

Hofmann, F. M. 2016. *Les fluctuations glaciaires dans le vallon de Rougnoux*. Saarbrücken: Éditions Universitaires Européennes.

Ivy-Ochs, S., H. Kerschner, P. W. Kubik, and C. Schlüchter. 2006a. Glacier response in the European Alps to Heinrich Event 1 cooling: the Gschnitz stadial. *Journal of Quaternary science,* 21**:** 115-130. DOI: 10.1002/jqs.955

Ivy-Ochs, S., H. Kerschner, A. Reuther, M. Maisch, R. Sailer, J. Schaefer, P. W. Kubik, H. Synal, et al. 2006b. The timing of glacier advances in the northern European Alps based on surface exposure dating with cosmogenic ^{10}Be, ^{26}Al, ^{36}Cl, and ^{21}Ne. In *In Situ-Produced Cosmogenic Nuclides and Quantification of Geological Processes,* eds. A. M. Alonso-Zarza, and L. H. Tanner, 43-60 pp. Boulder: Geological Society of America.

Ivy-Ochs, S., and F. Kober. 2008. Surface exposure dating with cosmogenic nuclides. *Eiszeitalter und Gegenwart. Quaternary Science Journal,* 57**:** 179-209. DOI: 10.3285/eg.57.1-2.7

Ivy-Ochs, S., H. Kerschner, A. Reuther, F. Preusser, K. Heine, M. Maisch, P. W. Kubik, and C. Schlüchter. 2008. Chronology of the last glacial cycle in the European Alps. *Journal of Quaternary Science,* 23**:** 559-573. DOI: 10.1002/jqs.1202

Ivy-Ochs, S., H. Kerschner, M. Maisch, M. Christl, P. W. Kubik, and C. Schlüchter. 2009. Latest Pleistocene and Holocene glacier variations in the European Alps. *Quaternary Science Reviews,* 28**:** 2137-2149. DOI: 10.1016/j.quascirev.2009.03.009

Ivy-Ochs, S. 2015. Glacier variations in the European Alps at the end of the last glaciation. *Cuadernos de investigación geográfica,* 41**:** 295-315. DOI: 10.18172/cig.2750

James, M. R., S. Robson, S. d'Oleire-Oltmanns, and U. Niethammer. 2017. Optimising UAV topographic surveys processed with structure-from-motion: Ground control quality, quantity and bundle adjustment. *Geomorphology,* 280**:** 51-66. DOI: 10.1016/j.geomorph.2016.11.021

Keiler, M., J. Knight, and S. Harrison. 2010. Climate change and geomorphological hazards in the eastern European Alps. *Philosophical Transactions of the Royal Society of London A: Mathematical, Physical and Engineering Sciences,* 368**:** 2461-2479. DOI: 10.1098/rsta.2010.0047

Kerschner, H., and S. Ivy-Ochs. 2008. Palaeoclimate from glaciers: Examples from the Eastern Alps during the Alpine Lateglacial and early Holocene. *Global and Planetary Change,* 60**:** 58-71. DOI: 10.1016/j.gloplacha.2006.07.034

Korschinek, G., A. Bergmaier, T. Faestermann, U. Gerstmann, K. Knie, G. Rugel, A. Wallner, I. Dillmann, et al. 2010. A new value for the half-life of ^{10}Be by heavy-ion elastic recoil detection and liquid scintillation counting. *Nuclear Instruments and Methods in Physics Research Section B: Beam Interactions with Materials and Atoms,* 268**:** 187-191. DOI: 10.1016/j.nimb.2009.09.020

Lal, D. 1991. Cosmic ray labeling of erosion surfaces: in situ nuclide production rates and erosion models. *Earth and Planetary Science Letters,* 104**:** 424-439. DOI: 10.1016/0012-821X(91)90220-C

Lambiel, C., B. Maillard, M. Kummert, and E. Reynard. 2016. Geomorphology of the Hérens valley (Swiss Alps). *Journal of Maps,* 12**:** 160-172. DOI: 10.1080/17445647.2014.999135

Le Roy, M., and P. Deline. 2009. Étude des fluctuations glaciaires de Petit Age de Glace dans le massif des Écrins: apports de la lichénométrie. *Collection EDYTEM. Cahiers de Géographie,* 8**:** 51-64.

Le Roy, M. 2012. Reconstitution des fluctuations glaciaires holocènes dans les Alpes occidentales. Apports de la dendrochronologie et de la datation par isotopes cosmogéniques produits in situ. PhD Thesis. Grenoble: Grenoble University

Le Roy, M., K. Nicolussi, P. Deline, L. Astrade, J.-L. Edouard, C. Miramont, and F. Arnaud. 2015. Calendar-dated glacier variations in the western European Alps during the Neoglacial: the Mer de Glace record, Mont Blanc massif. *Quaternary Science Reviews,* 108**:** 1-22. DOI: 10.1016/j.quascirev.2014.10.033

Le Roy, M., P. Deline, J. Carcaillet, I. Schimmelpfennig, M. Ermini, and A. Team. 2017. ^{10}Be exposure dating of the timing of Neoglacial glacier advances in the Ecrins-Pelvoux massif, southern French Alps. *Quaternary Science Reviews,* 178**:** 118-138. DOI: 10.1016/j.quascirev.2017.10.010

Lifton, N., T. Sato, and T. J. Dunai. 2014. Scaling in situ cosmogenic nuclide production rates using analytical approximations to atmospheric cosmic-ray fluxes. *Earth and Planetary Science Letters,* 386**:** 149-160. DOI: 10.1016/j.epsl.2013.10.052

Lifton, N. 2016. Implications of two Holocene time-dependent geomagnetic models for cosmogenic nuclide production rate scaling. *Earth and Planetary Science Letters,* 433**:** 257-268. DOI: 10.1016/j.epsl.2015.11.006

Lowe, J., and M. J. Walker. 2015. *Reconstructing Quaternary Environments*. London: Routledge.

Lucieer, A., S. M. d. Jong, and D. Turner. 2014. Mapping landslide displacements using Structure from Motion (SfM) and image correlation of multi-temporal UAV photography. *Progress in Physical Geography,* 38**:** 97-116. DOI: 10.1177/0309133313515293

Mackintosh, A. N., B. M. Anderson, and R. T. Pierrehumbert. 2017. Reconstructing Climate from Glaciers. *Annual Review of Earth and Planetary Sciences,* 45**:** 649-680. DOI: 10.1146/annurev-earth-063016-020643

Maillard, B., C. Lambiel, S. Martin, R. Pellitero Ondicol, E. Reynard, and P. Schoeneich. 2011. The ArcGIS version of the geomorphological mapping legend of the University of Lausanne. Retrieved 15.3. 2018, from. https://www.unil.ch/files/live/sites/igd/files/shared/recherche/Carto_geomorpho_Informations_et_bibliographie.pdf

Martin, L., P.-H. Blard, G. Balco, J. Lavé, R. Delunel, N. Lifton, and V. Laurent. 2017. The CREp program and the ICE-D production rate calibration database: a fully parameterizable and updated online tool to compute cosmic-ray exposure ages. *Quaternary geochronology,* 38**:** 25-49. DOI: 10.1016/j.quageo.2016.11.006

Masson-Delmotte, V., M. Schulz, A. Abe-Ouchi, J. Beer, A. Ganopolski, J. F. Gonzalez Rouco, E. Jansen, K. Lambeck, et al. 2013. Information from paleoclimate archives. In *Climate Change 2013: the Physical Science Basis. Contribution of Working Group I to the Fifth Assessment Report of the Intergovernmental Panel on Climate Change,* eds. T. F. Stocker, D. Qin, G.-K. Plattner, M. Tignor, S. K. Allen, J. Boschung, A. Nauels, Y. Xia, V. Bex, and P. M. Midgley. Cambridge, United Kingdom and New York, NY, USA: Cambridge University Press.

Mertes, J. R., J. D. Gulley, D. I. Benn, S. S. Thompson, and L. I. Nicholson. 2017. Using Structure from Motion to create Glacier DEMs and Orthoimagery from Historical Terrestrial and Oblique Aerial Imagery. *Earth Surface Processes and Landforms*. DOI: 10.1002/esp.4188

Monjuvent, G. 1978. Le Drac, morphologie, stratigraphie et chronologie quaternaires d'un bassin alpin. PhD Thesis. Paris: Université Paris-Diderot-Paris VII

Moran, A. P., S. Ivy-Ochs, M. Schuh, M. Christl, and H. Kerschner. 2016. Evidence of central Alpine glacier advances during the Younger Dryas–early Holocene transition period. *Boreas,* 45**:** 398-410. DOI: 10.1111/bor.12170

Ohmura, A., P. Kasser, and M. Funk. 1992. Climate at the equilibrium line of glaciers. *Journal of Glaciology,* 38**:** 397-411. DOI: 10.3189/S0022143000002276

Pellitero Ondicol, R. 2009. Application of an alpine geomorphological mapping system to an atlantic mountain environment: The Curavacas Massif (Cantabrian Range, Northwest Spain). *Journal of Maps,* 5**:** 194-205. DOI: 10.4113/jom.2009.1065

Pellitero, R., B. R. Rea, M. Spagnolo, J. Bakke, P. Hughes, S. Ivy-Ochs, S. Lukas, and A. Ribolini. 2015. A GIS tool for automatic calculation of glacier equilibrium-line altitudes. *Computers & Geosciences,* 82**:** 55-62. DOI: 10.1016/j.cageo.2015.05.005

Pellitero, R., B. R. Rea, M. Spagnolo, J. Bakke, S. Ivy-Ochs, C. R. Frew, P. Hughes, A. Ribolini, et al. 2016. GlaRe, a GIS tool to reconstruct the 3D surface of palaeoglaciers. *Computers & Geosciences,* 94**:** 77-85. DOI: 10.1016/j.cageo.2016.06.008

Penck, A., and E. Brückner. 1909. *Die Alpen im Eiszeitalter*. Leipzig: C.H. Tauchnitz.

Ponel, P., M. Court-Picon, M. Badura, F. Guiter, J.-L. de Beaulieu, V. Andrieu-Ponel, M. Djamali, M. Leydet, et al. 2011. Holocene history of Lac des Lauzons (2180 m asl), reconstructed from multiproxy analyses of Coleoptera, plant macroremains and pollen (Hautes-Alpes, France). *The Holocene,* 21**:** 565-582. DOI: 10.1177/0959683610385725

Putkonen, J., and T. Swanson. 2003. Accuracy of cosmogenic ages for moraines. *Quaternary Research,* 59**:** 255-261. DOI: 10.1016/S0033-5894(03)00006-1

Rasmussen, S. O., M. Bigler, S. P. Blockley, T. Blunier, S. L. Buchardt, H. B. Clausen, I. Cvijanovic, D. Dahl-Jensen, et al. 2014. A stratigraphic framework for abrupt climatic changes during the Last Glacial period based on three synchronized Greenland ice-core records: refining and extending the INTIMATE event stratigraphy. *Quaternary Science Reviews,* 106**:** 14-28. DOI: 10.1016/j.quascirev.2014.09.007

Reitner, J. M., S. Ivy-Ochs, R. Drescher-Schneider, I. Hajdas, and M. Linner. 2016. Reconsidering the current stratigraphy of the Alpine Lateglacial: Implications of the sedimentary and morphological record of the Lienz area (Tyrol/Austria). *E&G Quaternary Science Journal,* 65**:** 113-144. DOI: 10.3285/eg.65.2.02

Schimmelpfennig, I., J. M. Schaefer, N. Akçar, T. Koffman, S. Ivy-Ochs, R. Schwartz, R. C. Finkel, S. Zimmerman, et al. 2014. A chronology of Holocene and Little Ice Age glacier culminations of the Steingletscher, Central Alps, Switzerland, based on high-sensitivity beryllium-10 moraine dating. *Earth and Planetary Science Letters,* 393**:** 220-230. DOI: 10.1016/j.epsl.2014.02.046

Schoeneich, P. 1993. Comparaison des systèmes de légende français, allemand et suisse. In *Cartographie géomorphologique - Cartographie des risques. Actes de la Réunion annuelle de la Société Suisse de Géomorphologie, 19 au 21 juin 1992 aux Diablerets et à Randa,* eds. P. Schoeneich, and E. Reynard, 15-24 pp. Lausanne: Institut de Géographie Lausanne.

Schwander, J., U. Eicher, and B. Ammann. 2000. Oxygen isotopes of lake marl at Gerzensee and Leysin (Switzerland), covering the Younger Dryas and two minor oscillations, and their correlation to the GRIP ice core. *Palaeogeography, Palaeoclimatology, Palaeoecology,* 159**:** 203-214. DOI: 10.1016/S0031-0182(00)00085-7

Smith, M., J. Carrivick, and D. Quincey. 2016. Structure from motion photogrammetry in physical geography. *Progress in Physical Geography,* 40**:** 247-275. DOI: 10.1177/0309133315615805

Stone, J. O. 2000. Air pressure and cosmogenic isotope production. *Journal of Geophysical Research: Solid Earth,* 105**:** 23753-23759. DOI: 10.1029/2000JB900181

Tessier, L., M. Couteaux, and J. Guiot. 1986. An attempt at an absolute dating of a sediment from the last glacial recurrence through correlations between pollen analytical and tree-ring data. *Pollen et Spores,* 18**:** 61-76.

Uppala, S. M., P. Kållberg, A. Simmons, U. Andrae, V. d. Bechtold, M. Fiorino, J. Gibson, J. Haseler, et al. 2005. The ERA-40 re-analysis. *Quarterly Journal of the royal meteorological society,* 131**:** 2961-3012. DOI: 10.1256/qj.04.176

van der Beek, P., and P. Bourbon. 2008. A quantification of the glacial imprint on relief development in the French western Alps. *Geomorphology,* 97**:** 52-72. DOI: 10.1016/j.geomorph.2007.02.038

Vincent, C., A. Fischer, C. Mayer, A. Bauder, S. P. Galos, M. Funk, E. Thibert, D. Six, et al. 2017. Common climatic signal from glaciers in the European Alps over the last 50 years. *Geophysical Research Letters,* 44**:** 1376-1383. DOI: 10.1002/2016GL072094

von Grafenstein, U., H. Erlenkeuser, A. Brauer, J. Jouzel, and S. J. Johnsen. 1999. A Mid-European Decadal Isotope-Climate Record from 15,500 to 5000 Years B.P. *Science***:** 1654-1657. DOI: 10.1126/science.284.5420.1654

Westoby, M., J. Brasington, N. Glasser, M. Hambrey, and J. Reynolds. 2012. 'Structure-from-Motion'photogrammetry: A low-cost, effective tool for geoscience applications. *Geomorphology,* 179**:** 300-314. DOI: 10.1016/j.geomorph.2012.08.021

Wurth, G., S. Niggeman, D. K. Richter, and A. Mangini. 2004. The Younger Dryas and Holocene climate record of a stalagmite from Hölloch Cave (Bavarian Alps, Germany). *Journal of Quaternary Science,* 19**:** 291-298. DOI: 10.1002/jqs.837

Young, N. E., J. M. Schaefer, J. P. Briner, and B. M. Goehring. 2013. A ^{10}Be production-rate calibration for the Arctic. *Journal of Quaternary Science,* 28**:** 515-526. DOI: 10.1002/jqs.2642

APPENDICES

Appendix 1. Characteristics of the samples from the Rougnoux valley (VdR). The latitude, longitude and elevation of each sampled boulder were recorded with a handheld GPS and later corrected with the DEM of the southern Écrins massif. The height of the boulders was assessed with a folding rule. The sample thickness of the rock fragments in each sample set was measured with a caliper and subsequently averaged. The topographic shielding of the sampled boulders was estimated with a clinometer and a compass. The CRONUS Earth geometric shielding calculator (http://hess.ess.washington.edu/math/general/skyline_input.php, last accessed 27 March 2018) enabled the conversion into a topographic shielding factor.

Sample	Latitude [°N]	Longitude [°E]	Elevation [m a.s.l.]	Boulder height [m]	Lithology	Sample thickness [cm]	Topographic shielding factor
VdR-01	44.7570000	6.3367200	2189	0.75	Sandstone	5.2	0.953
VdR-02	44.7571983	6.3367701	2186	0.60	Sandstone	6.5	0.954
VdR-03	44.7573013	6.3368101	2184	0.70	Sandstone	3.6	0.941
VdR-04	44.7574997	6.3376698	2152	0.80	Sandstone	6.4	0.947
VdR-05	44.7574997	6.3377800	2151	0.40	Sandstone	5.7	0.941
VdR-06	44.7577019	6.3377500	2151	0.46	Sandstone	3.5	0.937
VdR-07	44.7563019	6.3383298	2160	1.20	Sandstone	10.0	0.932
VdR-08	44.7568016	6.3381500	2157	0.55	Sandstone	3.8	0.939
VdR-09	44.7580986	6.3382802	2142	0.45	Sandstone	5.0	0.936
VdR-10	44.7552986	6.3388400	2152	0.65	Sandstone	3.4	0.879
VdR-11	44.7566986	6.3392501	2126	1.75	Sandstone	2.6	0.896
VdR-12	44.7579002	6.3390799	2120	0.50	Sandstone	7.0	0.934
VdR-13	44.7626991	6.3421998	2104	0.55	Sandstone	3.0	0.930
VdR-14	44.7627983	6.3416200	2089	1.50	Sandstone	4.5	0.933
VdR-15	44.7630005	6.3409700	2069	0.75	Sandstone	5.6	0.936
VdR-16	44.7640991	6.3405600	2064	1.80	Sandstone	6.2	0.941
VdR-17	44.7639999	6.3406301	2067	1.05	Sandstone	4.1	0.941
VdR-18	44.7640991	6.3401599	2050	1.25	Sandstone	4.4	0.930
VdR-19	44.7644997	6.3375201	1979	0.80	Sandstone	5.2	0.928
VdR-20	44.7644997	6.3368702	1966	1.60	Sandstone	4.1	0.937
VdR-21	44.7645988	6.3360100	1945	0.35	Sandstone	1.6	0.936
VdR-22	44.7648010	6.3359199	1943	1.30	Sandstone	2.8	0.880
VdR-23	44.7631989	6.3353000	1975	1.05	Sandstone	4.6	0.939
VdR-24	44.7634010	6.3354402	1969	0.80	Sandstone	6.0	0.926
VdR-25-1	44.7635002	6.3352499	1964	0.50	Sandstone	2.5	0.926
VdR-25-2	44.7635002	6.3352499	1964	0.50	Sandstone	3.5	0.926
VdR-26	44.7638016	6.3342099	1957	1.90	Sandstone	1.6	0.948
VdR-27	44.7635002	6.3344798	1969	1.25	Sandstone	6.3	0.933
VdR-28	44.7635002	6.3344598	1968	1.40	Sandstone	6.7	0.933
VdR-29	44.7657013	6.3342400	1894	0.55	Granite	3.4	0.936
VdR-30	44.7657013	6.3340402	1885	0.35	Granite	3.0	0.923

Sample	Latitude [°N]	Longitude [°E]	Elevation [m a.s.l.]	Boulder height [m]	Lithology	Sample thickness [cm]	Topographic shielding factor
VdR-31	44.7655983	6.3338099	1874	0.75	Gneiss	2.7	0.934

Appendix 2. Characteristics of the samples from the Prelles valley (VdP) and the moraine down-valley from the Pré de la Chaumette (PdC) mountain cabin. The latitude, longitude and elevation of each sampled boulder were recorded with a handheld GPS and later corrected with the DEM of the southern Écrins massif. The height of the boulders was assessed with a folding rule. The sample thickness of the rock fragments in each sample set was measured with a caliper and subsequently averaged. The topographic shielding of the sampled boulders was estimated with a clinometer and a compass. The CRONUS Earth geometric shielding calculator (http://hess.ess.washington.edu/math/general/skyline_input.php, last accessed 27 March 2018) enabled the conversion into a topographic shielding factor.

Sample	Latitude [°N]	Longitude [°E]	Elevation [m a.s.l.]	Boulder height [m]	Lithology	Sample thickness [cm]	Topographic shielding
VdP-01	44.7430992	6.3312802	2396	0.60	Sandstone	6.3	0.943
VdP-02	44.7430992	6.3309398	2380	0.65	Gneiss	1.5	0.949
VdP-04	44.7452011	6.3222899	2263	1.30	Sandstone	5.9	0.970
VdP-05	44.7449989	6.3222198	2258	1.10	Sandstone	5.3	0.963
VdP-06	44.7450981	6.3222799	2259	0.90	Sandstone	2.4	0.958
PdC-01	44.7639008	6.3252201	1791	0.65	Granite	3.8	0.926
PdC-02	44.7636986	6.3253102	1793	1.05	Gneiss	1.4	0.915
PdC-04	44.7635994	6.3255000	1792	1.30	Gneiss	1.5	0.929
PdC-05	44.7634010	6.3254900	1790	2.00	Gneiss	1.3	0.918

Appendix 3. ^{10}Be concentrations in the samples from the Prelles valley and from the moraine near the Pré de la Chaumette mountain cabin. The ^{10}Be/^{9}Be ratios were corrected with ^{10}Be/^{9}Be ratios from batch-specific analytical blanks. Samples marked with * and ** were corrected with a ^{10}Be/^{9}Be ratio of 3.2559E-15 and 2.8946E-15, respectively.

Sample	Quartz [g]	Spike [atoms ^{9}Be]	^{10}Be/^{9}Be	Accelerator mass spectrometry error [%]	^{10}Be concentration [atoms ^{10}Be g^{-1}]	Uncertainty [atoms ^{10}Be g^{-1}]
VdP-1	20.9300	2.0446E+19	4.2801E-14	8.7	38,631*	3,697
VdP-2	14.9900	2.0606E+19	3.4912E-14	11.0	43,516*	5,347
VdP-4	21.0900	2.0416E+19	2.3252E-13	3.5	221,937*	7,836
VdP-5	21.0300	2.0440E+19	2.5221E-13	3.6	241,973*	8,812
VdP-6	21.0400	2.0280E+19	2.3972E-13	3.4	227,925*	7,947
PdC-1	11.1371	2.0365E+19	9.1951E-14	10.7	162,849**	18,085

Sample	Quartz [g]	Spike [atoms ^{9}Be]	^{10}Be/^{9}Be	Accelerator mass spectrometry error [%]	^{10}Be concentration [atoms ^{10}Be g^{-1}]	Uncertainty [atoms ^{10}Be g^{-1}]
PdC-2	21.0117	2.0286E+19	1.9016E-13	9.0	180,803**	16,471
PdC-4	8.9640	2.0327E+19	7.2063E-14	4.6	156,849**	7,731
PdC-5	20.9817	2.0379E+19	2.6467E-13	9.5	254,265**	24,519

Appendix 4. ^{10}Be concentrations in the samples from the Rougnoux valley. The ^{10}Be/^{9}Be ratios were corrected with ^{10}Be/^{9}Be batch-specific analytical blanks. Samples marked with * and ** were corrected with a ^{10}Be/^{9}Be ratio of 3.2559E-15 and 2.8946E-15, respectively.

Sample	Quartz [g]	Spike [atoms ^{9}Be]	^{10}Be/^{9}Be	Accelerator mass spectrometry error [%]	^{10}Be concentration [atoms ^{10}Be g^{-1}]	Uncertainty [atoms ^{10}Be g^{-1}]
VdR-01	21.0600	2.0367E+19	2.3318E-13	3.3	222,358*	7,509
VdR-02	21.0300	2.0412E+19	2.1607E-13	4.4	206,562*	9,221
VdR-03	21.0600	2.0371E+19	2.1075E-13	3.8	200,710*	7,697
VdR-04	21.0322	2.0377E+19	2.1633E-13	3.6	206,789**	7,565
VdR-05	21.0583	2.0333E+19	2.2700E-13	5.2	216,386**	11,505
VdR-06	19.3505	2.0307E+19	2.0601E-13	3.2	213,149**	6,897
VdR-07	21.0600	2.0404E+19	2.2398E-13	3.7	213,842*	8,019
VdR-08	21.0442	2.0303E+19	2.3194E-13	6.2	220,976**	13,892
VdR-09	21.0405	2.0309E+19	2.1300E-13	3.5	202,797**	7,280
VdR-10	21.0900	2.0458E+19	2.1663E-13	3.5	206,981*	7,397
VdR-11	2.9100	2.0483E+19	3.4739E-14	7.1	221,599*	18,031
VdR-12	17.8100	2.0458E+19	1.2089E-13	5.3	135,122*	7,478
VdR-13	21.0100	2.0472E+19	2.9129E-14	7.0	25,211*	2,102
VdR-14	21.0000	2.0515E+19	2.1546E-13	3.2	207,305*	6,818
VdR-15	21.0600	2.0531E+19	2.0165E-13	3.7	193,408*	7,360
VdR-16	21.0600	2.0505E+19	2.2367E-13	3.3	214,599*	7,274
VdR-17	10.3900	2.0731E+19	1.0204E-13	3.8	197,104*	7,907
VdR-18	2.2800	2.0487E+19	2.5864E-14	9.4	203,139*	22,774
VdR-19	21.0445	2.0301E+19	2.2562E-13	5.7	214,850**	12,499
VdR-20	14.4975	2.0317E+19	9.8701E-14	4.2	134,264**	5,891
VdR-21	21.0378	2.0282E+19	1.4279E-13	3.9	134,876**	5,410
VdR-22	21.0500	2.0503E+19	1.6291E-13	4.0	155,506*	6,464
VdR-23	21.0401	2.0335E+19	1.8791E-13	4.1	178,814**	7,544
VdR-24	20.9716	2.0321E+19	2.1645E-13	4.7	206,929**	9,796

Sample	Quartz [g]	Spike [atoms ^{9}Be]	^{10}Be/^{9}Be	Accelerator mass spectrometry error [%]	^{10}Be concentration [atoms ^{10}Be g^{-1}]	Uncertainty [atoms ^{10}Be g^{-1}]
VdR-25-1	21.0239	2.0363E+19	2.1266E-13	3.5	203,178**	7,239
VdR-25-2	21.0489	2.0266E+19	1.9151E-13	3.1	181,601**	5,786
VdR-26	21.0500	2.0551E+19	2.2958E-13	3.4	220,965*	7,672
VdR-27	21.0200	2.0527E+19	2.1783E-13	3.4	209,540*	7,320
VdR-28	21.0800	1.9846E+19	2.1898E-13	4.5	203,092*	9,290
VdR-29	7.3454	2.0331E+19	4.9287E-14	15.0	128,409**	20,576
VdR-30	11.1832	2.0343E+19	7.1655E-14	15.9	125,081**	20,706
VdR-31	9.7399	2.0359E+19	2.7915E-14	28.9	52,300**	16,913

Appendix 5. ^{10}Be exposure ages of the samples from the Rougnoux valley. The exposure ages were computed according to four scenarios ('CRONUS Earth', 'CRONUS Earth + snow', 'CREp', 'CREp + snow'). Exposure age uncertainties are given as σ.

Sample	Exposure age CRONUS Earth [ka]	σ CRONUS Earth [ka]	Exposure age CRONUS Earth + snow [ka]	σ CRONUS Earth + snow [ka]	Exposure age CREp [ka]	σ CREp [ka]	Exposure age CREp + snow [ka]	σ CREp + snow [ka]
VdR-01	10.6	0.5	11.4	0.6	10.3	0.4	11.0	0.4
VdR-02	10	0.6	10.7	0.6	9.7	0.5	10.4	0.5
VdR-03	9.6	0.5	10.3	0.6	9.4	0.4	10.0	0.4
VdR-04	10.3	0.5	11.0	0.6	10.0	0.4	10.7	0.5
VdR-05	10.8	0.7	11.5	0.8	10.5	0.6	11.2	0.6
VdR-06	10.5	0.5	11.2	0.6	10.2	0.4	10.9	0.4
VdR-07	11.1	0.6	11.8	0.6	10.8	0.5	11.5	0.5
VdR-08	10.8	0.8	11.6	0.9	10.5	0.7	11.2	0.7
VdR-09	10.2	0.5	10.9	0.6	9.9	0.4	10.6	0.4
VdR-10	10.8	0.6	11.6	0.6	10.5	0.4	11.2	0.5
VdR-11	11.5	1.0	12.3	1.1	11.2	0.9	11.9	1.0
VdR-12	7.0	0.5	7.4	0.5	6.9	0.4	7.3	0.4
VdR-13	1.3	0.1	1.4	0.1	1.3	0.1	1.3	0.1
VdR-14	10.8	0.5	11.5	0.6	10.5	0.4	11.2	0.4
VdR-15	10.2	0.6	11.0	0.6	10.0	0.4	10.7	0.5
VdR-16	11.4	0.6	12.2	0.6	11.1	0.4	11.9	0.5
VdR-17	10.3	0.6	11.0	0.6	10.1	0.5	10.7	0.5
VdR-18	10.9	1.3	11.6	1.4	10.6	1.2	11.3	1.3
VdR-19	12.2	0.9	13.0	0.9	11.9	0.7	12.7	0.8
VdR-20	7.5	0.4	8.0	0.5	7.4	0.3	7.9	0.4

Sample	Exposure age CRONUS Earth [ka]	σ CRONUS Earth [ka]	Exposure age CRONUS Earth + snow [ka]	σ CRONUS Earth + snow [ka]	Exposure age CREp [ka]	σ CREp [ka]	Exposure age CREp + snow [ka]	σ CREp + snow [ka]
VdR-21	7.5	0.4	8.0	0.4	7.4	0.3	7.9	0.4
VdR-22	9.3	0.5	10.0	0.6	9.2	0.5	9.9	0.5
VdR-23	10.0	0.6	10.7	0.6	9.9	0.5	10.5	0.5
VdR-24	11.9	0.7	12.8	0.8	11.7	0.6	12.5	0.7
VdR-25-1	11.4	0.6	12.2	0.6	11.2	0.4	11.9	0.5
VdR-25-2	10.3	0.5	11.0	0.5	10.1	0.4	10.8	0.4
VdR-26	12.1	0.6	13.0	0.7	11.8	0.5	12.7	0.5
VdR-27	12.0	0.6	12.9	0.7	11.7	0.5	12.6	0.5
VdR-28	11.7	0.7	12.5	0.7	11.4	0.6	12.2	0.6
VdR-29	7.5	1.2	8.0	1.3	7.5	1.1	8.0	1.3
VdR-30	7.5	1.3	8.0	1.4	7.4	1.2	7.9	1.3
VdR-31	3.2	1.0	3.4	1.1	3.2	1.1	3.4	1.1

Appendix 6. ^{10}Be exposure ages of the samples from the Prelles valley and the moraine near the Pré de la Chaumette mountain cabin. The exposure ages were computed according to four scenarios (CRONUS Earth, CRONUS Earth + snow, CREp, CREp + snow. Exposure age uncertainties are given as σ.

Sample	Exposure age CRONUS Earth [ka]	σ CRONUS Earth [ka]	Exposure age CRONUS Earth + snow [ka]	σ CRONUS Earth + snow [ka]	Exposure age CREp [ka]	σ CREp [ka]	Exposure age CREp + snow [ka]	σ CREp + snow [ka]
VdP-1	1.7	0.2	1.8	0.2	1.6	0.2	1.7	0.2
VdP-2	1.8	0.2	1.9	0.3	1.7	0.2	1.9	0.3
VdP-4	9.9	0.5	10.6	0.6	9.7	0.4	10.3	0.4
VdP-5	10.9	0.6	11.7	0.6	10.6	0.4	11.3	0.5
VdP-6	10.1	0.5	10.8	0.6	9.8	0.4	10.5	0.4
PdC-1	10.5	1.2	11.2	1.3	10.4	1.1	11.1	1.2
PdC-2	11.5	1.1	12.3	1.2	11.4	1.0	12.2	1.1
PdC-4	9.9	0.6	10.5	0.7	9.8	0.5	10.5	0.6
PdC-5	16.2	1.7	17.2	1.8	15.8	1.5	16.9	1.6

Appendix 7. ^{10}Be exposure ages and associated uncertainties from the Prelles valley [ka]. The ^{10}Be exposure age in the bracket was excluded due to internal uncertainties higher than 12%.

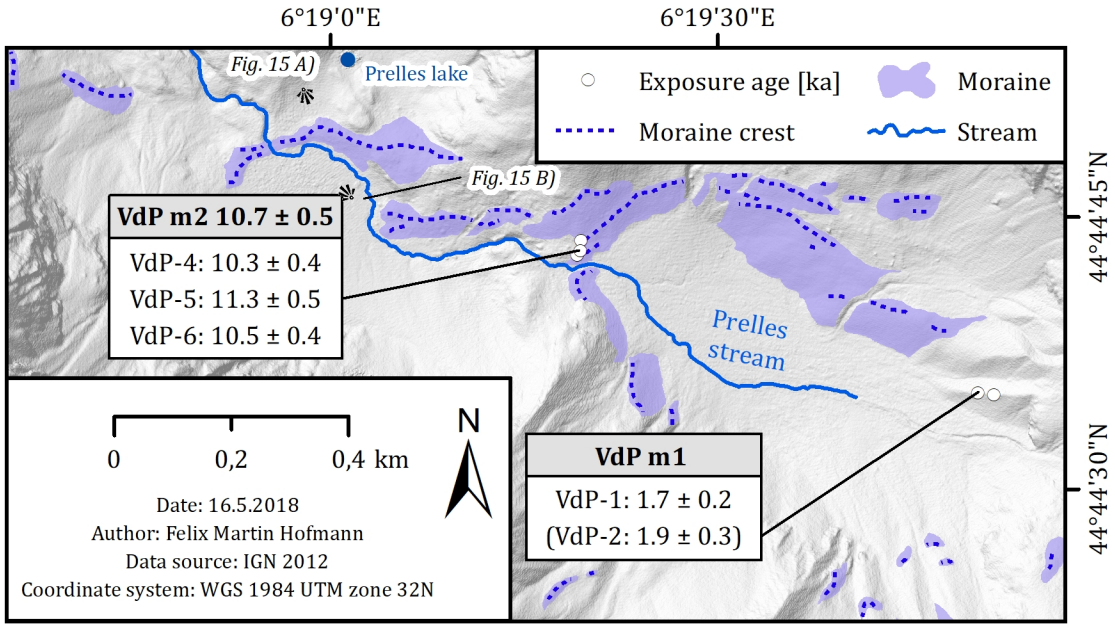

Appendix 8. ^{10}Be exposure ages and associated uncertainties from the frontal moraine near the Pré de la Chaumette mountain cabin [ka].

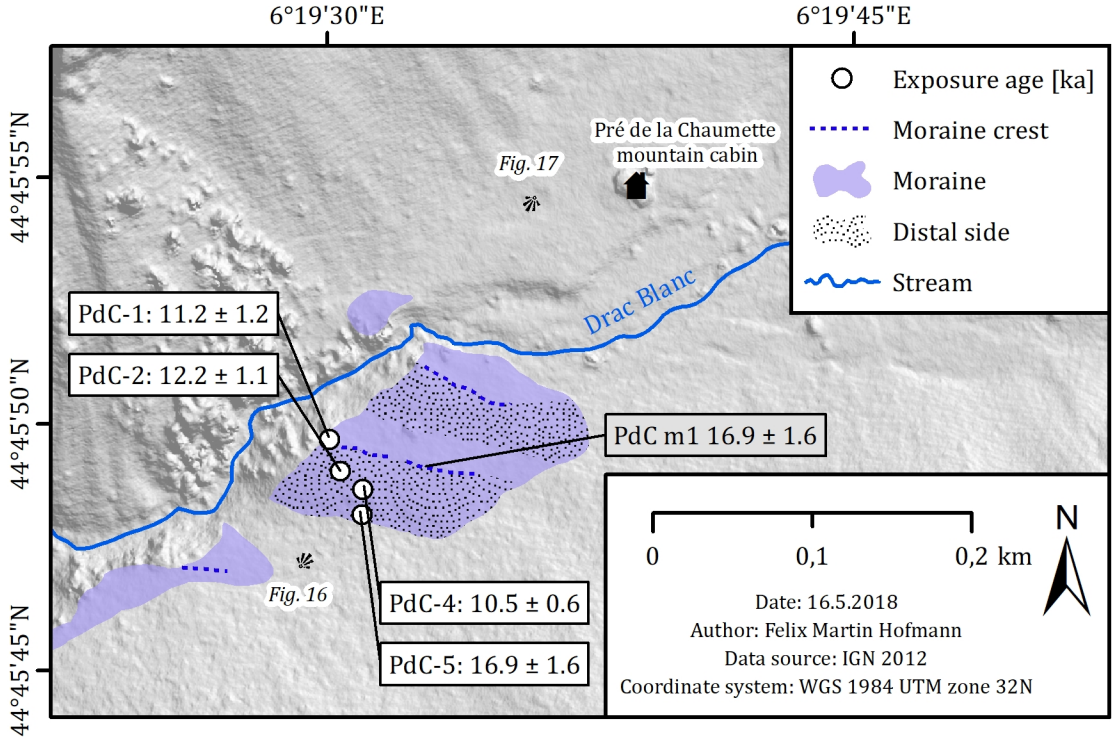

Appendix 9. ^{10}Be exposure ages and associated uncertainties from the Rougnoux valley [ka]. The ^{10}Be exposure ages in brackets were excluded due to internal uncertainties higher than 12%. Exposure ages and landform ages which were excluded due to stratigraphical considerations, are shown in grey.

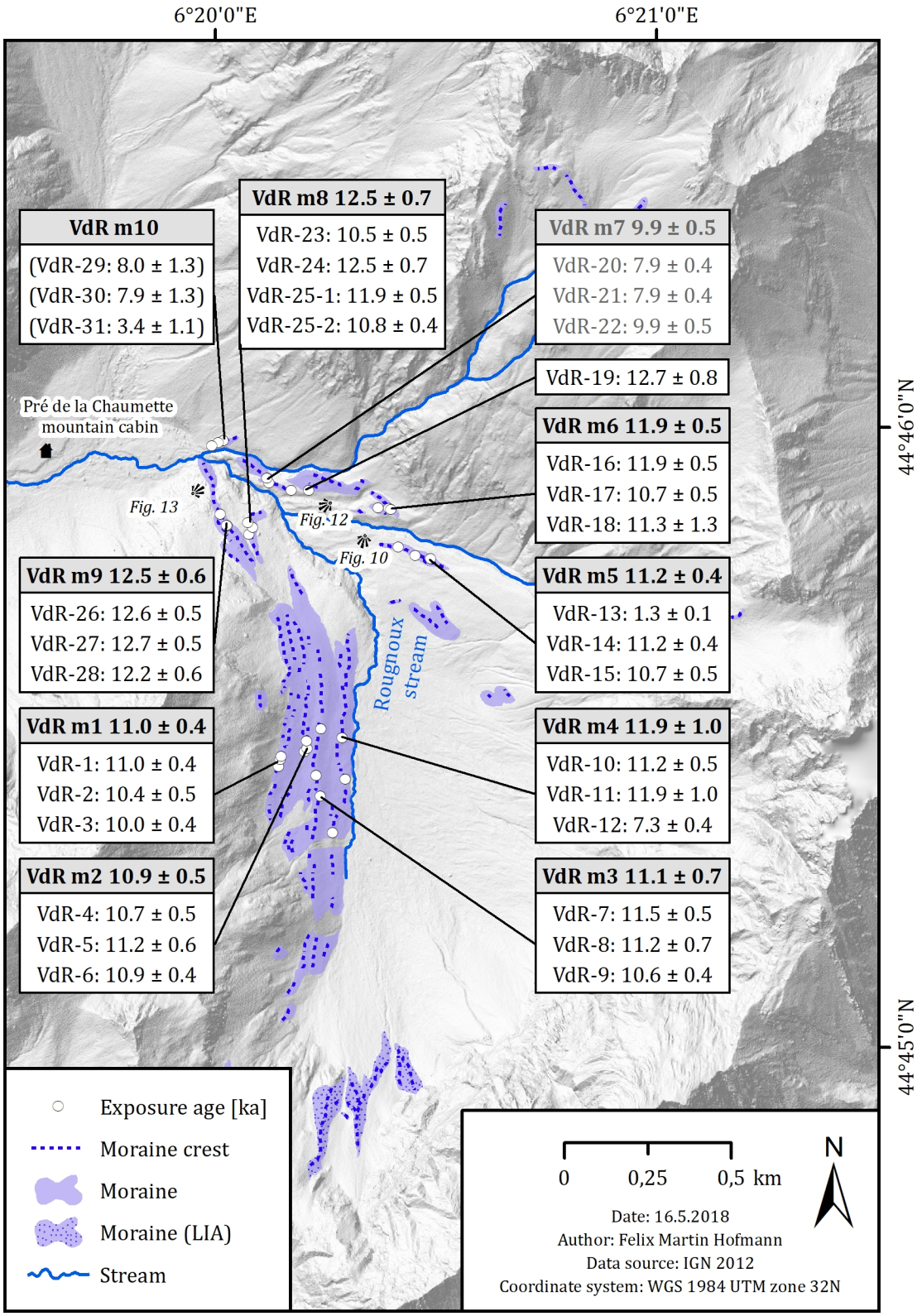

Appendix 10. Geomorphological map of the area around the Pré de la Chaumette mountain cabin.

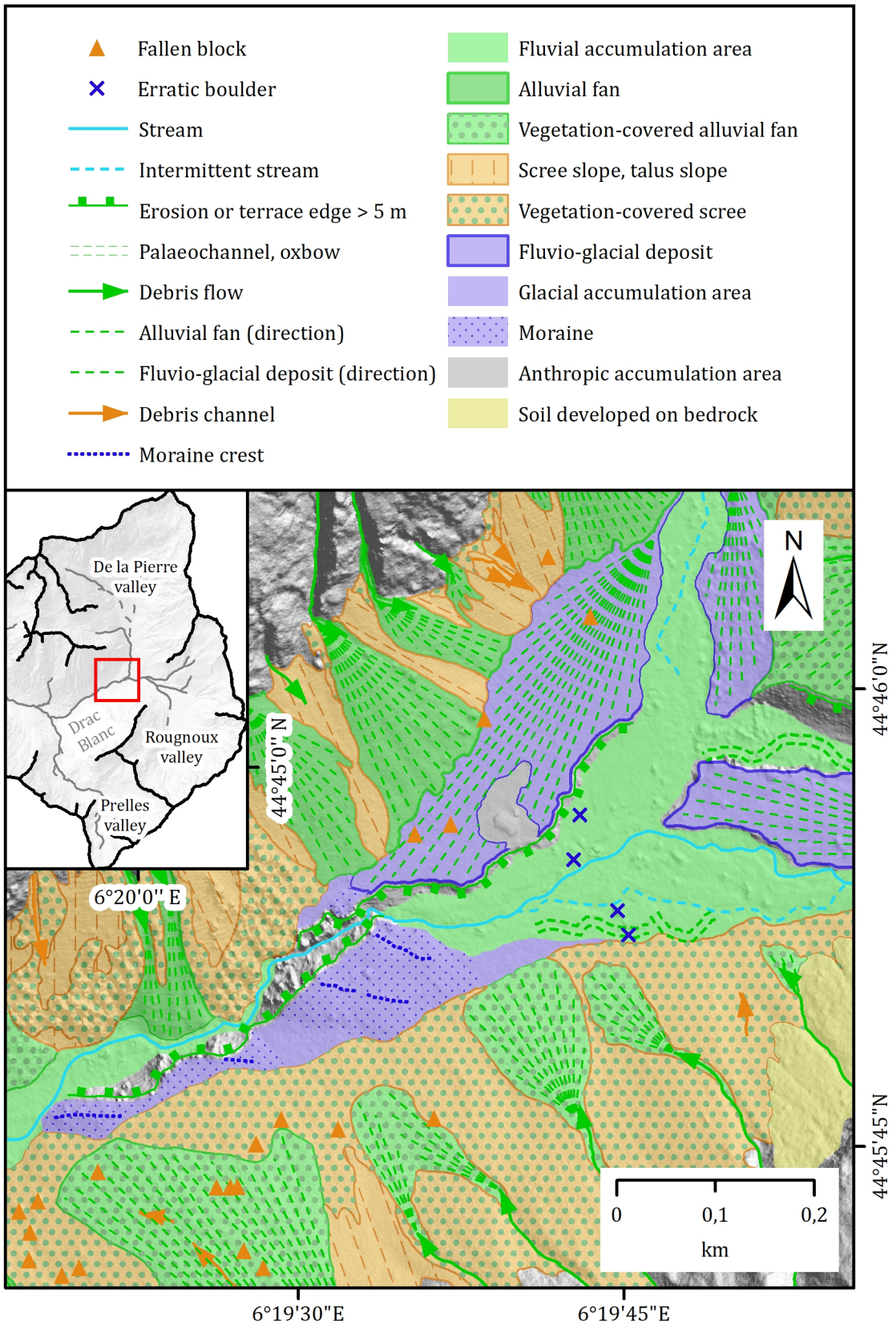

Date: 9.4.2018; Author: F.M. Hofmann; Data source: IGN 2012; Coordinate system: WGS 1984 UTM zone 32N

Appendix 11. Geomorphological map of the Prelles valley.

Appendix 12. Geomorphological map of the Rognoux valley.